Seismic deformation behavior of several types of multi-tier reinforced soil retaining walls

(数種類の多層擁壁の地震変形挙動)

Albano Acacio Ajuda

Supervisor: Prof. Jiro Kuwano

Graduate School of Science and Engineering, Saitama University,

Japan

December 7, 2020

Saitama, Japan

This work presents results from a series of 1g shaking table test on earthquake-induced deformation of hybrid retaining walls. The hybrid walls were constructed in two-tiers, the first using soil nailed wall and the second using MSE wall. During the experimental program, digital image analysis technique was employed to capture the sand movement and shear strains. The experimental results confirm the applicability of the modified Monono-Okabe theory for retaining walls systems. It was found that the deformation of the hybrid model walls was due to compaction of the backfill and shear deformation. The failure surface consisted of a planar geometry extending from the toe of the soil nail wall propagating upwards towards the backfill surface, passing behind geogrid reinforcement layers. The critical acceleration and development of the active wedge of failure was found at 5% of the hybrid wall height, and a few seconds later of seismic shaking, intense strain-softening within the active wedge of failure appeared from the heel of the wall towards the backfill surface at a changing angle towards the critical state intersecting the active failure wedge. The deformation of the hybrid walls is conditioned by the nail lengths rather than the geogrid reinforcement lengths. For reinforced soil wall constructed in two tiers the failure mechanism of the model walls consisted in a two-part failure wedge, extending from the toe of the lower tier towards the backfill surface passing behind reinforcement layers of the upper tier towards the backfill surface. The maximum horizontal displacements of reinforced soil wall decrease with increase in offset length of tiered wall. By observing the sand deformation, two deformation zones—shear deformation zone near the facing of the lower tier and compaction zone below the upper tier soil block, the compaction zone of lower tier increased with increase in offset length. It was found that by increasing the offset distance of the upper tier lesser amount of lateral deformation in both tiers. Increasing the reinforcement while maintaining the same offset distance also reduce the

amount of lateral displacement. A critical offset distance is defined as a distance by which the upper and lower tier does not rotates to the outward direction as a rigid body.

Keywords: Earthquake, soil nail, reinforced soil wall, deformation, strain localization, shear strains.

Contents

Chapter 1: Introduction

Background and objectives of research

Geogrid reinforced soil method is widely utilized and contributes towards the improvement of stability for many kinds of earth structures. By using this method, steep embankment or vertical soil wall can be constructed easily and economically comparing to the other conventional methods. Moreover, this method has advantage on environment because waste material can be reduced by constructing steep soil structures. From these backgrounds, application rate of this method is increasing recently. It is well known that the seismic performance of geogrid reinforced soil wall (GRSW) is much higher than that of the other conventional retaining walls. Tatsuoka et al. (1996) reported the damages of some kinds of retaining structures due to the Hyogo-Ken-Nambu earthquake that occurred in 1995. According to their report, the GRSWs having a full-height rigid facing for railway showed very small displacement although they were located in severe shaken areas, and the other conventional retaining walls collapsed at almost the same area. As for the GRSW having divided facing panels for roadway, damages caused by Hyogoken-Nambu earthquake were also reported by Nishimura et al. (1996). They reported that the GRSWs subjected to seismic intensity of 6 or more showed no clear failure and maintained adequate stabilities even after the earthquake.

In recent years, many departments of transportation have been working to keep pace with population growth by considering major infrastructure improvements to their highways. The successive expansion of the highway system to meet increasing demand has made extension of the right-of-way economically prohibitive. The use of earth

retaining walls has allowed highway upgrades to be constructed within existing right-of ways, consequently lowering the additional cost of acquiring separate lands. The primary function of earth retaining walls in highway constructions is to retrofit and maximize the use of existing space and structures. Engineers can use earth retaining walls to provide steep slopes of reinforced soil to reduce the required width for widening existing traffic lanes in constricted areas. Various types of earth retaining structures have been used successfully in the last two decades. Around the world, mechanically stabilized earth (MSE) retaining walls and soil nail walls are commonly incorporated into highway construction. Typical applications of such systems include but are not limited to: Widening within existing rights-of-way; adding a lane of traffic; Adding a turn-around lane under a bridge abutment; Repairing failed slopes and retaining structures; Unlike the conventional systems that serve to retain soil behind a vertical cut, these two techniques are based on the concept of soil reinforcement that use passive inclusions in the soil mass to create a gravity structure to improve soil stability. In soil nail walls, the native undisturbed soil, adjacent to the excavation is strengthened so that it can stand unsupported at larger depths which would normally require installation of sheet piling or soldier pile bracings. This technique is composed of two major elements: a) layers of reinforcing members that are placed in predrilled holes and grouted to improve the bond strength between the nail and the adjacent soil when nail stresses are mobilized and b) a shotcrete facing typically placed on the soil face which soil nails are attached into. Construction of soil nail walls is performed in vertical steps, with construction starting at the top of the excavation and proceeding down. Once an excavated level is reinforced with soil nails, first temporary and then permanent facings are applied to retain the soil. Mechanically stabilized earth walls, on the other hand, are composed of three major components: a) reinforcements which are placed in the backfill

soil in unstressed condition, b) layers of granular soil backfill with drainage blankets and c) facing elements which are provided to retain fill material and to prevent slumping and erosion of steep faces. Unlike soil nail walls, MSE walls are constructed by placing reinforced fill from the "bottom up."

From the point of view described above, the objectives of the research presented in this dissertation is:

a) To understand the failure and deformation behaviour of the GRSW during an earthquake. Especially, special attention is focused on the effect of material properties, pullout characteristics of geogrid.
b) To understand the failure and deformation behaviour of the MSE/Soil nail hybrid reinforced soil retaining walls during earthquake;
c) Investigate the sand movement behind a two-tier reinforced soil wall during seismic shaking;

Review of the physical modelling of reinforced structures

A wide range of geotechnical problems can be investigated using physical modelling techniques and the evaluation of the behaviour of soil structures with geosynthetics is no exception. Small-scale physical modelling of reinforced soil structures tested at the 1g gravity field has been sued in the past to provide insight tin failure mechanisms (Lee et al., 1973; Juran and Christopher, 1989; Palmeira and Gomes, 1996). However, with the model tests under the 1g gravity field, the behaviour of soil mass could not be simulated properly because of the dominance of self-weight forces in geotechnical engineering. The use of finite element analyses has also been used to investigate failure mechanisms of reinforced soil structures (Hird et al., 1990; San et al., 1994). However,

while standard finite element techniques are useful for analysis of structures under working stress conditions, modelling of failure in frictional materials requires special techniques to handle the localization of deformations, such as specific continuum formulations or the use of adaptive mesh refinement to capture slip discontinuities (Zienkiewicz and Tayler 1991). In order to replicate the gravity induced stresses of a prototype structure in a 1/N reduced model, it is necessary to make a test with the model in a gravitational field N times larger than that of prototype structure. Although modelling limitations are often difficult to overcome when seeking a direct comparison between the performance of centrifuge models and full-scale prototype structures, many of these limitations can be avoided when the purpose is to validate analytic or numerical tool. Thus, the combination of experimental centrifuge modelling results with analytic predictions is a useful approach to investigate the performance of reinforced soil structures at failure. Some of the earliest tests were performed by Bolton and Pang (1982) on vertical wall models made with dry sand reinforced using metallic strips and rods. They suggested a simple anchor theory for design of reinforced soil walls based on active pressures exerted on the facing area attributable to a strip. The vertical stresses used to compute the active pressures included a contribution from the overturning effect of the backfill. Their main conclusions were that the distribution of vertical stress under the reinforced soil mass was close to being uniform, and that the use of the active earth pressure coefficient underestimated the acceleration at failure in the models.

Review of seismic performance of GRSWs

Several researchers studied the seismic performance of reinforced embankment or soil wall on experimentally and numerically. The first experimental investigation about the seismic stability of the reinforced embankment was made by Uesawa et al. (1972). They

made the shaking table tests with the model reinforced and non-reinforced embankment having 1.5m wall height. As a result, the non-reinforced embankment showed large deformation and collapsed. To the contrary, stability of the reinforced embankment could be maintained although some differential settlement at crown was observed.

Richardson and Lee (1975) reported results of shaking table tests of vertical reinforced soil wall having 30mm wall height. Aluminum belt and magnetic tape were used for the model reinforcement in order to investigate the effect of kind of reinforcement. In the case of aluminum belt, the wall collapsed due to pullout of the belt. On the other hand, magnetic tape broken, and the wall collapsed. Furthermore, simple equation for horizontal earth pressure distribution acting on the wall facing during earthquake was proposed based on the test results. They also suggested the validity of the proposed equation comparing to the results obtained from the equivalent linear response analyses. Continuously, Richardson et al. (1977) conducted the full scale model test with blasting. It was reported that the tensile force occurred in the reinforcement was much smaller than the values calculated by above equation and increment factor of earth pressure during earthquake was correspond to about 0.5~0.8a/g(a: base acceleration, g: gravitational acceleration). Koga et al. (1986, 1987, 1992, 1988) conducted the shaking table test using the model reinforced embankment with 300mm in height. They focused on the slope gradient, laying spacing and length of the reinforcement and kinds of the reinforcement. As a consequence, spacing and rigidity of reinforcement were effective to reduce the deformation of the reinforced embankment. Furthermore, it was addressed that upper most extensive reinforcement could restrict deformation effectively. Finally, stability analysis was proposed based on the pseudo-static method. Murata et al. (1989, 1990, 1991) and Tateyama et al. (1990) proposed the GRSW having full height rigid facing wall. For developing the method, full scale (wall height = 2.5m) and medium

scale (wall height = 1.0m) shaking table tests were conducted. They reported that the GRSW having a rigid facing has much higher seismic stability as compared with that of the GRSW having divided facing panel wall. At the same time, the full scale shaking table test was conducted on the symmetrical vertical reinforced soil wall covered with geogrid on whole surface. It seems that seismic stability of GRSW can be improved greatly by laying the geogrid on the whole surface.

Sakaguchi et al. (1993, 1994, 1995, 1998) conducted the large scale model shaking tests of the GRSW having the lightweight hollow concrete blocks for the facing wall. They reported that the stains occurred in the geogrid increased with the increment of the seismic acceleration. Besides the gravity field tests, the centrifuge shaking table tests were also conducted with the same scale model. They reported that strain in the geogrid was proportion to the centrifugal acceleration and length of geogrid was most effective to restrict the residual displacement. Compaction of the backfill was also effective for the reduction of residual displacement. Furthermore, simple chart to estimate the residual displacement was proposed. Sato et al. (1993, 1994, 1995, 1998) made the centrifuge shaking table test on the seismic stability of GRSW. Special attention was focused on the effect of kinds of wall facing (soil bag, soil cement wall and paper), spacing of geogrid, density of backfill and so on.

As a result, the GSW having FS=1.2 at kh =0.2 based on the manual of the PWRI maintained their sufficient stability against the middle earthquake. Watanabe et al. (2003) investigated the reasons for relatively good seismic performance of GRSW with full height rigid wall facing based on 1G model shaking table tests. In the case of conventional retaining walls, earth pressure acting on the wall was supported by the bearing capacity of the base. Therefore, when the bearing stress reached to the capacity of the base and local toe failure occurred, the wall collapsed rapidly. On the

other hand, in the case of GRSW, since the wall loads were spread over the wider and more flexible base of the reinforced soil zone. Kato et al. (2002) reported the instability of GRSW constructed on the slope based on the results of 1G model shaking table test. Furthermore, the new type GRSW with soil nails below the base of facing was suggested to overcome such instability. Based on these results, rigidity of base supporting GRSW was considered sufficiently, when the GRSW was constructed at mountain area after 2004 Niigataken Chuetsu earthquake (Kitamoto et al., 2006; JSCE, 2006). As for toe condition, Bathurst et al. (2002, 2005) investigate the influence of toe constraint of the GRSW with full height rigid wall using a series of 1m high shaking table test. In the test, 40~60 % of the peak total horizontal earth load were measured at the toe of the wall. Such value was much higher than the value calculated by NCMA method (1998) and AASHTO (2002). Bathurst et al. (2002) also investigated the seismic stability of the GRSW with segmental block type wall. They reported that the stability of the GRSW depended on the share capacity between segmental blocks

References

Lee, K. L., Adams, B. D., and Vagneron, J. J. 1973. Reinforced earth retaining walls, Journal of the Soil Mechanics Division, ASCE, Vol. 99, No. SM10, pp. 745-764

Juran, I. and Christopher, B. R. 1989. Laboratory model study on geosynthetic reinoforced soil retaining walls, Journal of Geotechnical Engineering, ASCE, Vol. 115, No. 7, pp. 905-926.

Palmeria, E. M. and Gomes, R. C. 1996. Comparisons of predict and observed failure mechanisms in model reinforced soil wall, Geosynthetic International, Vol. 3, No. 3, pp. 329-347.

Hird, C. C., Pyrah, I. C., and Russell, D. 1990. Finite element analysis of the collapse of reinforced embankments on soft clay, Geotechnique, Vol. 40, No 4, pp. 633-640.

San, K., Leshchinsky, D. and Matsui, T. 1994. Geosynthetic reinforced slopes: Limit equilibrium and Finite element analyses, Soils and Foundations, Vol. 34, No. 2, pp. 79-85.

Zienkiewicz, O. C. and Taylor, R. L. 1991. The finite element method 4th edition, Vol. 2, McGraw-Hill, New York.

Bolton, M. and Pang, P. 1982. Collapse limit states of reinforced earth retaining walls, Geotechnique, Vol. 32, No. 4, pp. 349-367

Uesawa, H., Nasu, M., Komine, T. and Yasuda, Y. 1972. Experimental research on seismic stability of embankment by large shaking table, Report for Railway Technological Research.

Richardson, G. N. and Lee. K. L. 1975. Seismic design of reinforced earth, Journal of Geotechnical Engineering Division, ASCE, Vol. 101, No. GT2, pp. 167-188.

Richardson, G. N., Feger, D., Fong, A. and Lee. K. L. 1977. Seismic testing of reinforced earth walls, Journal of Geotechnical Engineering Division, ASCE, Vol. 103, No. GT1, pp. 1-17.

Koga, Y., Taniguchi, E., Itoh, Y., Sakaguchi, M., Nakanishi, A. and Sakami, T. 1986. Model shaking table tests on geotextile reinforced embankment, Proc. of 1st Symposium on Geotextile, pp. 57-60.

Koga, Y., Taniguchi, E., Itoh, Y., Sakaguchi, M., Nakanishi, A. and Sakami, T. 1987. Model shaking table tests and stability analysis method for the reinforced embankment on inclined ground, Proc. of 2nd Symposium on Geotextile, pp. 57-60.

Koga, Y., Itoh, Y., Washida, S. and Shimazu, T. 1988. Seismic resistance of reinforced embankment by model shaking table tests, Proc. of International Symposium on Theory and Practice of Earth reinforcement, pp. 413-418.

Koga, Y. and Washida, S. 1992. Earthquake resistant design method of geotextile reinforced embankments, Proc. of International Symposium on Reinforced Practice, pp. 255-260.

Murata, O., Tateyama, M. and Tatsuoka, F. 1989. Middle scale seismic test for the embankment having the short sheet reinforcement and wall, Proc. of 44th Annual conference of JSCE, pp. 56-57 (in Japanese).

Murata, O., Tateyama, M. and Tatsuoka, F. 1990. Middle scale seismic test for the embankment having the short sheet reinforcement and wall, Proc. of 25th Annual conference of JGS, pp. 2019-2022 (in Japanese).

Murata, O., Tateyama, M. and Tatsuoka, F. 1991. A reinforcing method for earth retaining walls using short reinforcing members and a continuous rigid facing, Proc. of ACSE Geotechnical Engineering Congress, ASCE, pp. 935-946

Chapter 2: Experimental Investigation on Earthquake-Induced Deformation of Hybrid Retaining Wall and Strain Softening of Backfill Soil

Author 1

- *Albano Ajuda, PhD Candidate*
- *Department of Civil and Environmental Engineering, Saitama, Japan*

Author 2

- *Jiro Kuwano, Professor*
- *Department of Civil and Environmental Engineering, Saitama, Japan*

Abstract

This work presents results from a series of 1g shaking table test on earthquake-induced deformation of hybrid retaining walls. The hybrid walls were constructed in two-tiers, the first using soil nailed wall and the second using MSE wall. During the experimental program, digital image analysis technique was employed to capture the sand movement and shear strains. The experimental results confirm the applicability of the modified Monono-Okabe theory for retaining walls systems. It was found that the deformation of the hybrid model walls was due to compaction of the backfill and shear deformation. The failure surface consisted of a planar geometry extending from the toe of the soil nail wall propagating upwards towards the backfill surface, passing behind geogrid reinforcement layers. The critical acceleration and development of the active wedge of failure was found at 5% of the hybrid wall height, and a few seconds later of seismic shaking, intense strain-softening within the active wedge of failure appeared from the heel of the wall towards the backfill surface at a changing angle towards the critical

state intersecting the active failure wedge. The deformation of the hybrid walls is conditioned by the nail lengths rather than the geogrid reinforcement lengths.

Introduction

Reinforced soil walls using geosynthetics and steel are well-established construction technologies, and it has been used for over four decades due to improved seismic performance and cost-effectiveness compared to conventional retaining walls such as gravity-type and cantilever type retaining walls. Many of the constructed reinforced soil walls demonstrated very high seismic stability from previously recorded earthquakes. For example, Kuwano et al. (2014) reported that 90% of the reinforced soil wall showed no damage, although a massive tsunami accompanied the earthquake. Seismic behaviour of geosynthetic reinforced soil wall and conventional retaining walls has been extensively investigated using shaking table model Test (Matsuo et al. 1998, Koseki et al. 1998a, Watanbe et al. 2003, Ling, et al. 2005, Sabermahani et al. 2009, Anastasopoulos et al. 2010, Watanabe 2011, Munoz and Kiyota, 2020). Soil nails also have demonstrated very high seismic performance. For example, (Vucetic et al. 1989) reported that during the Loma Pietra earthquake, no evidence of damage was reported in soil nailed walls, although the soil nailed walls were subjected to near-fault ground motion. Seismic behaviour of soil nailed walls in reduced-scale model is reported in (Yazdandoust 2018, Tufenkjian and Vucetic 2000).

In the case where reinforced soil wall needs to be constructed in high sloping ground, the retaining wall selection would be preferable a shored reinforced soil wall (SMSE) walls (Lee et al. 2010 and Morrison et al. 2007) or multi-tier geosynthetics reinforced soil wall (GRS) walls (Yoo et al. 2011, Mohamed et al. 2014, Liu et al. 2014,

Bhattacharjee and Amin 2019). However, some construction constraints may arise. For example, it is necessary to excavate a large amount of soil to allow bottom-up placement of the reinforcement layers and wall panels, a temporary shoring may be needed to stabilize the excavation during the MSE wall construction and therefore, all this process leads to an increase in the total construction cost and time. To overcome these issues, as an alternative solution for those wall types, hybrid retaining walls have been proposed recently to be used in a cut/fill ground condition in particular for road projects, as illustrated in Figure 1. The solution consists of stabilizing the excavation using nails and then constructing the MSE wall on top of the soil nailed wall and, therefore, reducing the amount of the reinforcement layers, wall height, the excavation and backfill volume. Very few studies have reported the behaviour of hybrid retaining walls Turner and Jensen (2005) showed a successful case study for landslide stabilization using soil nail and MSE walls. Alhabshi (2006) investigated using numerical simulation the effect of reinforcement length. It suggested that the ideal reinforcement length to height ratio range between 0.8-1.0. Then, Wei (2013) investigated the response of hybrid wall subjected to surcharge loading, he found that the failure plane consists of two zones: the first zone located in the reinforced area of the soil nail wall, and the second located behind the MSE reinforcement layers. Meantime, investigations on the seismic deformation behaviour of hybrid retaining walls are still very limited. Yazdandoust (2019) reported failure surfaces with a two-part wedge geometry consisting of a concave curve in the soil nailed block and an inclined line in the MSE soil block. Moreover, investigations on detailed failure mechanisms regarding sand deformation and strain localization behind hybrid and soil nailed walls are still unknown. The present paper investigates the earthquake-induced deformation of a hybrid retaining wall, focusing on facing lateral deformation, progressive failure, and

strain softening of the backfill soil. In addition, for the author's best knowledge, there is no experimental evidence of the applicability of the modified Monono-Okabe theory's proposed by Koseki et al. (1998b) for retaining walls, which is discussed from the experimental observations.

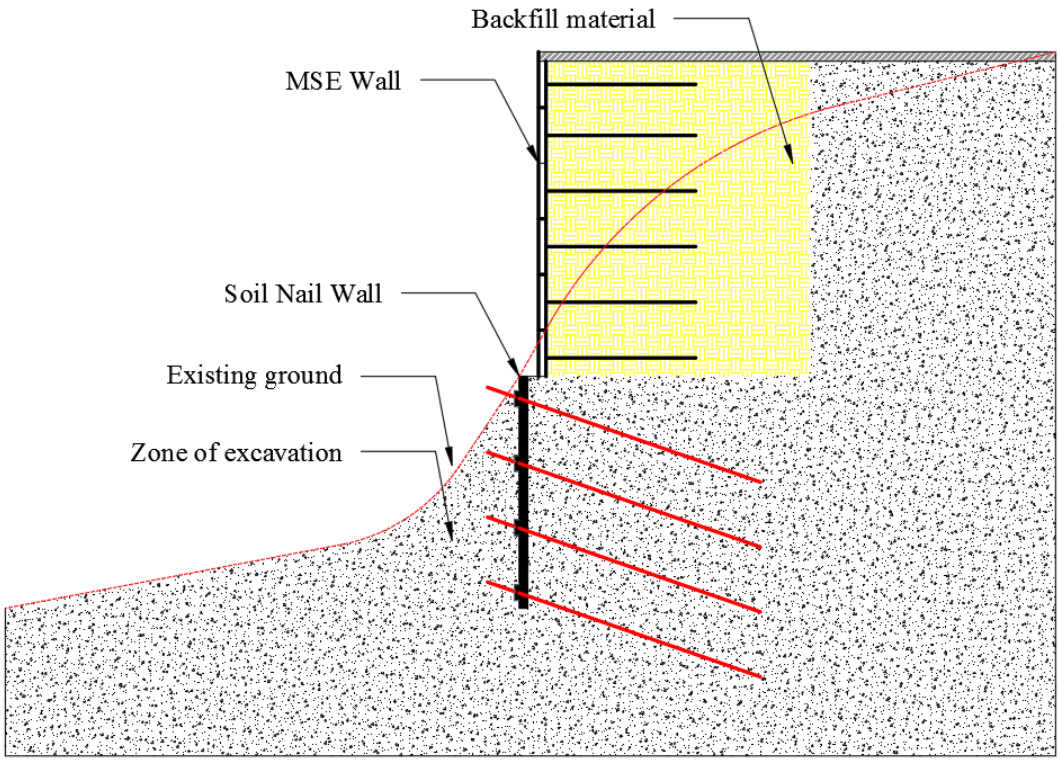

Figure 1 Example of application of hybrid reinforced soil retaining wall

Test setup

Shaking table facility

A computer-controlled shaking table is used to simulate the seismic loading, as shown in Figure 2. The shaking table is built with the following dimension: 1,300 mm (long) by 1,000 mm (wide) seated on a pair of low friction bearing rails constrained to the horizontal corresponding to a single degree of freedom.

Similitude laws

In the present study, similitude proposed by Iai (1989) was used to scale-down a prototype hybrid wall to a reduced-scale wall by taking a geometric factor of 15. Table 1 shows a summary of the similitude implemented in the current study. The reduced-scale modelling and the corresponding prototype are discussed individually for each hybrid retaining wall component in the following sections.

Model container

The soil and wall are constructed inside a rigid container built with the following dimensions: 1,300 mm (long), 600 mm (wide), and 650 mm (high) as shown in Figure 3. On one side of the container was constructed using Plexiglas in order to visualize the deformation during shaking. The container was perfectly bolted to the shaking table to keep the plane strain condition. According to Lomardi et al. (2015), using absorbing boundaries can minimize the generation of reflection of body waves. Therefore, at the far end boundary of the container, a 50 mm foam damper was installed. Lubricant was used at the side walls of the container to minimize friction between the soil and wall sides. However, Watanbe et al. (2003) conclude that sidewall friction of the soil container on the response acceleration and failure angle is negligible.

Figure 2 Shaking table facility

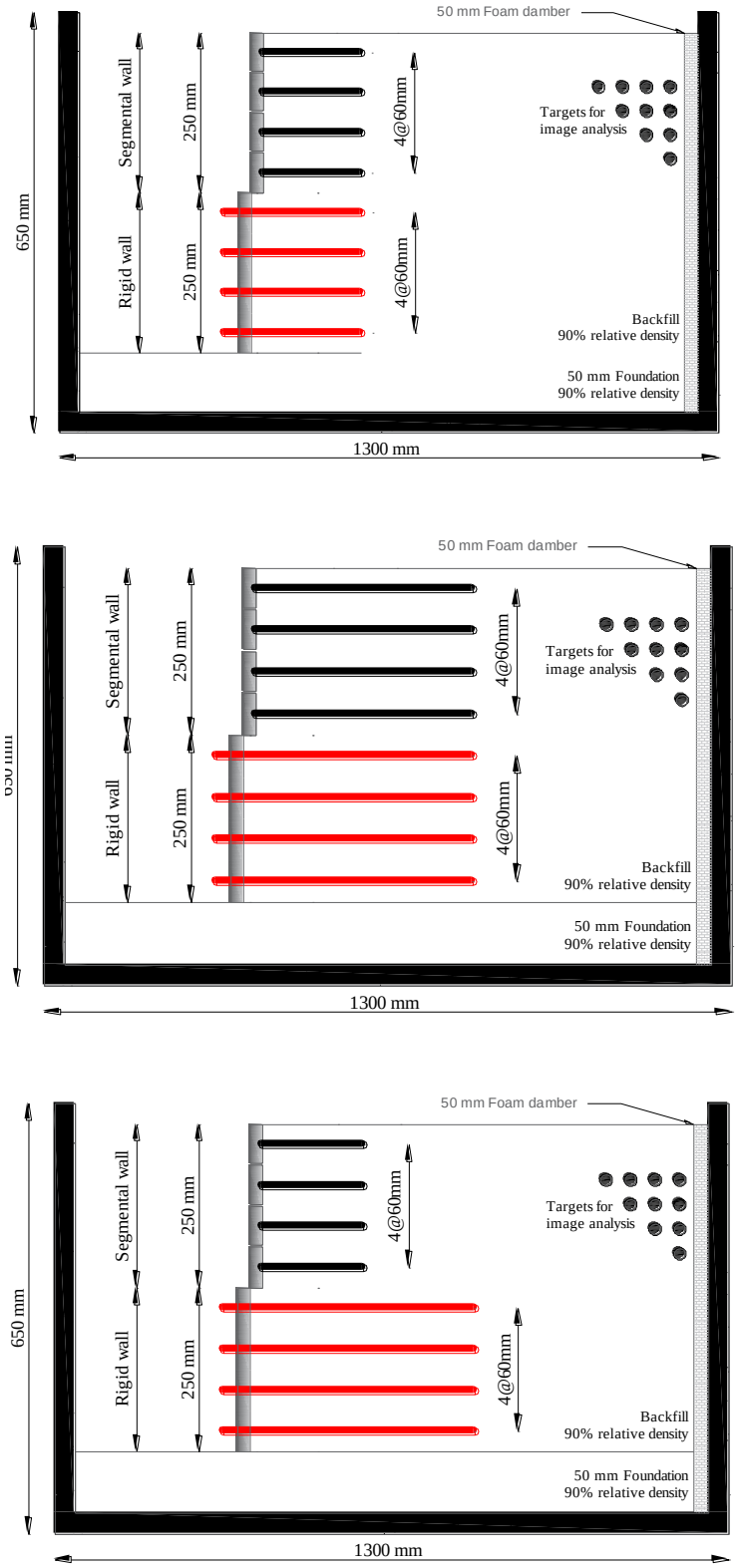

Figure 3 Tested models

Model soil

In this study, air drained Toyoura sand with 90% relative density was used for both foundation and backfill. This density corresponds to a model ground of well-compacted sand to construct railways and road embankment Nakajima et al. (2010). Moreover, sandy soil was also used by Gassler (1988) to investigate the failure of a nearly vertical soil nail wall using reduced-scale and field tests. Based on the plane strain compression test results, as shown in Figure 4, the values of the mobilized internal friction angle at peak and residual strength are equal to 51 and 43 degrees, respectively, with the corresponding maximum shear strains.

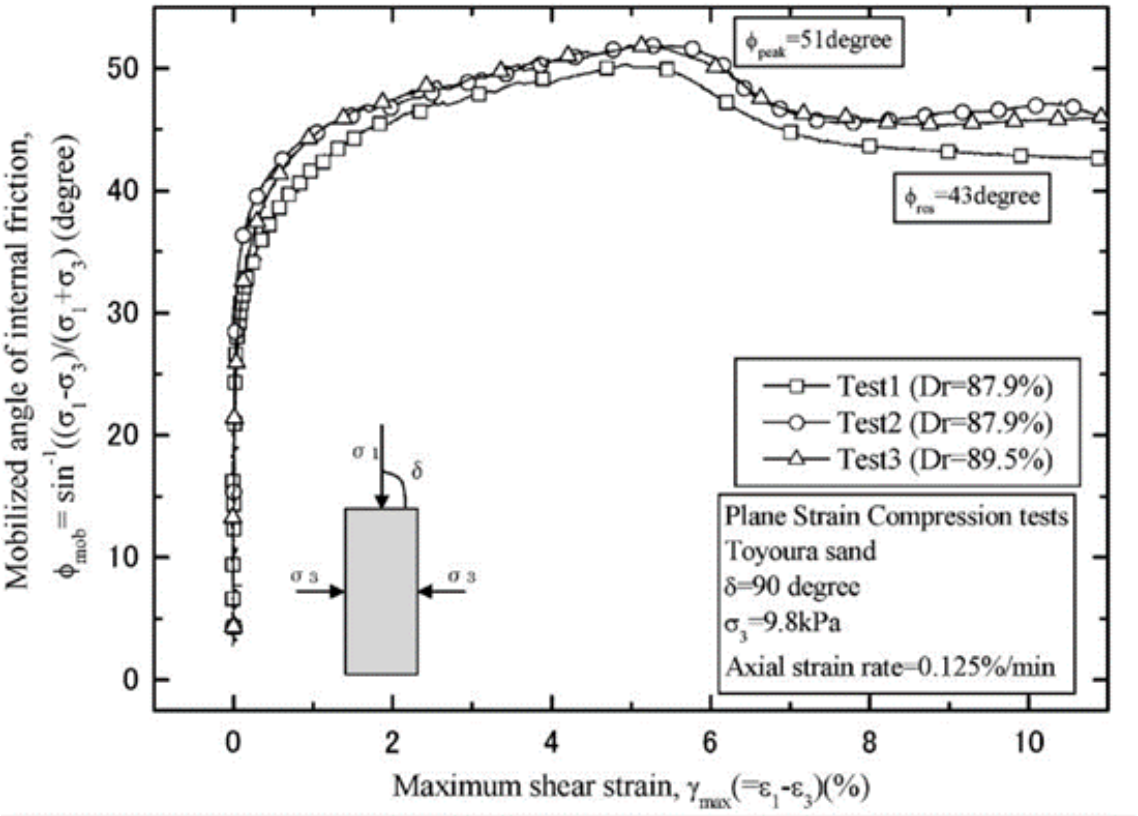

Figure 4 Soil properties Munaf, 1988

Model wall

According to Yazdandoust (2018), traditional soil nail and geosynthetics reinforced soil wall height ranges from 3.0 to 14.0 m with an average of 8.0 m. Different types of walls have been used in previous reduced-scale models. Richardson et al. (1977) conducted seismic testing using 280 mm wall height; (Watanbe et al. 2003 and Koseki et al. 1998) constructed reduced-scale models using 500 mm high walls. Therefore, considering the size of the shaking table and the container, the reduced-scale hybrid retaining wall height was set to 500 mm, which corresponds to a 7.5 m wall high at the prototype scale. The hybrid walls are divided into two-tiers, the first is the lower tier constructed using a rigid full-height soil nail wall, and the upper was built using segmental panels. The wall models are illustrated in Figure 5 and 6. The segmental panels are not fixed to each other and can rotate freely. Therefore, local buckling or bulging deformation is expected.

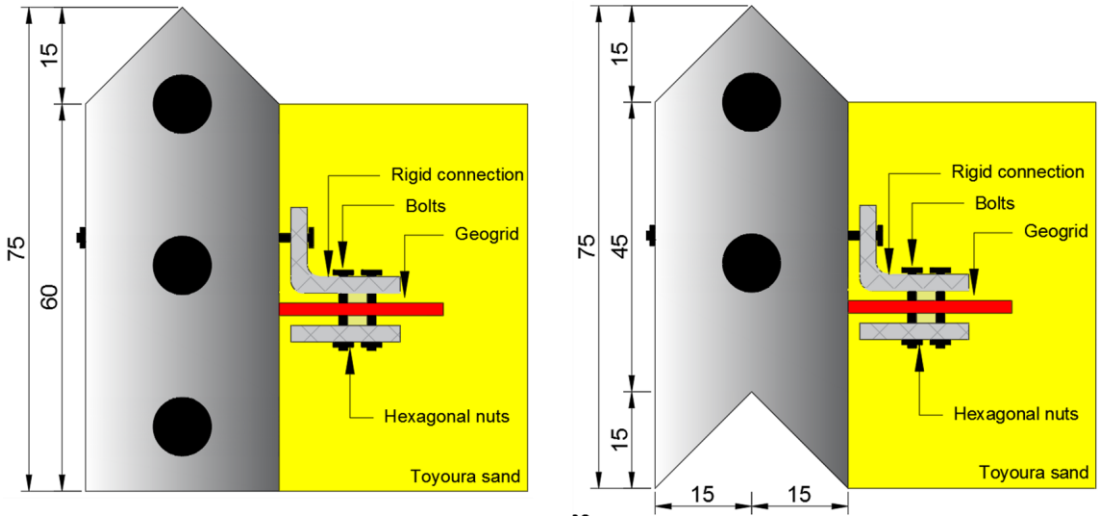

Figure 5 Model segmental walls

Model reinforcement

In hybrid retaining walls, two types of reinforcement material are used, geosynthetics and soil nail as shown in Figure 6. In this study, geogrids with a tensile strength of 22 kN/m was used as reinforcement material for the MSE wall. The reinforcement can be scaled base on strength, stiffness, or geometry. Punched-drawn uniaxial geogrids typically have the aperture size in the longitudinal direction between 300 mm and 500 mm, Xiao et al. (2016). Taking the scale factor of 1/15, the aperture of the model geogrid in the longitudinal direction (shaking direction) should be between 20 mm and 33 mm. The model geogrid used in this study has a longitudinal aperture of 25 mm. The length of the geogrids is set to 200 mm and 300 mm, corresponding to an L/H = 0.8, 1.2, which is beyond the minimum recommended L/H = 0.7 by FHWA design guidelines. The geogrids were laid in the backfill soil at a vertical spacing of 60 mm, which corresponded to the prototype of 0.9 m. According to Wu and Payeur (2015), MSE walls have been constructed with vertical spacing between 0.3 and 1.0 m to save

construction costs. It should be noted that the interaction between sand and reinforcement at the near the backfill surface can be less than at the prototype scale to the corresponding reinforcement layers at depth, as noted by El-Emam & Bathurst (2007).

Figure 6(a) Reinforcement material for the MSE walls

For soil nailed walls, according to FHWA design guidelines, solid bars diameter varies from 100 mm to 200 mm, taking the scale of 1/15, the diameter in model scale should be between 7 mm and 13 mm. Therefore, the nails used have a diameter of 12 mm correspond to 180 mm at the prototype, which falls between the recommended values. Another important consideration in modelling the nails is the soil-nail interfaces as it affects the lateral wall deformation. According to Luo et al. (2000) it is preferable to use a soil nail with a rough surface to achieve higher shear resistance. Furthermore, Sharma et al. (2019) conducted a series of pull out tests on soil nail in cohesionless soil to investigate the effect of nail surface roughness on pull out behaviour, it was reported

that a nail with a smooth surface showed a linear-perfectly plastic behaviour while a rough surface nail showed a strain-softening behaviour. In the present experimental program, nails with a rough surface were used to simulate the soil-reinforcement behaviour at the prototype. According to design guidelines by AS4678 (2002), nail horizontal and vertical spacing should not be more than 2.0 m; therefore, on reduced scale the spacing should not be more than 130 mm. In Test 1, the four nails were laid at a horizontal spacing of 50 mm, while in Test 2 and Test 3, the two nails were laid at a horizontal spacing of 130 mm at a vertical spacing of 60 mm. Table 2 shows a summary of the experimental program.

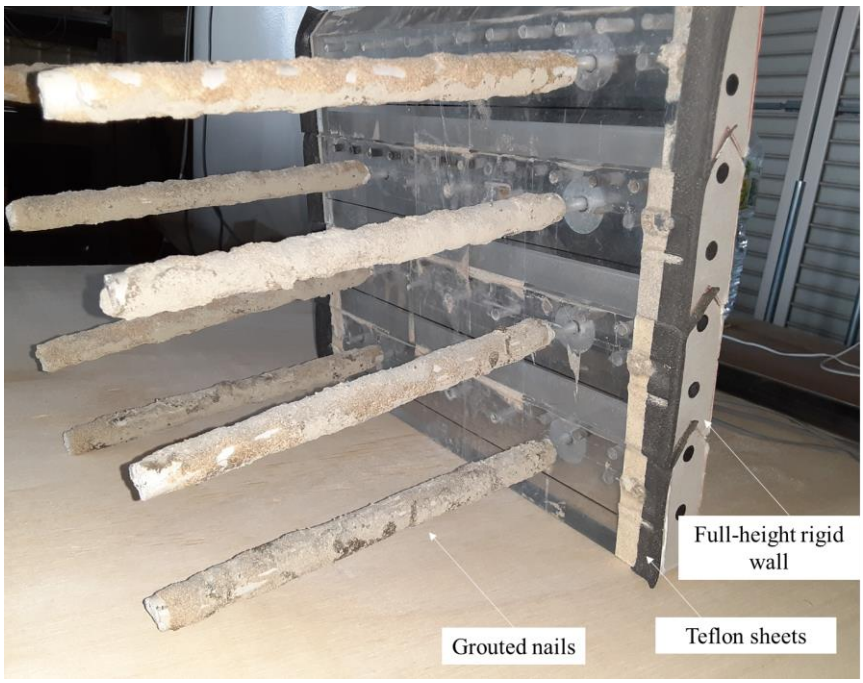

Figure 6(b) Reinforcement material (Soil nails) for the soil nailed walls

Construction sequence

The reduced-scale hybrid retaining wall construction started from the bottom of the rigid container by air-draining the foundation soil. The soil nail wall was placed into the desired position and braced, then the backfill soil was constructed while installing the reinforcement at a vertical spacing of 60 mm and optical targets at 30 mm horizontally.

Pre-installed grouted nails were used, it should be noted that a direct installation through the pre-drilled holes on the shaking table test would be complicated as compared to field construction. Because the nails are pre-installed, loads could develop and mobilize before the excavation depth for a nail layer. Therefore, installation induced soil nail loads and soil stresses could not be simulated in the shaking table model test. In addition, the nails are laid horizontally, which is different from the field. According to Hong et al. (2005) nail inclination has very little effect on reduced scale shaking table models. A similar construction technique is reported by (Yazdandoust 2019 and Moradi et al. 2020). Once the soil nail construction finished, unbracing took place from the top of the nail wall towards the bottom to simulate the excavation stress-path. The MSE wall construction started from the top of the soil nail backfill. The segmental panels are installed one by one while installing reinforcement layers and optical targets towards the top.

Input ground motion

All models were subjected to a simple sinusoidal wave with a predominant frequency of 5 Hz. The ground motion amplitude started at 0.1g with increments of 0.1g until complete failure occurred on the hybrid retaining walls or measurement was impossible. Each shaking stage was held for 10 seconds, corresponding to 50 cycles. This simple input motion and frequency allowed to generate large facing and backfill deformation.

Image analysis for shaking table models

A series of optical targets were placed into the backfill in contact with the plexiglass; the movement of the targets allowed the identification of failure geometry, sand deformation, and distribution of shear stains. The camera used in this research is GoPro Hero 5 at 2.7k and 30 frames per second (FPS). The camera was attached to the shaking

table using a special design frame, so it could shake at the same phase with the shaking table, eliminating the need for additional correction. The camera is mounted about 1.0 m away from the container Plexiglas. The resulting displacement of each target is in image space (units of a pixel) and therefore, calibration is required to convert into (cm); this is achieved by placing a series of fixed markers dots on the Plexiglas whose position is known in (cm) relatively to the container, a similar technique is reported in Watanabe et al. (2005).

Experimental Test results

Seismic failure mechanism

Figure 7(a) and (c) shows the failure mechanism of the tested models during shaking. In general, the hybrid walls were stable during the static condition, and no evidence of lateral deformation is recorded. By inputting the seismic waves, failure surfaces started to appear from the top of the backfill in the interface between the reinforced and unreinforced zone in the MSE wall and propagated towards the bottom-most geogrid layer. With continued application of seismic waves, inclined failure surfaces appear from the backfill surface in the unreinforced zone and propagated to the end of the last geogrid layer (counting from the top). Once the hybrid wall reaches its failure stage, the inclined failure surface penetrates the soil nail block reinforced zone, intersecting the wall toe. Figure 7(b) shows the illustration of the failure mechanism. For instance, in geosynthetics reinforced soil walls constructed in tiered configuration and with small offset distance, the failure surface crosses both the lower tier and the upper tier, as reported by Mohamed et al. (2014) under static loading and Liu et al. (2014) under seismic loading. The measured failure surface (first) angle during 0.4g was 51 degrees to the horizontal, this stage corresponds to the critical acceleration at 5% of the total

hybrid wall height, and therefore the active wedge of failure was formed. Shortly after the facing lateral deformation passed the critical acceleration, the backfill rapidly deformed to the outward direction together with the facing wall, a new failure surface (second) was formed with an angle of 41 degrees, similar behaviour is observed in Test 2 with much shallower failure surfaces. However, in Test 3, only one failure surface was possible to observe. Similar behaviour was reported by Watanabe et al. (2011) in gravity-type retaining walls. Figure 7(c) shows the failure mechanism of hybrid retaining walls regarding the efficiency of different reinforcement arrangements. It is observed that independently the arrangement of the reinforcement layers, the failure mechanism is the same. However, by increasing the reinforcement length, the failure surface angles become shallower, as can be observed in Test 2 and Test 3 compared to Test 1. Differently, Yazdandoust (2019) reported that the failure surfaces remained the same independently the nail length. This is because the extended reinforcement layers can hold more soil mass together, delaying the formation of the failure surfaces. Moreover, the failure surface angles of Test 2 and Test 3 was almost the same; this behaviour suggests that seismic stability of the hybrid retaining wall is governed by the nail lengths rather than the MSE reinforcement length and for economic design, increasing the nail length while maintaining the geogrid shorter can be an effective way while increasing the seismic stability.

The backfill settlements were also dependent on the reinforcement arrangement. In Test 1, a steep settlement with a “U” shape deformation is observed while in other Tests, the backfill settles uniformly throughout its length. Bearing capacity is also observed associated with rotation of each wall type and sliding of the soil nail while in Test 2 and 3, the walls mainly slide horizontally due to an increase in the reinforcement length,

which also justifies the shape of the backfill settlements. It should be noted that the bearing capacity on the MSE wall was not observed, this is due to the restrain mechanism of the soil nail wall top.

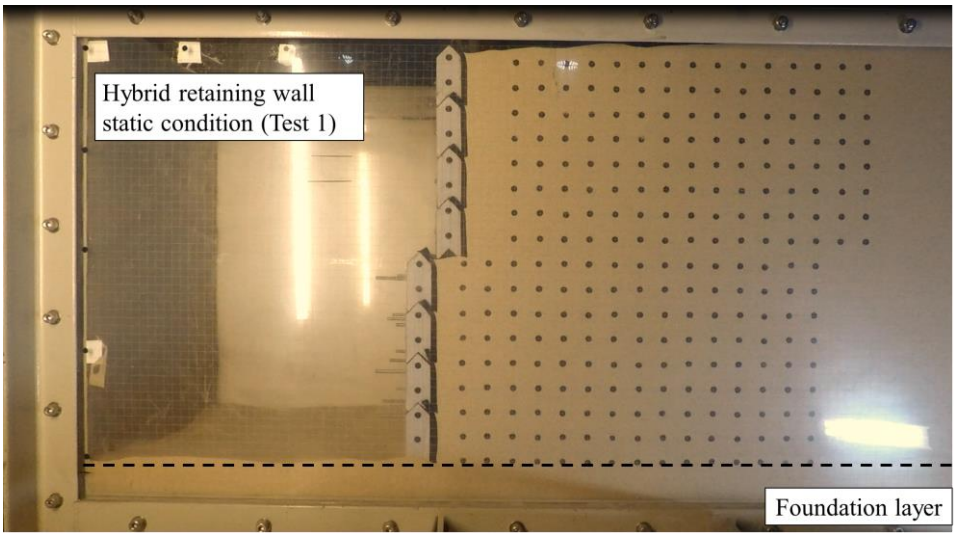

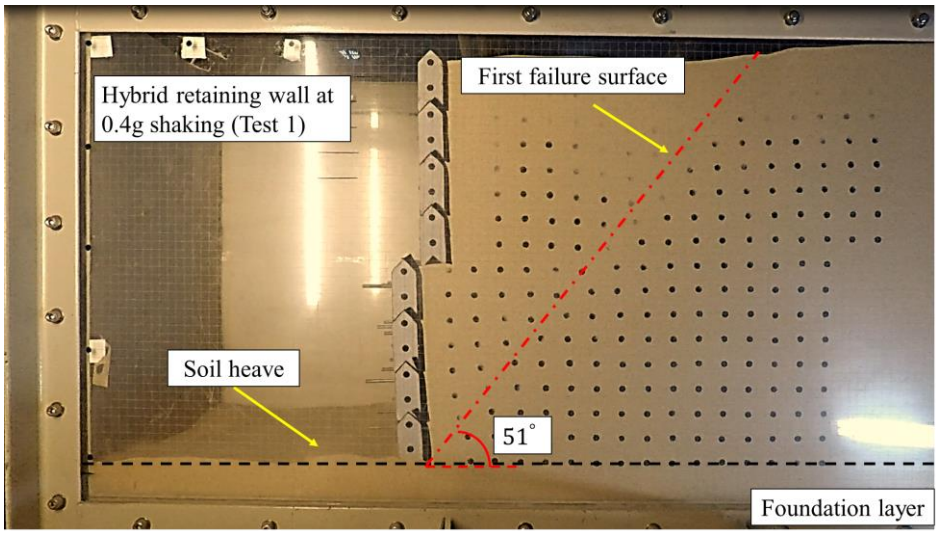

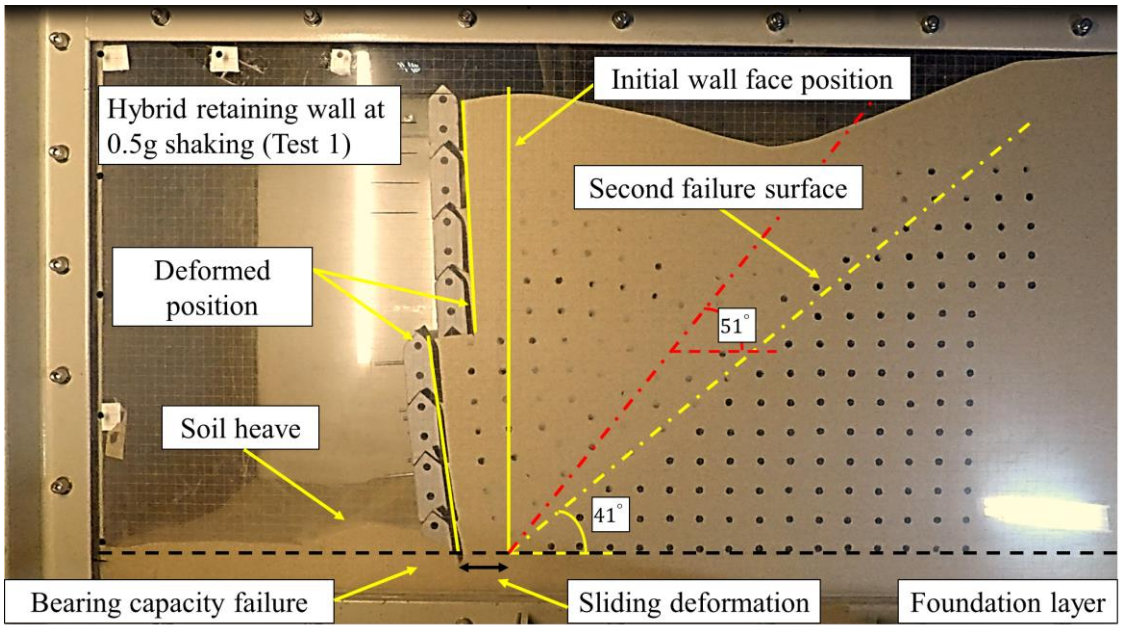

Figure 7(a) Failure process during seismic shaking in Test 1

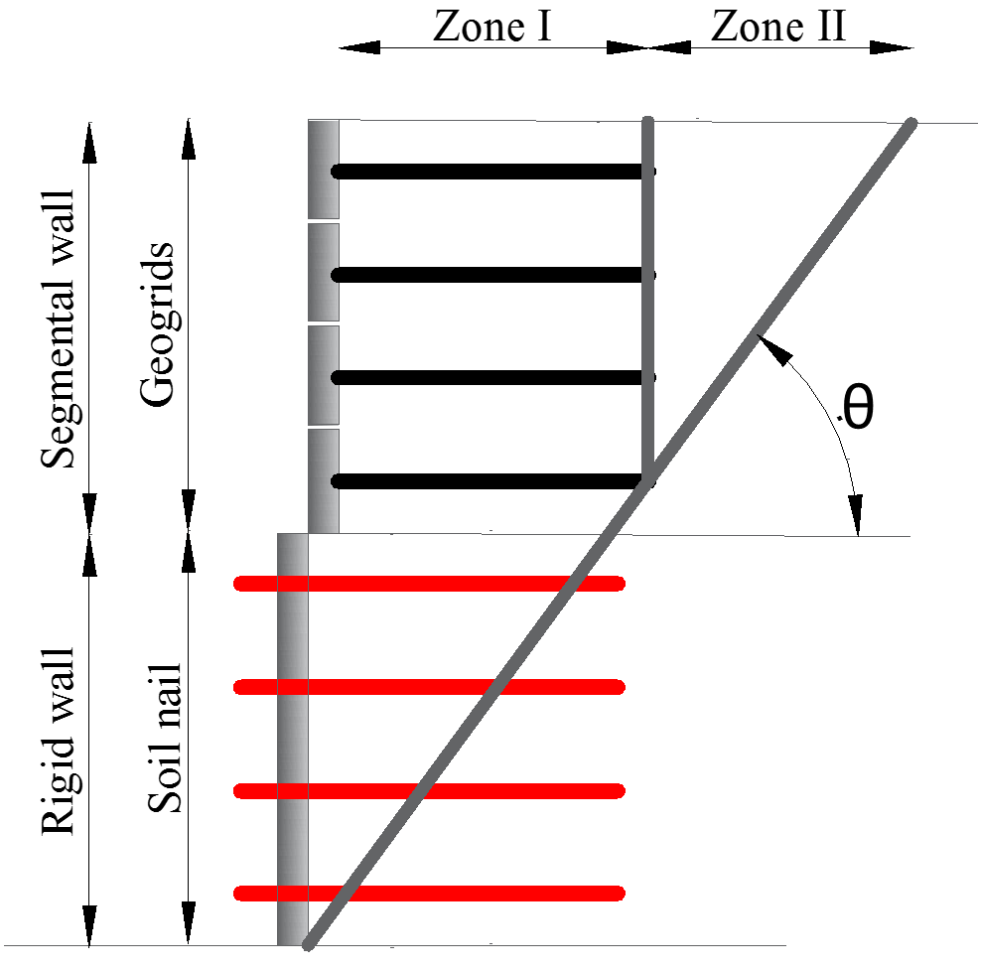

Figure 7(b) Schematic representation of the failure surfaces on hybrid reinforced soil retaining walls

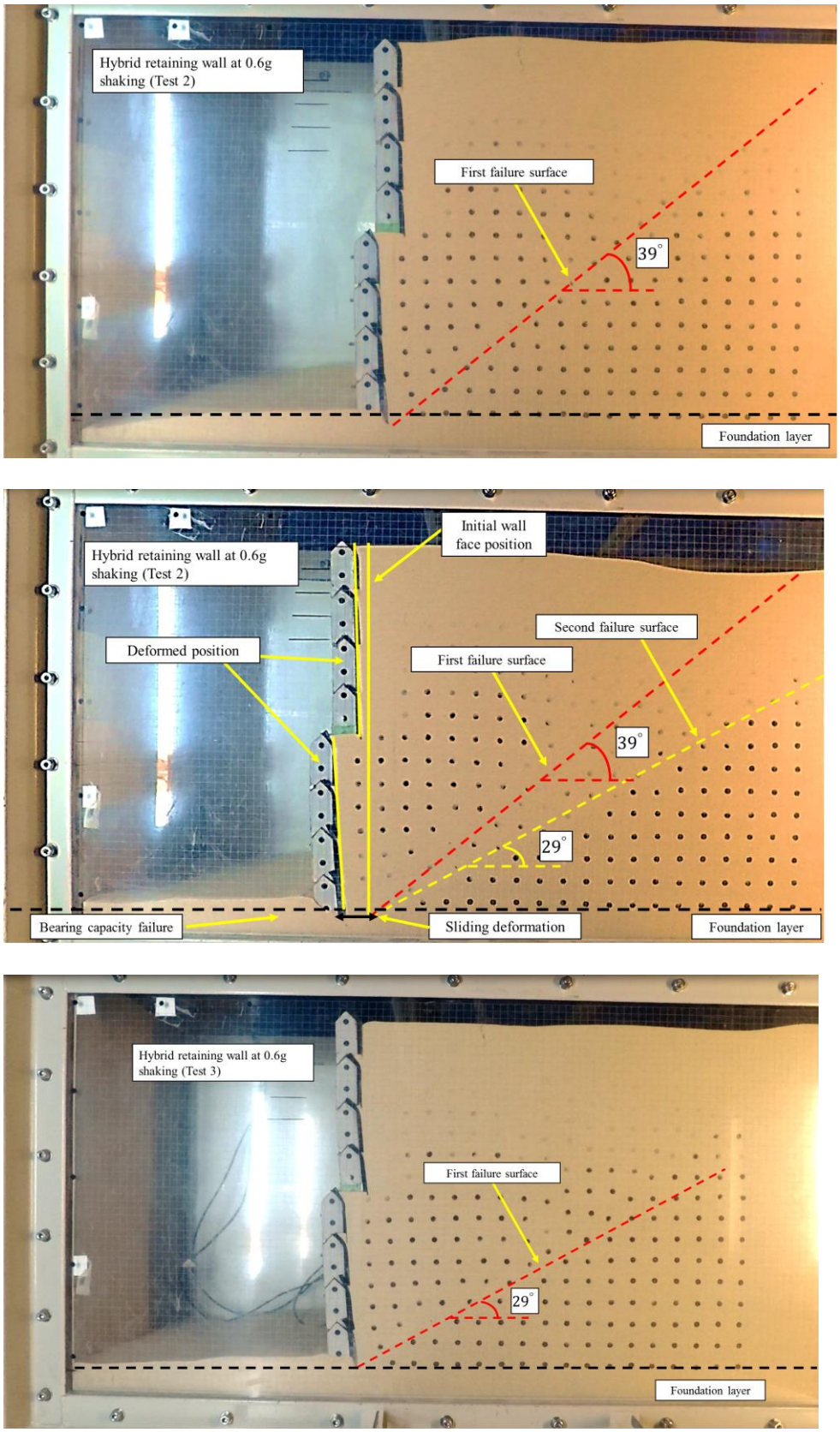

Figure 7(c) Failure process during seismic shaking in Test 2

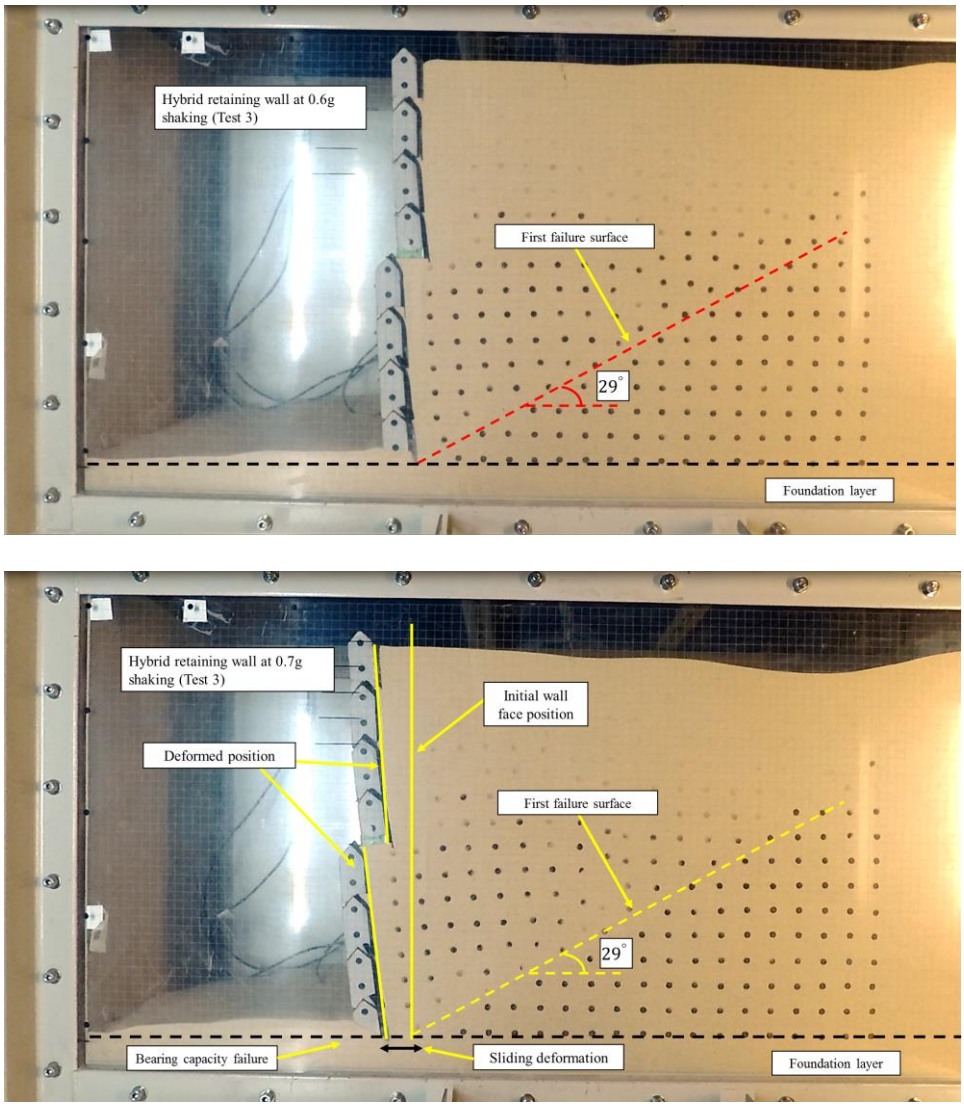

Figure 7(c) Failure process during seismic shaking in Test 3

Facing lateral deformations

Figure 8(a) shows the relationship between the base input acceleration and wall top displacement. It can be observed that the top displacement increased steadily until some critical acceleration. This critical acceleration was depended on the reinforcement arrangement. In Test 1 the critical acceleration was observed during the peak ground acceleration of 0.4g, while in Test 2 and Test 3 was the same at 0.6g. This behaviour suggests that by increasing the reinforcement length, the model walls can sustain extended ground motion amplitudes of about 0.2g increments. The critical acceleration

and development of the active wedge of failure were observed when the top reached 5% of the total hybrid wall height, which agrees with the observation by Yazdandoust (2019). The amount of top displacement between the soil nailed and the MSE wall was almost the same.

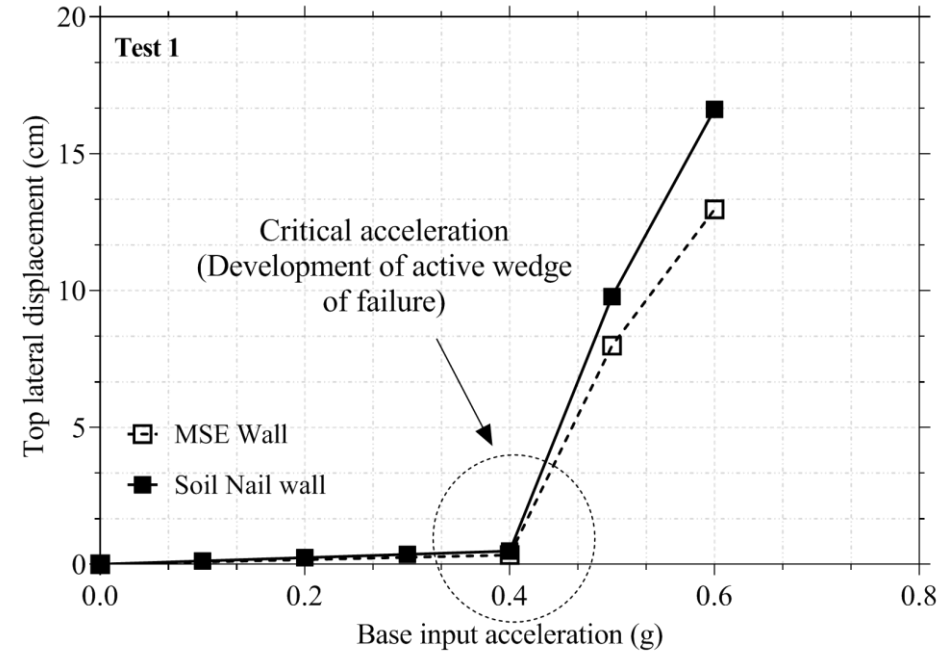

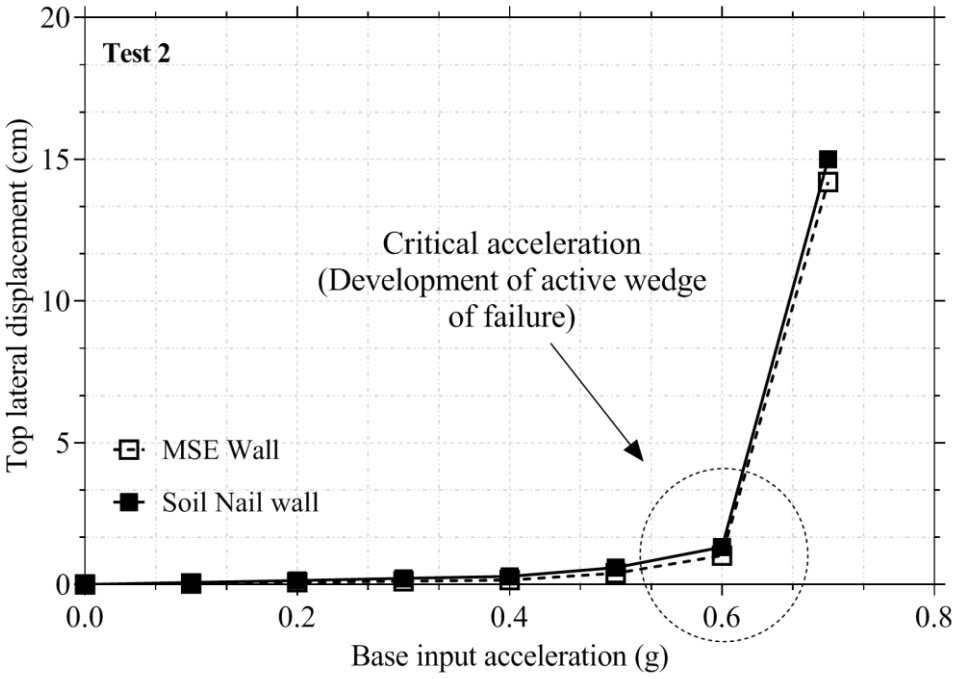

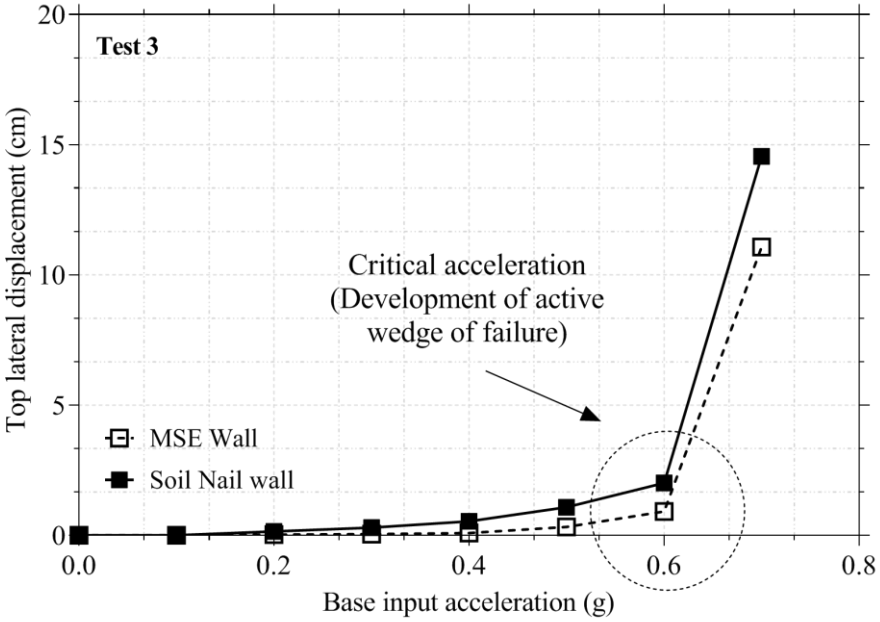

Figure 8(a) Facing top lateral displacement with base shaking

Figure 8(b) shows the relationship between the facing elevation with base input acceleration. Facing lateral deformation increased linearly from the heel of the soil nail wall towards the top of the MSE wall in Test 1. The deformation modes consisted of overturning and sliding, the later was predominant, and therefore the backfill soil underwent shear deformation; this type of deformation is observed in all tests. Test 2 and Test 3, the facing lateral deformation was slightly different; the amount of sliding and overturning was similar, about 0.5 cm and 2 cm, respectively. The soil nail face deformed linearly from the heel towards the top; however, the MSE wall showed bulging deformation with a convex shape geometry. This behaviour is attributed to the rigidity of the soil nail block due to the extended nail lengths since the soil nail block act as a foundation base; consequently, the walls vibrate at a different phase. Another reason could be attributed to the low confining pressure at the top of the wall. The amount of facing lateral deformation was significantly reduced in Test 2 and Test 3 as

compared to Test 1 from 8 cm to 0.5 cm during 0.6g shaking amplitude, which is attributed to the increase in nail length. To conclude, for economic design, increasing the nail and reducing the geogrid length, satisfactory seismic stability can be achieved.

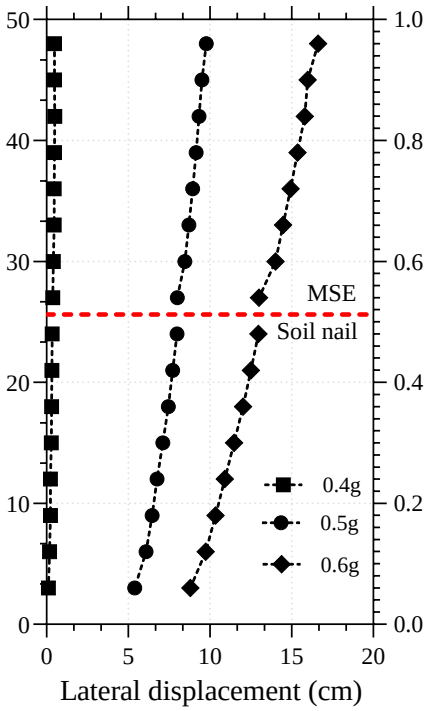

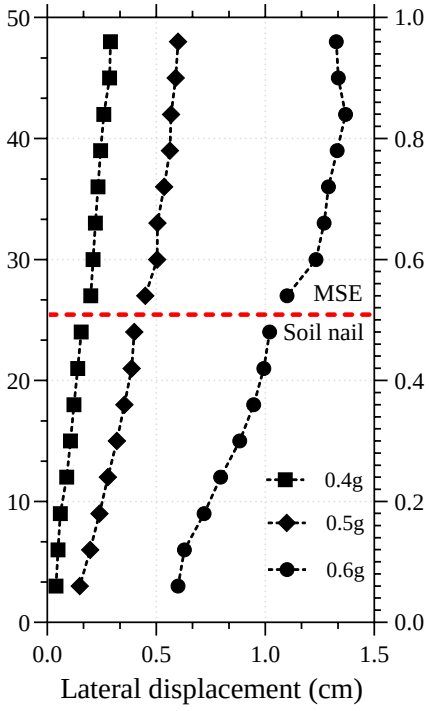

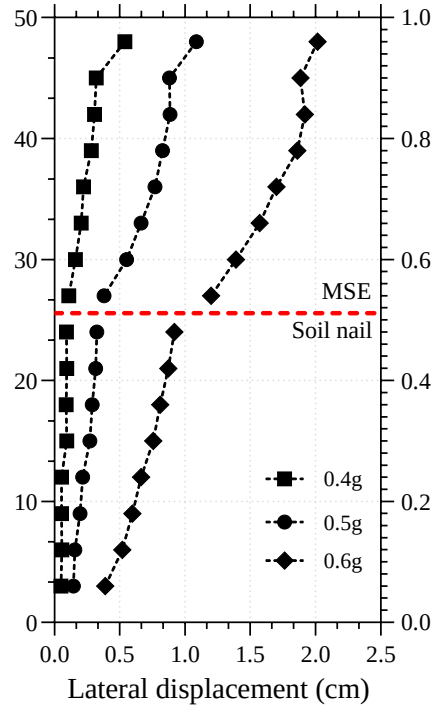

Figure 8(b) Facing lateral deformation with facing elevation and base shaking

Deformations of the sand

Figure 9(a)-(c) shows the total sand deformation calculated from the vertical and horizontal displacements of the targets in the soil nail block with an increase in base acceleration between 0.4g to 0.5g in Test 1 and 0.6g to 0.7g in Test 2 and Test 3. In general, deformation in the active zone behind the wall is confined in a triangular area bounded by a failure line at 34 degrees to the horizontal for Test 1 and 29 degrees for Test 2 and Test 3. The failure line delineates a "dead zone" and an active zone where the soil mass slides along the inclined failure surface to the back of the retaining wall corresponding to the active wedge of failure. The size and the amount of sand deformation increased with an increase of base shaking and downward thrust exerted by the MSE soil block, but the failure line does not alter during seismic shaking. It was observed that only a slight sand deformation at very low seismic shaking was necessary to create the active wedge of failure in the backfill soil. The amount of facing lateral deformation and soil deformation inside the active zone by the time of formation of the active zone was less than 0.3 cm, which is not large enough to fully mobilize the shear strength of the soil. The amount of soil deformation along a horizontal plane is linearly reduced with distance from the wall face towards the retaining zone and vertically from the top of the wall.

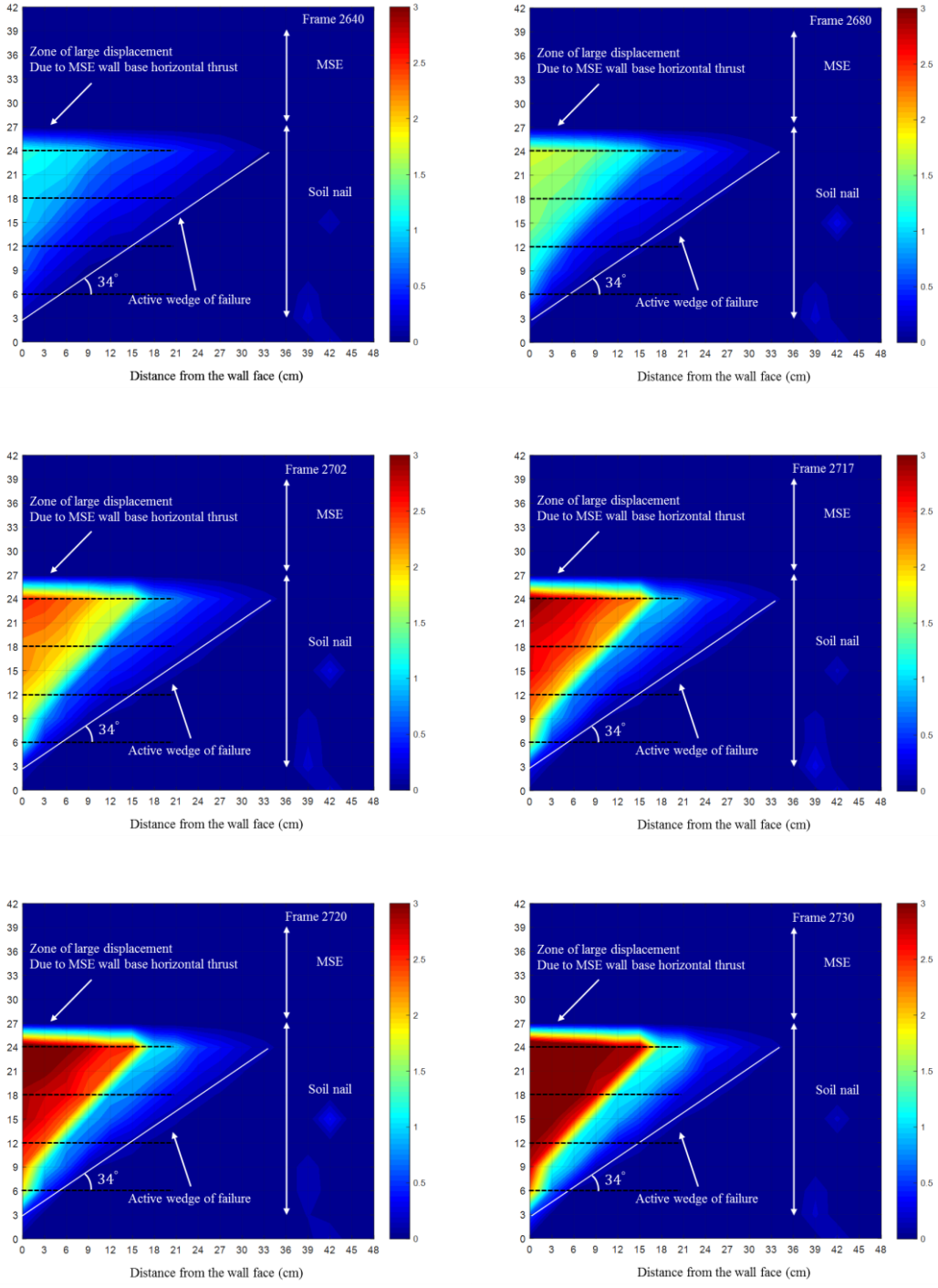

Figure 9(a) Sand deformation in Test 1

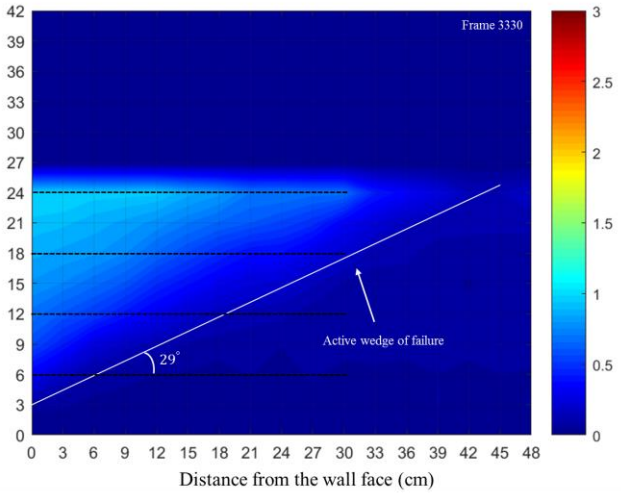

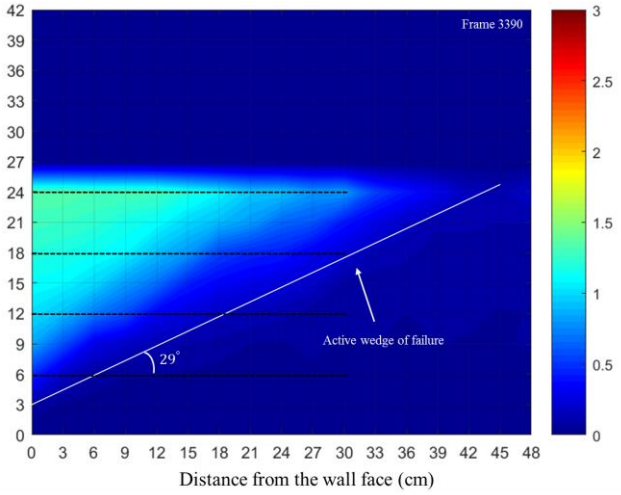

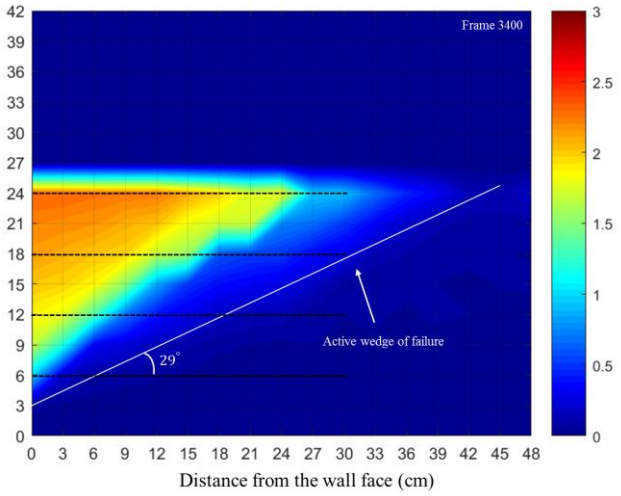

Figure 9(b) Sand deformation in Test 2

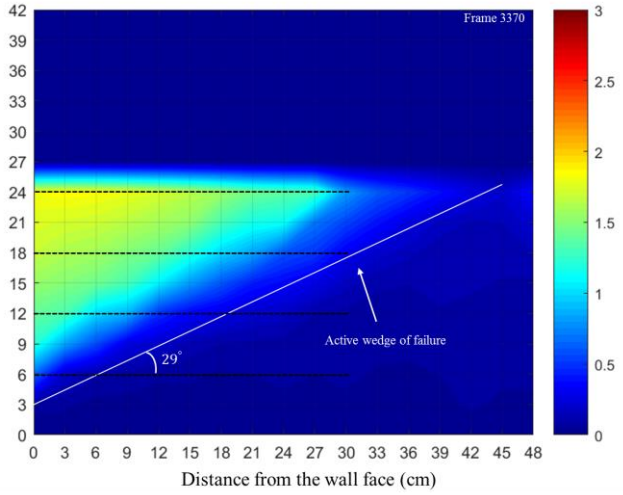

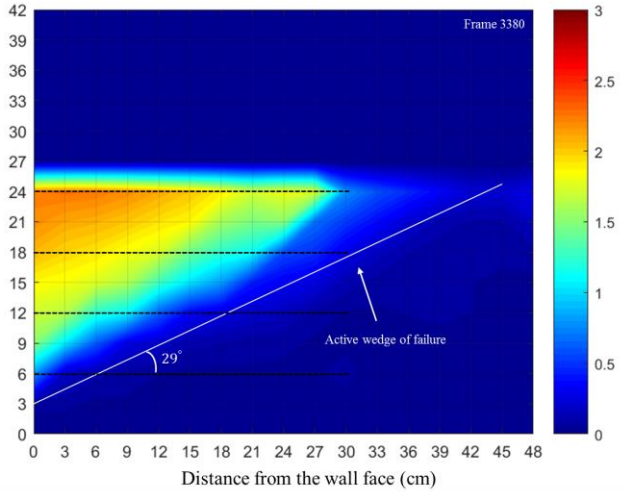

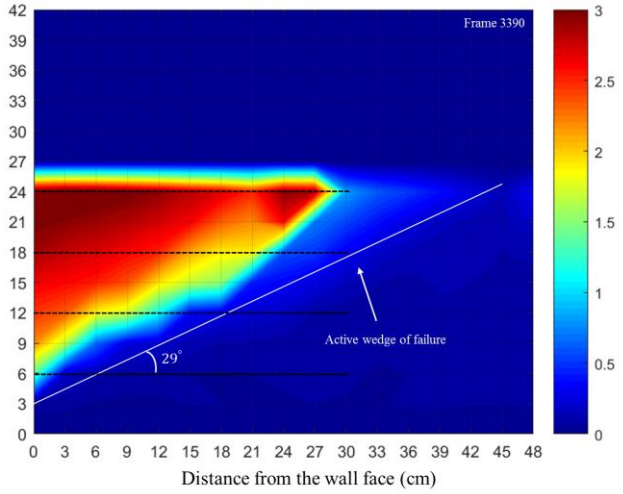

Figure 9(c) Sand deformation in Test 3

After some wall rotation to the outward direction, multiple rupture surfaces formed in the active zone near the wall top as a result of high stresses imposed by the seismic inertia forces and base thrust of the MSE soil block as shown in Figure 9(d) and therefore, stresses should reach their peak rapidly in these locations, similar behaviour is reported by Bransby and Milligan (1975) on cantilever sheet pile walls. The inclination of the multiple rupture surfaces is linear as assumed in coulomb theory and seems constants from the backfill surface towards the wall toe and different from the active wedge of failure. The rupture surfaces progressed downwards and horizontally from the top of the wall merging into a single one as the wall rotates, as can be seen during frame 2730. It can be concluded that soil wedge changes due to the seismic inertial force and downward pressure exerted by the MSE soil block; the latter tend to act as a surcharge with different magnitudes as the wall rotates during seismic shaking, which then alters the weight of soil and density as observed by Berg (1991) which attributed this behaviour to sand porosity (degree of compaction), they also reported that size of the active failure zone increased with the surcharge load. Furthermore, in geosynthetics reinforced soil walls in tiered arrangement reported by Liu et al. (2014) large reinforcement load in the interface between the two-tier wall was observed, and it was attributed to a down-drag force on the facing imposed by the seismic compression of the backfill soil. Moreover, according to Khosravi et al. (2016) by increasing the magnitude of the surcharge, an increment in the vertical and horizontal earth pressure in the upper zone of the wall can be expected. Our observation suggests that the earth pressure distribution behind the hybrid retaining wall would be quite different from a typical single tier retaining wall. For instance, in simple retaining walls, the coulomb earth pressure theory assumes that the wall yields and the whole backfill soil reached a plastic state and fails as a rigid body. However, this behaviour does not reflect the hybrid wall

since the upper-tier outward movement is restrained by the lower-tier wall top, and only the lower can deform. However, the MSE wall induces additional rotation on the soil nail wall by sliding of the wall toe, and therefore a different seismic earth pressures distribution on the hybrid wall compared to a traditional retaining wall should be expected. This seismic earth pressure should be correctly quantified and incorporated in seismic lateral earth pressure when designing a hybrid retaining wall as it leads to destabilization of the hybrid system as also recommended by Liu et al. (2014).

Shear strains distribution

Figure 10 shows the distribution of maximum shear strain in the soil nail backfill soil for Test 1, between peak ground acceleration of 0.4g and 0.5g. Due to small amount of facing and backfill deformation in Test 2 and Test 3 it is not presented. The shear strains were calculated from the horizontal and vertical targets installed in the backfill. Generally, it possible to observe that the shear strain magnitude increased with base acceleration or shaking time. When the ground motion reached, a peak of 4 m/s2 definitive failure surface was observed corresponding to the onset of the active wedge of failure, as can be observed in frame 2370 and 2400. At this stage, the maximum shear strain level was in the order of 5%, which coincides with the observation of the plane strain compression test corresponding to the peak strength of the backfill soil. This threshold value to the failure strain levels at peak stress state was also reported by Nakajima et al. (2009).

It is evident from the distribution of shear strains that the definitive failure surface is linear, extending from the heel of the soil nail wall crossing the nail elements towards the top as observed from the images recorded by the camera. The definitive failure surface angle was about 34 degrees which coincide with the observation of the sand

deformation in Figure 9, therefore, it can be concluded that the definitive failure surface is formed at a very low seismic shaking or very small amount of soil displacement. The definite failure surface angle remained constant throughout all seismic shaking stages while softening location is being slowly formed within the active wedge at slightly higher shear strain values as the hybrid wall continued to experience sliding and shear deformation of the subsoil. It should be noted that the definitive failure surface is observed before the ultimate failure of the hybrid wall and, therefore, can be considered the pre-failure stage when the wall achieved instability in the critical state and consequently, this failure surface will control the sand deformation as show in Figure 9 as well as the mobilization of seismic lateral earth pressure during different shaking steps. In addition, the definite failure surface at the critical state is consistent with Been et al. (1991). However, the failure surface angle is dependent on the reinforcement length, as shown in Figure 7. The amount of soil compaction might be different in longer nails, so the soil densification and void ratio might be different. Consequently, the critical failure surface angle might be much lower than 34 degrees as reported by Been et al. (1991). Similarly, Watanabe et al. (2011) reported that the failure surface angle is determined in the critical state. It should be noted that in their case, the retaining wall backfill is not reinforced. Furthermore, they reported that the seismic active earth pressure has an upper limit which is determined by the force equilibrium of the soil wedge in a critical state when the retaining wall lost its stability.

After a slight increase in base acceleration or shaking time, the facing wall continued to rotate, slide together with shear deformation of the subsoil, then strain-softening was observed within the active wedge of failure, which started from the heel of the soil nail wall as well as close to the soil-wall interface and progressed upwards to the backfill

surface as can be seen during frame 2650. Differently from the definite failure surface, the zone of intense strain softening was not stationary but moved away towards the retained zone intersecting the active wedge of failure. Bolton and Steedman (1985) reported that the shear resistance angle mobilized along the failure plane dropped from 55 degrees to 33 degrees. They also reported that the base thrust is transmitted through the softening locations and the plane of sliding is determined to contribute to the greatest degree of strain localization. Besides, by observing the Figures 9 it is thought that after the creation of the active wedge of failure, the Toyoura sand was in a "loose state" and as the extreme shaking continues, as well the downward thrust exerted by the MSE wall soil, the backfill continues to experience dynamic densification and, consequently the sand progressively becomes denser which may be the reason for the rapid drop on the shear strength after reaches is peak strength. The failure surface of the zone of intense strain-softening did not cross the failure surface of the active wedge of failure, which can be considered as the limit by which the backfill soil is damaged. The strain levels within the zone of intense strain-softening remained constant about 10% once it was formed, in other words, at its residual strength. These large post-peak shear strain values allowed the soil void ratio to increase to its critical where the maximum possible dilation is achieved. The initially measured angle of the zone of intense strain-softening was about 71 degrees, measured in frame 2650, which is approximate to "45 degrees + (Φpeak)/2 = 70.5 degree". It should be noted that shear strains in other parts of the backfill was still at around 5%, corresponding to the mobilized friction angle at the peak, and as the shear resistance along the failure surface is reduced, the backfill soil becomes more damaged, this failure surface then drops to about 34 degrees as shown in frame 2730 and consequently the seismic earth pressure should increase as described in the modified Monono-Okabe theory proposed by Koseki et al. (1998b). In addition, the

zone of intense-strain softening did not cross the initially developed active wedge of failure and therefore, it can be concluded that there is a limit by which the backfill becomes damaged and finally, the failure surface in the critical state will be the responsible for the mobilization of seismic earth pressures at very high earthquake-induced deformations. Moreover, this limit may depend on the reinforcement characteristics such as nail length as can be observed in Figure 7.

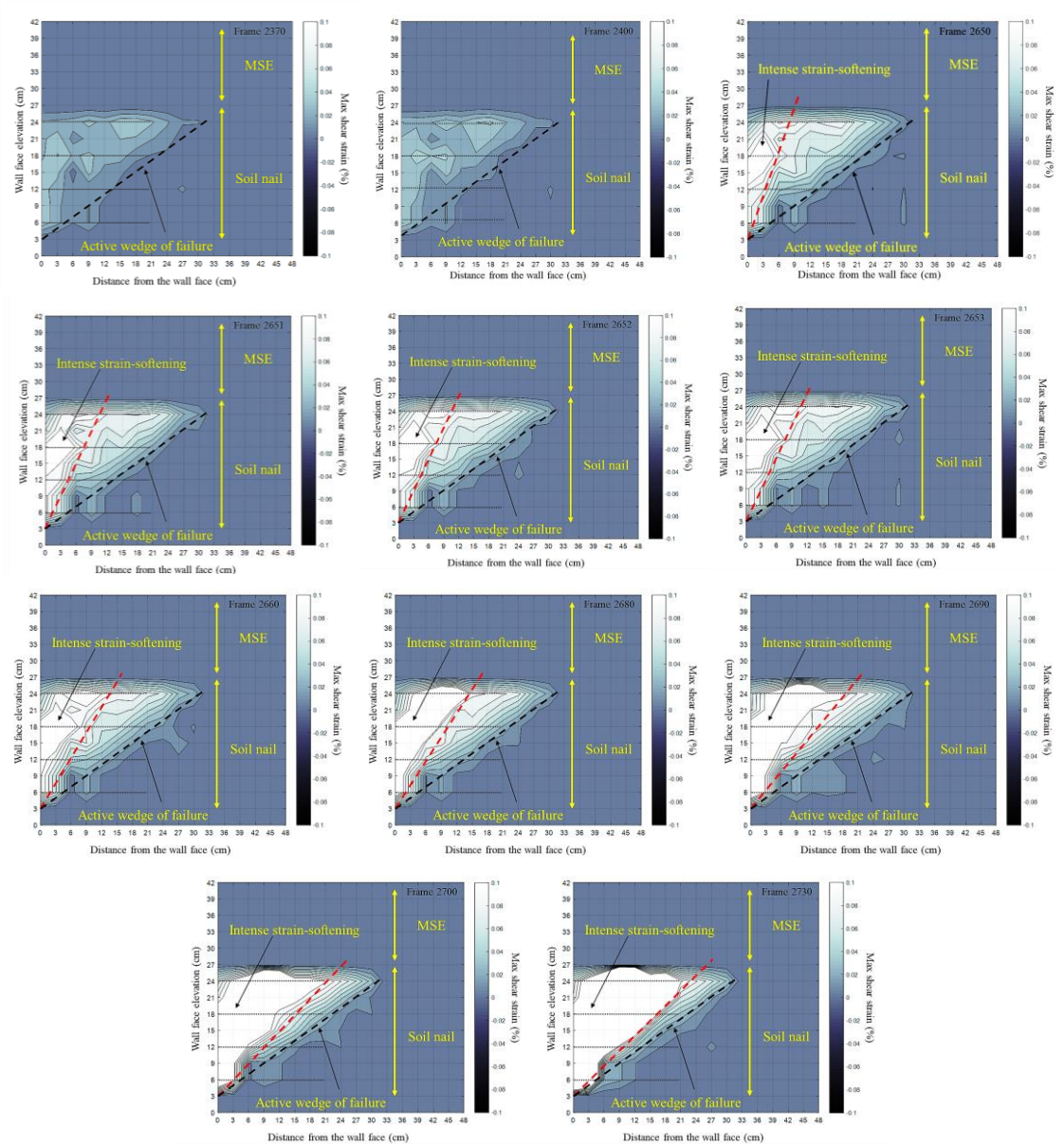

Figure.10 Maximum shear strains (Test 1) in the soil nail block.

Conclusion

In recent years, hybrid retaining wall using geosynthetics and soil nails have been proposed as alternative solution for conventional single tier, multi-tier geosynthetics reinforced soil walls and shored walls in order to further minimize the construction cost. This paper present results from 1g shaking table test to investigate the earthquake-induced deformation and strain softening behind hybrid retaining walls with particular focus to the soil nailed wall. The following is the summary of the experimental findings: The failure mechanism observed in the present test agrees with the Modified Monono-Okabe Theory proposed by Koseki et al. (1998); After the initial active wedge was developed, intense-strain softening was observed within the active wedge. The amount of damaged backfill soil increased towards the failure surface in the critical state, as the wall continued to rotate to the outward direction. In addition, there is a limit by which the backfill soil becomes damaged in the critical state. The failure mechanism of the hybrid retaining walls consisted of a planar failure surface extending the wall toe of the soil nail crossing the nail elements towards the backfill surface passing behind the MSE reinforcement layers, a combination of internal and external stability, respectively. For economic design of hybrid reinforced retaining walls, increasing the nail length beyond the recommended values by the current design codes while reducing the geosynthetics reinforcement length can be an effective approach while maintain satisfactory seismic performance.

Table 1. Scaling factors

Characteristic	Scaling factor (prototype/model)
Length	λ
Density	λ
Strain	$\lambda^{0.5}$
Time	$\lambda^{0.75}$
Stress	λ
Displacement	$\lambda^{1.5}$
Acceleration	1

Table 2. Test program

Test name	Nail length (mm)	Number of nails pe lift	Nail horizontal spacing (mm)	Geogrid length (mm)	Vertical spacing (mm)
Test 1	200	4	50	200	60
Test 2	300	2	130	300	
Test 3	300	2		200	

References

Alhabshi, A., 2006. Finite element Based Design Procedures for MSE/Soil Nail Hybrid Retaining Wall System. Doctoral thesis, Texas Tech Univerisity. http://hdl.handle.net/2346/14852

Anastasopoulos , I., Georgarakos, T., Georgiannou, V. & Kourkoulis, D., 2010. Seismic performance of bar-mat reinforced-soil retaining wall: Shaking table testing versus numerical analysis with modified kinematic hardening constitutive model. Soil Dynamics and Earthquake Engineering, pp. 1089-1105. https://doi.org/10.1016/j.soildyn.2010.04.020

Been, K., Jefferies, M. G. & Hachey, J., 1991. The critical state of sands. Geotechnique, 41(3), pp. 365-381. https://doi.org/10.1680/geot.1991.41.3.365

Berg, V. D., 1991. Effects of surface loading behind earth retaining walls. Deform Soils Displac Strct, pp. 767-771.

Bhattachrjee, A. & Amin, M. U., 2019. Behaviour of Two-Tiered Geosynthetic-Reinforced Soil Walls. INAE Letters, pp. 91-100. https://doi.org/10.1007/s41403-019-00069-7

Bolton, M. & Steedman, R., 1985. Modelling the seismic resistance of retaining structures. San Francisco , s.n., pp. 1845-1848.

Bransby, P. L. & Milligan, G. W. E., 1975. Soil deformation near cantilever sheet pile walls. Geotechnique, Volume 2, pp. 175-195. https://doi.org/10.1680/geot.1975.25.2.175

El-Emam, M. M. & Bathurst, R. J., 2007. Influence of reinforcement parameters on the seismic response of reduced-scale reinforced soil retaining walls. Geotextiles and Geomembranes , 25(1), pp. 33-48. https://doi.org/10.1016/j.geotexmem.2006.09.001

Gassler, G., 1988. Soil-nailing - theoretical basis and practical design.. Fukuoka, Kyushu, Japan, Proceedings of the International Geotechnical Symposium on Theory and Practice of Earth Reinforcement.

Hong, Y.-S., Chen, R.-H., Wu, C.-S. & Chen, J.-R., 2005. Shaking table test and stability analysis of steep nailed slopes. Canadian Geotechnical Journal. https://doi.org/10.1139/t05-055

Iai, S., 1989. Similitude for shaking table tests on soil-structure-fluid model in 1g gravitational field. Soils and Foundations, 29(1), pp. 105-118. https://doi.org/10.3208/sandf1972.29.105

Khosravi, M. H., Pipatpongsa, T. & Takemura, J., 2016. Theoretical analysis of earth pressure against rigid retaining walls under translation mode. Soils and Foundations, pp. 664-675. https://doi.org/10.1016/j.sandf.2016.07.007

Koseki, J. et al., 1998a. Shaking and Tilt Table Test of Geosynthetics-Reinforced Soil and Convetional-Type Retaining Walls. Geosynthetics International, pp. 73-96. https://doi.org/10.1680/gein.5.0115

Koseki, J. et al., 1998b. A modified procedure to evaluate active earth pressure at high seismic laods. Soils and Foudnations, pp. 209-216. https://doi.org/10.3208/sandf.38.Special_209

Kuwano, J., Miyata, Y. & Koseki, J., 2014. Performance of reinforced soil walls during the 2011 Tohoku earthquake. Geosynthetics International, pp. 389-402. https://doi.org/10.1680/gein.14.00008

Lee, Y. -B., Ko, H. -Y. & McCartney, J., 2010. Deformation response of shored MSE walls under surcharge loading in the centrifuge. Geosynthetics International, pp. 389-402. https://doi.org/10.1680/gein.2010.17.6.389

Ling, H. I., Mohri, Y. & Burke, C., 2005. Large-scale shaking table test on modular block reinforced soil retaining walls. Journal of geotechnical and geoenviromental engineering. https://doi.org/10.1061/(ASCE)1090-0241(2005)131:4(465)

Liu, H., Yang, G. & Ling, H. I., 2014. Seismic response of multi-tiered reinforced soil retaining walls. Soil Dynamics and Earthquake Engineering, pp. 1-12. https://doi.org/10.1016/j.soildyn.2014.01.012

Lomardi, D., Bhattacharya, S., Scarpa, F. & Bianchi, M., 2015. Dynamic response of geotechnical rigid model container with absorving boundaries. Soil dynamics and Earthquake Engineering, pp. 46-56. https://doi.org/10.1016/j.soildyn.2014.09.008

Luo, A. Q., Tan, A. S. & Yong, Y. K., 2000. Pullout resistance mechanism of a soil nail reinforcement in dilative soils. Soils and Foundations, pp. 47-56. https://doi.org/10.3208/sandf.40.47

Matsuo, O., Yokoyama, K. & Saito, Y., 1998. Shaking table tests and analysis of geosynthetic-reinforced soil retaining walls. Geosynthetics International , pp. 97-126. https://doi.org/10.1680/gein.5.0116

Mohamed, S. B., Yang, K.-H. & Hung, W.-Y., 2014. Finite element analysis of two-tier geosynthetic-reinforced soil walls: Comparison involving centrifuge test and limit equilibrium results. Computers and Geotechnics, pp. 67-84. https://doi.org/10.1016/j.compgeo.2014.04.010

Moradi, M., Babaki, A. P. & Sabermahani, M., 2020. Effect of Nail Arrangement on the Behaviour of Convex Corner Soil-Nailed Walls. Journal of Geotechnical and Geoenviromental Engineering. https://doi.org/10.1061/(ASCE)GT.1943-5606.0002235

Morrison, K. F., Harrison, F. E., Collin, J. G. & Anderson, S. A., 2007. Full-scale Testing of a Shored Mechanically-Satbilized Earth (SMSE) Wall Employing Short Reinforcement, Geosynthetics in Reinforcement and Hydraulic Applications , ASCE. https://doi.org/10.1061/40909(228)6

Munaf, Y. (1988): Study on seismic performance of soil retaining walls by tilting and shaking table test, PhD Thesis, University of Tokyo.

Munoz, H. & Kiyota, T., 2020. Deformation and localisation behaviour of reinforced gravelly backfill using shaking table tests. Journal of Rock Mechanics and Geotechnical Engineering, pp. 102-111. https://doi.org/10.1016/j.jrmge.2019.06.008

Nakajima, S., Koseki, J., Watanabe , K. & Tateyama, M., 2009. A simplified procedure to evaluate earthquake-induced residual displacement of convetional type retaining walls. Soils and Foundations, pp. 287-303. https://doi.org/10.3208/sandf.49.287

Richardson, G. N., Feger, D., Fong, A. & Lee, K. L., 1977. Seismic testing of reinforced soil earth walls. Journal of Geotechnical Engineering, pp. 1-17. https://doi.org/10.1016/0148-9062(77)90166-8

Sabermahani, M., Ghalandarzadeh, A. & Fakher, A., 2009. Experimental study on seismic deformation modes of reinforced-soil walls. Geotextiles and Geomembranes, Volume 27, pp. 121-136. https://doi.org/10.1016/j.geotexmem.2008.09.009

Sharma, M., Samanta, M. & Punetha, P., 2019. Experimental Investigation and Modeling of Pullout Response of Soil Nails in Cohesionless Medium. International Journal of Geomechanics. https://doi.org/10.1061/(ASCE)GM.1943-5622.0001372

Tufenkjian, M. R. & Vucetic, M., 2000. Dynamic Failure Mechanism of Soil-Nailed Excavation Models in Centrifuge. Journal of Geotechnical and Geoenvironmental Engineering. https://doi.org/10.1061/(ASCE)1090-0241(2000)126:3(227)

Turner, J. P. & Jensen, W., 2005. Landslide stabilization using soil nail and mechanical stabilized earth walls: Case study. Journal of geotechnical and geoenviromental engineering. https://doi.org/10.1061/(ASCE)1090-0241(2005)131:2(141)

Vucetic, M. et al., 1989. Analysis of soil-nailed excavations stability during the 1989 Prieta earthquake. Earth structures and Engineering characterization of ground motion.

Watanabe, K. J. & Tateyama, M., 2011. Seismic earth pressure exerted on retaining walls under a large seismic loading. Soils and Foundations , pp. 379-394. https://doi.org/10.3208/sandf.51.379

Watanabe, K., Koseki, J. & Tateyama, M., 2005. Application of high speed digital CCD cameras to observe static and dynamic deformation characteristics of sand. Geotechnical Testing Journal , pp. 432-435. https://doi.org/10.1520/GTJ12646

Watanbe, K. et al., 2003. Behaviour of Several Types of Model retaining Walls Subjected to Irregular Excitation. Soils and Foundations. https://doi.org/10.3208/sandf.43.5_13

Wei, Y., 2013. Development of Equivalent Surcharge Loads for the Design of Soil Nailed Segment of MSE/Soil Nail Hybrid Retaining Walls Based on Results from Full-

Scale Wall Instrumentation and Finite Element Analysis. Doctoral thesis. Texas Tech Univerisity. http://hdl.handle.net/2346/50627

Wu, J. T. H. & Payeur, J.-B., 2015. Connection stability analysis of segmental geosynthetic reinforced soil (GRS) walls. Transportation Infrastructure Geotechnology. https://doi.org/10.1007/s40515-014-0013-4

Xiao, C., Han, J. & Zhang, Z., 2016. Experimental study on performance of geosynthetic-reinforced soil model walls on rigid foundations subjected to static footing loading. Geotextiles and Geomembranes. https://doi.org/10.1016/j.geotexmem.2015.06.001

Yazdandoust, M., 2018. Seismic performance of soil-nailed walls using 1g shaking table test. Canadian Geotechnical Journal, pp. 1-18. https://doi.org/10.1139/cgj-2016-0358

Yazdandoust, M., 2019. Shaking table modeling of MSE/soil nail hybrid retaining walls. Soils and Foundation, pp. 241-252. https://doi.org/10.1016/j.sandf.2018.05.013

Yoo, C., Jang, Y. & Park, I., 2011. Internal stability of geosynthetic-reinforced soil walls in tiered configuration. Geosynthetics International, 18(2), pp. 74-83. https://doi.org/10.1680/gein.2011.18.2.74

Chapter 3: Capturing compaction zones behind a two tier reinforced soil wall during seismic shaking

Author 1
Albano Ajuda, PhD Candidate
Department of Civil and Environmental Engineering, Saitama, Japan

Author 2
Jiro Kuwano, Professor
Department of Civil and Environmental Engineering, Saitama, Japan

Abstract

This work presents a series of shaking table test on seismic deformation behaviour of model two-tier reinforced soil wall with focus on the deformation of the lower tier. During the experimental program, facing displacement and deformation of the sand was monitored using digital image analysis technique. The failure mechanism of the model walls consisted in a two-part failure wedge, extending from the toe of the lower tier towards the backfill surface passing behind reinforcement layers of the upper tier towards the backfill surface. The maximum horizontal displacements of reinforced soil wall decrease with increase in offset length of tiered wall. By observing the sand deformation, two deformation zones—shear deformation zone near the facing of the lower tier and compaction zone below the upper tier soil block, the compaction zone of lower tier decreased with increase in offset length. It was found that by increasing the offset distance of the upper tier lesser amount of lateral deformation in both tiers. Increasing the reinforcement while maintaining the same offset distance also reduce the amount of lateral displacement. A critical offset distance is defined as a distance by which the upper and lower tier does not rotates to the outward direction as a rigid body.

Introduction

Geosynthetics reinforced soil walls (GRSW) using single tier are well documented construction technique. Many of the past earthquake events demonstrated a very high seismic stability, for example during the Great Tohoku Earthquake about 90% of the constructed GRSW showed no damage, although a massive tsunami accompanied the earthquake. Seismic performance of single tier GRSW have been conducted using different research methodologies. Numerical methods (Hatami & Bathrust 2006, Damians, et al. 2015, Huang, et al. 2009, Hatami & Bathrust 2005, Guler et al. 2007, Lee et al. 2010, Bathurst & Hatami 1998). Shaking table test (Koseki et al., 1998, Matsuo et al. 1998, Watanabe et al. 2003, Ling et al. 2005, Krishna & Latha, 2007, Sabermahani et al. 2009, Guler & Enunlu 2009, Guler & Selek 2014, Panah et al. 2015, Yazdandoust 2017, Xu et al. 2020, Xu et al. 2020, Munoz & Kiyota 2020). Tatsuoka et al. (1998) concluded that the two-part wedge geometry is a valid failure geometry for geosynthetic-reinforced soil walls with a full height rigid facing and short reinforcement lengths based on shaking table tests. The pattern and location of the failure shape is controlled by reinforcement length. Tatsuoka et al. (1998) proposed a modified two-part wedge method. They concluded that the size of failure wedge from the modified two-part wedge method was typically smaller than what would be predicted from conventional two-part wedge analysis and more realistic according to experimental observations. Latha and Santhanakumar (2015) found that reinforcement has a greater influence in controlling lateral displacements in modular-block reinforced soil walls as compared to walls with full-height facing panels. Latha and Krishna (2008) found that backfill compaction had an insignificant influence on the wall seismic response at smaller base excitations.

Evidence of reinforced soil wall satisfactory seismic performance can be found in the literature. Collin (1992) reported that in the Loma Prieta earthquake with a peak horizontal ground acceleration (PGA) equal to 0.41 g, two reinforced soil retaining walls which were designed for PGA = 0.2 g did not showed any damage. Even some walls which had not been designed for any level of seismic load were found to perform well in an earthquake with PGA = 0.32 g. Tatsuoka et al. (1998) reported that a reinforced soil retaining at Tanata in Japan, which was designed for PGA = 0.2 g showed essentially no damage when subjected to the 1995 Kobe earthquake (PGA = 0.83 g).

Multi-tier reinforced soil walls can be used for aesthetics, construction cost reduction and improved stability as shown in Figure 1. Investigation on deformation behaviour of multi-tier GRS wall are reported using several methodologies and under different loading condition, the most common research is under static loading, Yoo et al. (2011) reported that the reinforcement length of the lower tier has a greater effect on the overall wall stability than the upper tier reinforcement length. In addition, they reported planar failure surfaces in both tiers. Bhattacharjee and Amin (2019) investigate the effect of offset distance in tiered walls, they reported that the maximum lateral stress on wall facing decreases with increase in tier offset. They observed variations in soil strain, two distinct deformation zones are identified in tiered walls, shear deformation zone near the facing at the bottom of the wall and compaction zone below the upper tier wall. Numerical, Liu et al. (2014) reported that multi-tiered configuration reduced the residual lateral facing displacement and the average reinforcement load using segmental reinforced soil walls, they also found that multi-tiered configuration with adequate tier-

offset could significantly reduce the residual lateral facing displacement and the average reinforcement load.

Seismic response of multi-tier geosynthetics reinforced soil wall are still very limited. Safaee et al. (2020) conducted a series of shaking table test and they found that multi-tiered wall models exhibited much smaller residual lateral displacements than single walls at the facings using wrap-around facing walls. Experimental investigation of detailed failure mechanism and sand deformation behind tiered walls is unknow. The present study investigates the seismic deformation behaviour of two-tier segmental reinforced soil wall with focus to the deformation of the lower tier. Parameters such as facing lateral deformation, failure mechanism, sand deformation are discussed.

Physical modelling

Shaking table facility

A computer-controlled shaking table is used to simulate the seismic loading. The shaking table is built with the following dimension: 1,300 mm (long) by 1,000 mm (wide) seated on a pair of low friction bearing rails constrained to the horizontal corresponding to a single degree of freedom.

Model container

The soil and wall are constructed inside a rigid container built with the following dimensions: 1,300 mm (long), 600 mm (wide), and 650 mm (high) as shown in Figure 3. On one side of the container was constructed using Plexiglas in order to visualize the deformation during shaking. The container was perfectly bolted to the shaking table to keep the plane strain condition. According to Lombardi et al. (2015), using absorbing

boundaries can minimize the generation of reflection of body waves. Therefore, at the far end boundary of the container, a 50 mm foam damper was installed. Lubricant was used at the side walls of the container to minimize friction between the soil and wall sides. However, Watanbe et al. (2003) conclude that sidewall friction of the soil container on the response acceleration and failure angle is negligible.

Similitude laws

In 1 g shaking table testing of model reinforced soil walls, scaling laws proposed by Iai (1989) have been widely used to convert the response predictions for prototype structures in the field (El-Emam and Bathurst, 2004; Hong et al., 2005; Bathurst et al., 2007; Latha and Santhanakumar, 2015). Taken in consideration a size of the shaking table a geometric factor of 15 was adopted in this study. Table 1 shows a summary of the similitude implemented in the current study. The reduced-scale modelling and the corresponding prototype are discussed individually for each two-tier reinforced soil wall component in the following sections.

Model soil

In this study, air drained Toyoura sand with 90% relative density was used for both foundation and backfill with the following properties: This density corresponds to a model ground of well-compacted sand to construct railways and road embankment Nakajima et al. (2010).

Model walls

According to Yazdandoust (2018), traditional soil nail and geosynthetics reinforced soil wall height ranges from 3.0 to 14.0 m with an average of 8.0 m. Different types of walls have been used in previous reduced-scale models. Richardson et al. (1977) conducted seismic testing using 280 mm wall height; (Watanbe et al. 2003 and Koseki et al. 1998) constructed reduced-scale models using 500 mm high walls. Therefore, considering the size of the shaking table and the container, the reduced-scale two-tier reinforced soil wall height was set to 500 mm, which corresponds to a 10 m wall high at the prototype scale. The segmental panels are not fixed to each other and can rotate freely. Therefore, local buckling or bulging deformation is expected, similar walls have been conducted by Izawa and Kuwano (2011).

Table 3 Test program

Test name	Reinforcement length (L1)	Reinforcement length (L2)	Offset distance (D)	Acceleration of catastrophic collapse
T101	200	200	50	0.6g
T102	200		100	0.7g
T103	200		200	0.8g
T104	300		100	0.8g
T105	300		200	0.7g

Model reinforcements

Geosynthetics can be scaled based on geometry, stiffness or strength. The tensile strength-strain behaviour and soil-reinforcement interaction are two key points to model

the reinforcement in reduced-scale tests Viswanadham and Mahajan (2007). In this study, the original geogrid had a tensile strength of 22 kN/m. However, in order to meet the similitude laws, the geogrid was modified by cutting the ribs as shown in Figure. Consequently, the tensile strength of the geogrid was reduced to about 5.5 kN/m which used as reinforcement material for the MSE wall. Therefore, taking the scale factor of 15, the tensile strength of the model reinforcement at the prototype scale correspond to 2,200 kN/m. A similar procedure is reported in Xiao et al. (2016). The length of the geogrids is set to 200 mm and 300 mm, corresponding to an L/H = 0.8 and 1.2, respectively, which is beyond the minimum recommended L/H = 0.7 by FHWA design guidelines. The geogrids were laid in the backfill soil at a vertical spacing of 60 mm, which corresponded to the prototype of 0.9 m. According to Wu and Payeur (2015), MSE walls have been constructed with vertical spacing between 0.3 and 1.0 m to save construction costs.

Input seismic motions

The predominant frequencies of earthquake records can typically vary within the range between 0.1 Hz and 10 Hz Varnier and Hatami (2011). Previous studies have demonstrated that an input harmonic wave is typically more aggressive than an actual ground motion record of the same amplitude and predominant frequency Bathurst and Hatami (1998). In the present research, all tested models were subjected to a sinusoidal wave with a predominant frequency of 5 Hz. Each shaking stage was increased about 0.1g increments, each step was held of 10 seconds. The waveform was applied until full collapse occurred or measurement was impossible.

Experimental seismic results

Seismic failure mechanism of single tier walls

In single tier reinforced soil wall, the major failure mode was overturning of the wall top to the outward direction together with mall amount of sliding component, it should be noted that bulging deformation was not observed in single tier walls. With continued shaking the wall face progressively rotates causing large backfill surface settlements. Failure shows the failure mechanism of a single tier wall during shaking. It can be observed that the failure (shear strains) started from the top of the backfill soil in the interface between the reinforced and unreinforced zone and propagated to the bottom most geogrid layer as the wall rotates. After a certain magnitude of acceleration was further attained inclined failure surface begin to appear from the backfill surface in the unreinforced zone towards the backfill of the reinforced zone intersecting the last geogrid layers. Finally, once the reinforced soil wall achieved instability, the failure surface penetrated the reinforced zone intersecting the toe of the wall panel at this stage the active wedges was fully formed and irreversible facing lateral deformation was observed. It can be observed that increasing the reinforcement length the failure surface formation process is the same. However, the failure surface angles become shallower in the case of longer reinforcement.

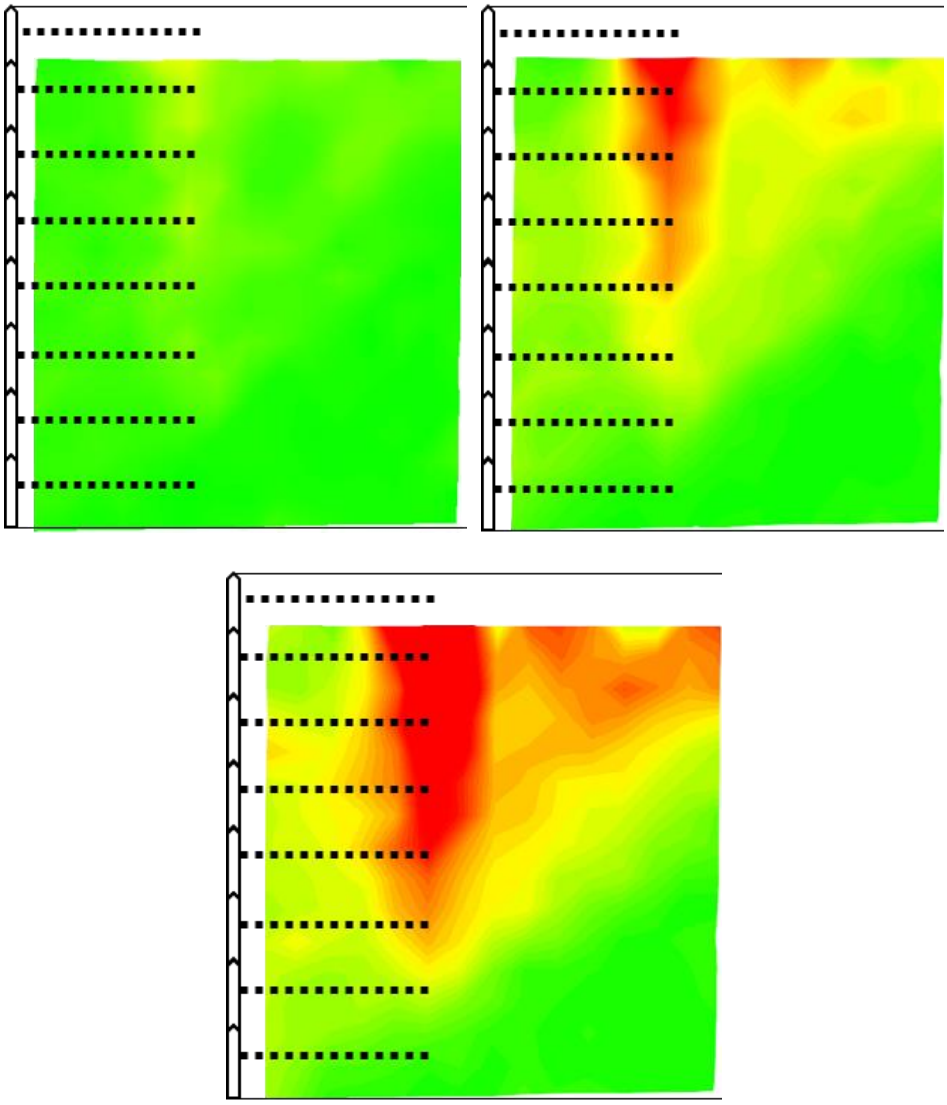

Figure 2 Shear strain distributin of single tier reinfirced soil wall

Seismic failure mechanism of two-tier walls

In conventional design approaches, the extent of failure surface in GRS walls is the determining factor in selecting an efficient length for reinforcement layers. In a safe design, the failure surface should pass through reinforcement layers indicating that the failure mechanism is governed by the reinforced soil region rather than the unimproved soil region. Three typical forms of deformation modes for single reinforced soil walls include bulging, overturning, and base sliding (Sabermahani et al., 2009). Figure shows

the failure mechanism of all tested model walls. In general, the failure mechanism observed in all tests was similar to a single tier reinforced soil wall with a two-wedge geometry. Differently, (Yoo et al. 2011 and Mohamed et al. 2014) reported planar failure surfaces under static loading. The failure surface appeared from the top of the backfill towards the bottom-most geogrid layer. As the seismic waves continued to be applied inclined failure surfaces appeared from the backfill surface in unreinforced zone towards the last geogrid layer and soon after the model walls reached failure stage, the inclined failure surface penetrated the reinforced zone intersecting the wall toe. It should be noted that no failure surface was observed in upper tier reinforced zone, a similar behaviour is reported by Safaee et al (2020). For instance, in Liu et al. (2014) the failure surface was observed in the upper tier.

In test 101, the failure mechanism was similar to wall constructed in a single tier reinforced soil wall. The reinforced zone of the lower and upper tier rotated together as a rigid block while the retained zone moved downwards to the back of the wall. By increasing the offset distance, only the lower tier behaves as a rigid block while the upper tier backfills experience smeared deformation as shown in Test 102 and 103. Figure shows the failure mechanism of Test 104, despite the offset distance, the reinforced zone in the lower and upper tier behaves as a rigid block like Test 101. This behaviour is attributed to the extended reinforcement length in the lower tier and due to the reinforcement length of the upper tier which coincides to the lower tier length, consequently the reinforced soil mass rotates as a unit. In test 105, no obvious failure surfaces can be observed, the lower tier wall was very rigid and only the upper tier collapsed while the lower tier was still intact. This is attributed to the combination of an increase in the reinforcement length and offset distance which means that the walls

behave independently. In test 101, the failure surface angles in both the reinforced and retained zone was about 45 degrees from the horizontal. In test 102, the failure surface angles were the same as test 101; however, the failure surface's length in the reinforced zone was slightly longer due to extended reinforcement length. In test 103, the failure surface angle followed test 102 despite the offset distance.

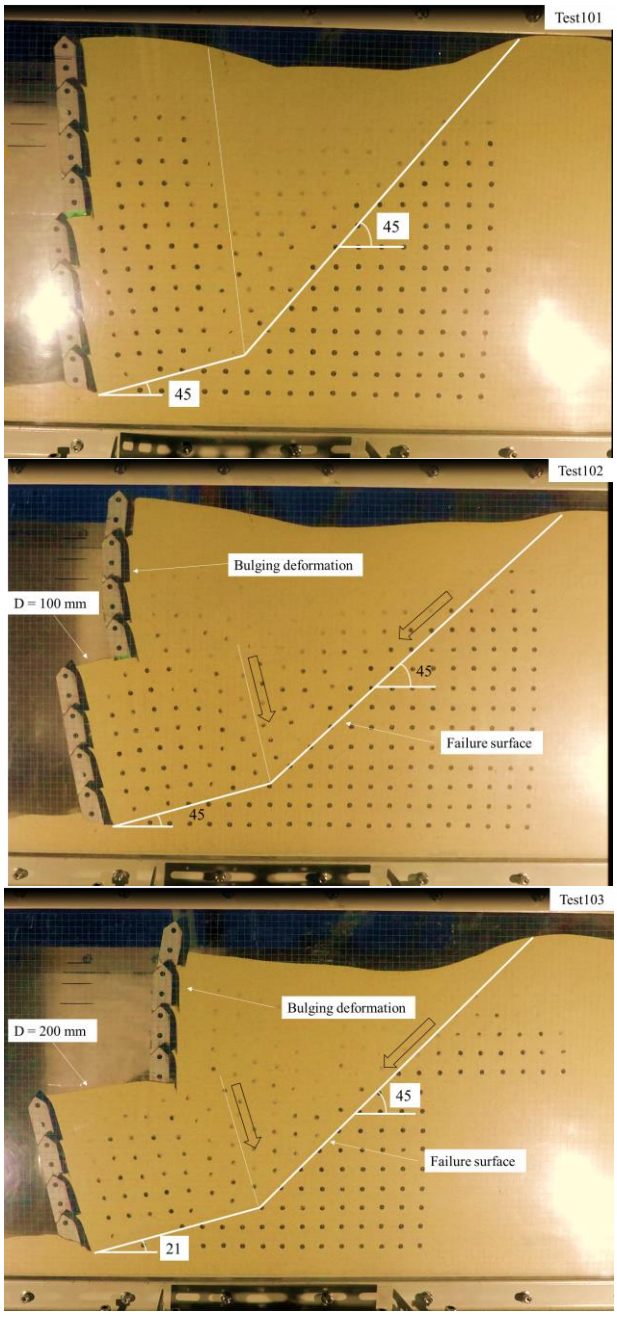

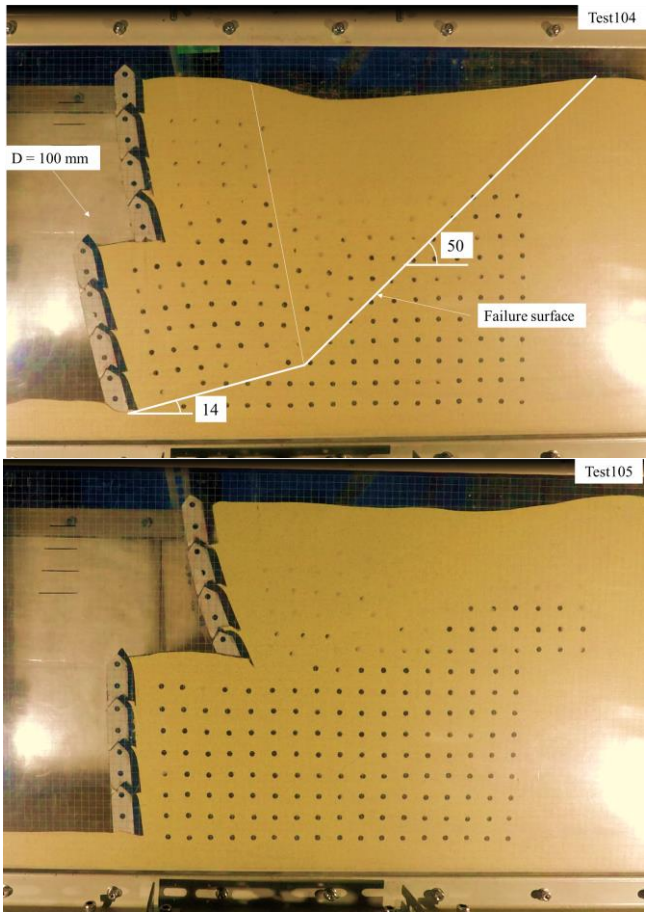

Figure 3 Failure process of a two-tier reinforced soil wall

Critical offset distance is been investigated using different methodologies, according to several experiments critical offset distance was found between 0.7 to 0.8 of the wall heights of the lower tier. In the present series of test, a critical offset distance was found about 0.8H, in addition the critical offset distance can be defined as the distance by which the lower and upper tier does not rotate as rigid block. Therefore for test 101 and 104, it is necessary to increase the reinforcement length of the lower or upper tier at least 1.5 times the reinforcement length of each tier or increase the offset distance, so the lower and upper tier can deform independently reducing the amount of seismic inertia forces on both tiers.

Figure 3 also shows the backfill settlement profiles for each model walls by the end of seismic shaking. The backfill settlements were very distinct for each wall depended of the reinforcement length and offset distance. In test 101, the backfill took a “U” shape geometry behind the reinforcement layers with a maximum by the end of the reinforcement layers, similar behaviour is observed in test 102 and test 104. However, in test 103 the backfill settled uniformly from the wall face towards the retaining zone with an inverted L shape deformation and the maximum settlement is observed in the retained zone attributed to the bulging deformation of the facing. While in test 105, the backfill settled uniformly thought the backfill length included in the reinforced zone, this behaviour can be attributed to the effect of offset distance and the wall height. In all tests it was observed bearing capacity failure on the lower tier; contrary, in the upper it was not observed, this is because the upper tier's wall toe is placed just on top of the reinforcement layers of the lower tier consequently preventing such failure. Differently, if the upper tier's offset distance goes beyond the reinforcement length of the lower tier, bearing capacity failure will be observed in both tiers.

Seismic facing displacement

Figure 4 shows the relationship between facing elevation and base shaking, for comparison purposes, only displacement at 0.5g and 0.6g are discussed here. In general, the deformation of the two-tier walls depended on the reinforcement length of the lower tier and the offset distance of the upper-tier wall. The deformation of the tested model consisted of sliding, overturning, and bulging deformation. In all cases, the lower tier facing lateral displacement increased linearly from the base towards the top with base shaking, and the differences were observed only in the upper tier wall.

The facing lateral deformation of Test 101 and Test 104 was similar and with the most significant displacement among all tested models. This behaviour is attributed to the

reinforced soil block's deformation, which rotates as a rigid body together with the facing wall; consequently, the seismic inertia forces induced by the upper tier on the lower tier are much more significant. Therefore, it is suggested here that the offset distance should be large enough to avoid a rigid body rotation of both tiers. The facing lateral deformation in test 101 was linear from the toe of the lower tier towards the top of the upper tier. The amount of sliding deformation was the greatest comparing to the rest of the model tests. In test 102, the lower tier deforms linearly toward the top, while in the upper tier bulging deformation with a convex shape geometry can be observed, the amount of bulging increased with an increase in base input acceleration. Test 104 also showed bulging deformation; however, the amount of bulging deformation was slightly reduced, which is attributed to the increase in the reinforcement length of the lower tier. Safaee et al. (2020) also found bulging deformation on multi-tier reinforced soil walls during seismic shaking.

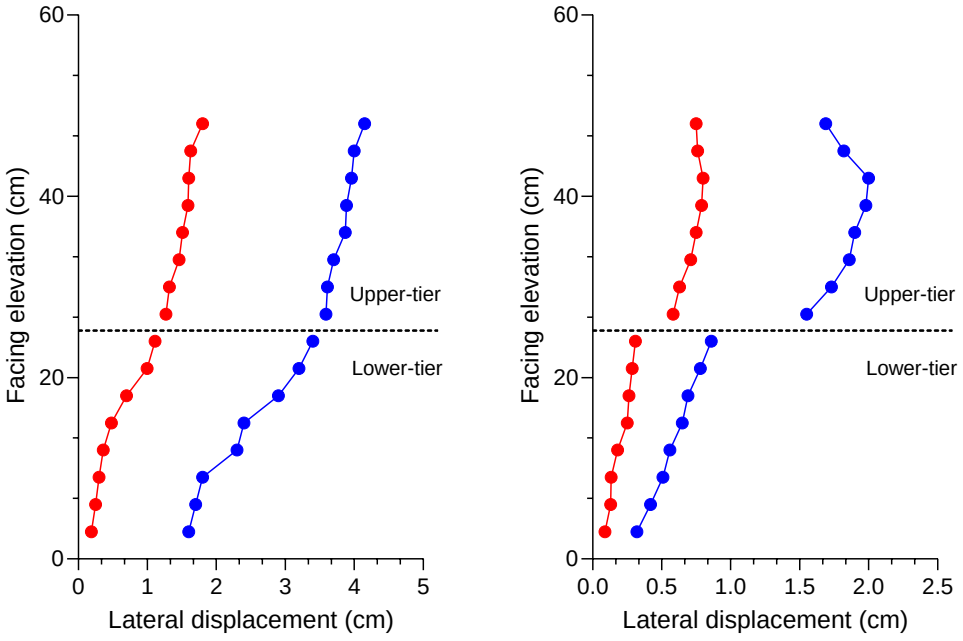

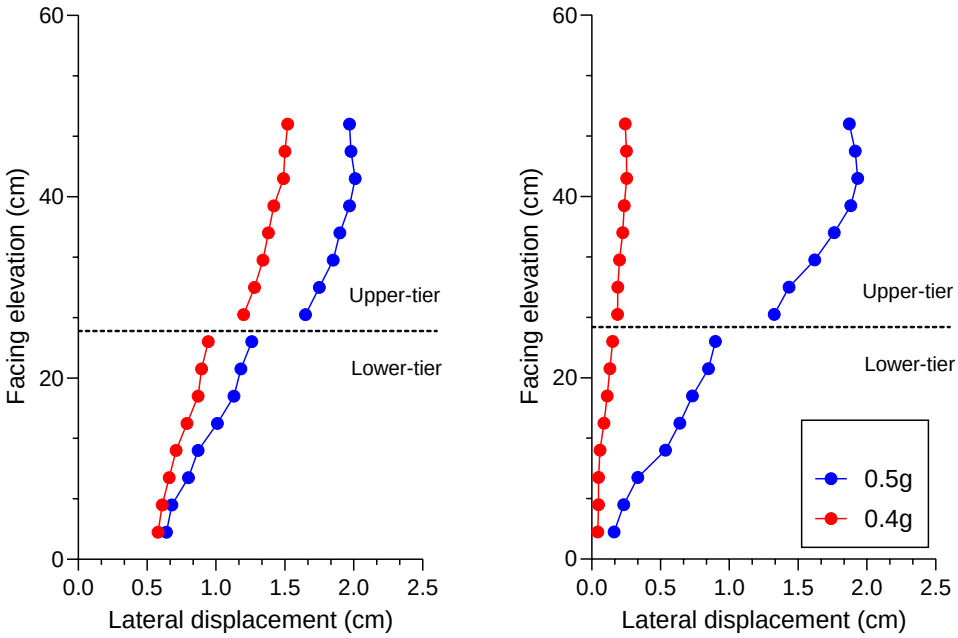

Figure 4 Facing lateral deformation for T102, T103, T104 and T105 respectively

Sand deformation of the lower tier

Figure 5 and 6 shows the total sand deformation. In general, the sand deformation behind the lower tier increased with an increase in base input motion and downward thrust exerted by the upper-tier wall; consequently, the upper-tier wall induced compaction on the lower tier backfill soil near the interface while the lower tier backfill base underwent shear deformation of the reinforced zone together with the shear deformation of the subsoil. In all cases, the active wedge of failure was triggered when the facing wall and backfill deformation showed a minimal amount of lateral deformation, between 0.001H ~ 0.006H, which is not large enough to mobilize the shear strength of the backfill soil. Therefore, the active failure in the backfill may occur at a seismic level far below the level where the wall's ultimate external failure occurs. For instance, according to Terzaghi (1920) the amount of outward wall displacement to trigger the active failure of the backfill associated with the mobilization of the peak friction angle in the shear band (or failure plane) is known to be very small; for a wall

rotating about its base, the outward displacement at the wall top is about 0.1% of the wall height from the at rest condition. The figure shows the total sand deformation during seismic shaking for the test T102. The deformation in the wall active zone is confined in a two-edge failure line approximately degrees from the horizontal. The displacement values within the active zone increased from zero at the toe of the wall to a maximum at the top. The size of the active wedge near the wall top of the lower tier was depended on the reinforcement length and offset distance. By increasing the reinforcement length and offset distance, the size and length also increase linearly from the facing wall towards the end of the reinforcements; this is because the amount of mobilized soil by the reinforcement layers also increased. This behaviour is similar to the one reported by Berg which performed small-scale model tests to study the effect of surcharge loading on earth retaining walls, where it was found that the lateral force applied by the strip footing on the non-yielding wall decreased as the distance from the wall increased and the sand porosity decreased and the shear bands, the borders between moving particles and particles, are increased in length as the footing vertical stress increased.

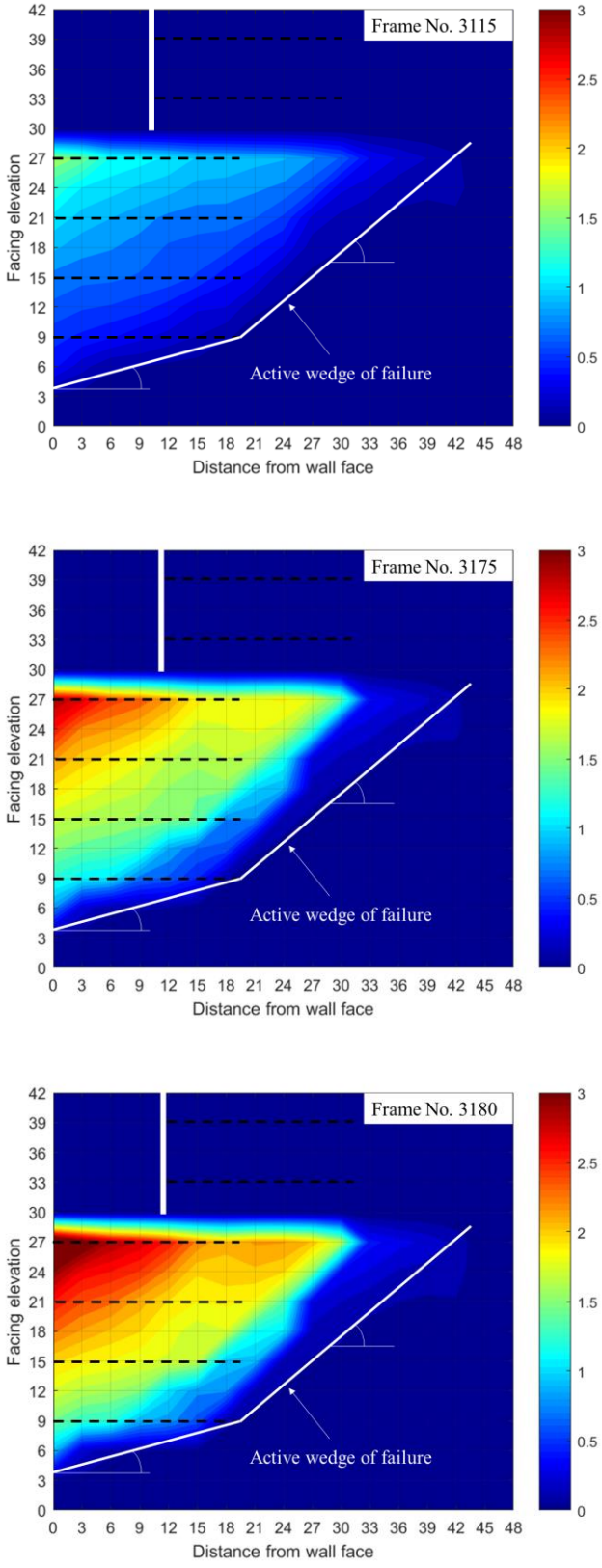

Figure 5 Sand total displacement Test 102 during ground shaking

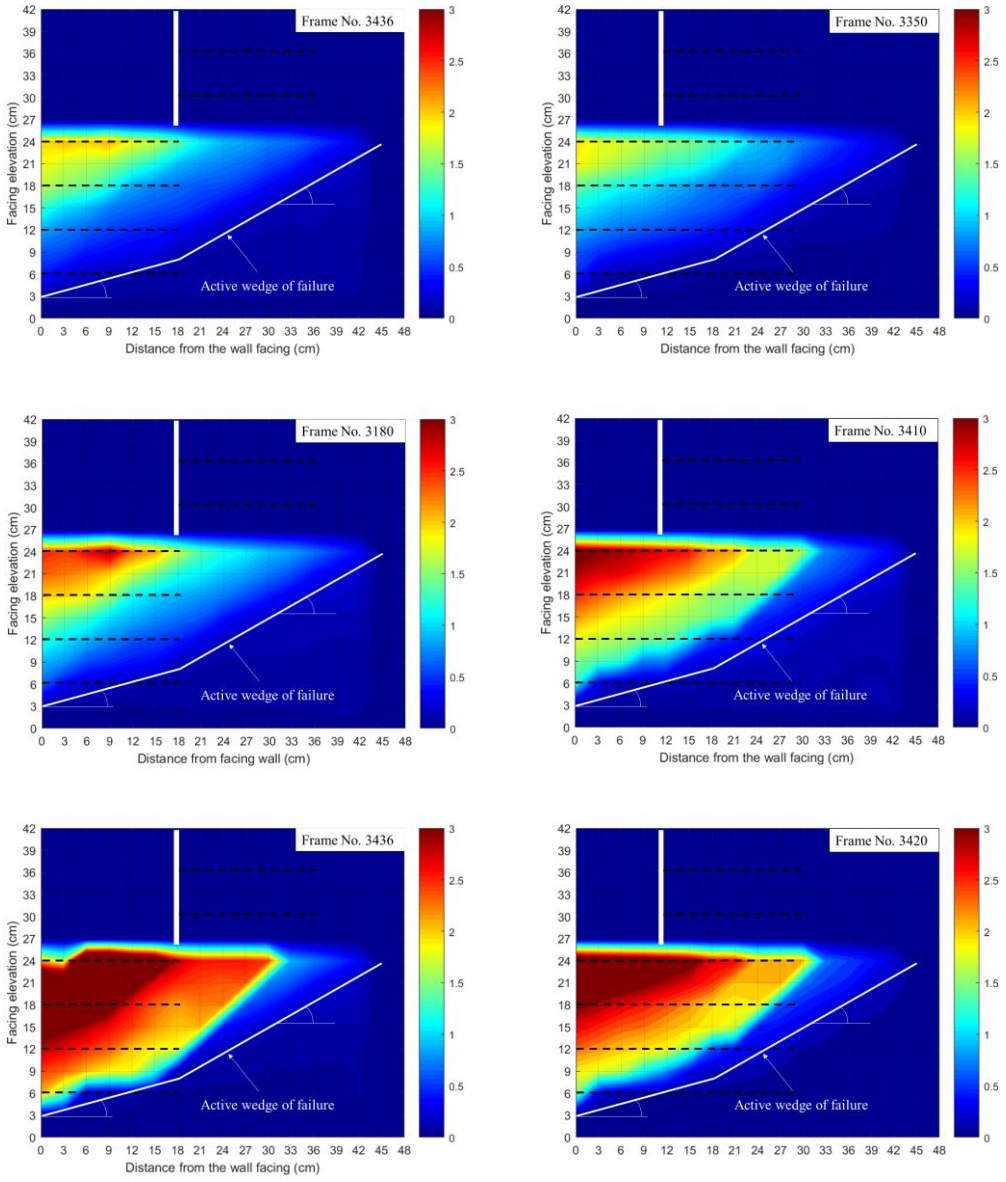

Figure 6 Total sand displacements a) Test 103 and b) Test 104 during ground shaking

The highest displacement values within the active zone are observed within the full length of the top-most reinforcement layer as shown in Test 103 while in Test 104 the highest displacement values are only recorded within half-length of the top-most reinforcement layer. As the wall rotates to the outward direction, multiple rupture surfaces were observed in the backfill soil in each tested wall. Each rupture surface corresponds to a particular displacement value. The rupture surfaces with the highest

displacement values were located near the lower tier wall and the interface between the tiers, which decreased with depth as well linearly from the facing wall toward the retaining zone. Consequently, high stresses in the interface between the two tiers is expected, which should be correctly quantified and incorporated in the seismic lateral earth pressure when designing tiered walls as it led to the whole system destabilization. The rupture surfaces geometry was distinct in each wall despite that the active wedge of failure showed a two-wedge geometry in all cases. For instance, in conventional retaining walls, the rupture surfaces within the backfill soil follow the same geometry of the active wedge of failure. In Test 103 and Test 102, the rupture surfaces took a linear geometry as assumed in coulomb theory from the top of the lower tier wall. However, the active wedge of failure was maintained with a two-wedge geometry, and as the wall rotates continued to rotate to the outward direction due to seismic inertia forces, the linear rupture surface then took a two-wedge geometry. Differently, in Test 103, the rupture surface close to the wall top of the lower tier was initially with a two-wedge geometry from its formation until the total collapse of the wall.

Figure 7 and 8 shows the horizontal distribution of sand movement. In general, the horizontal displacement was more significant than vertical displacement, which is attributed to the dilation of the sand and the spread of the active zones in the failure envelopes that pushed the soil outward during ground shaking. Figure shows the distribution of vertical soil displacement during ground shaking. The vertical soil displacement and the active wedge during seismic shaking were not uniform, as observed in the horizontal displacement. It is possible to notice two distinct zones of high compaction. The first located near the top of the lower tier, and the second is located below the upper tier's reinforced zone. In these zones, the soil is being

compressed as the wall rotates to the outward direction causing the shear zone to increase its size during seismic shaking. The amount of soil compaction was larger in the second region, which is attributed to the drag-down forces induced by the upper tier's soil block and soil block of the retaining zone, which tend to move toward the back of the reinforced zone of the lower.

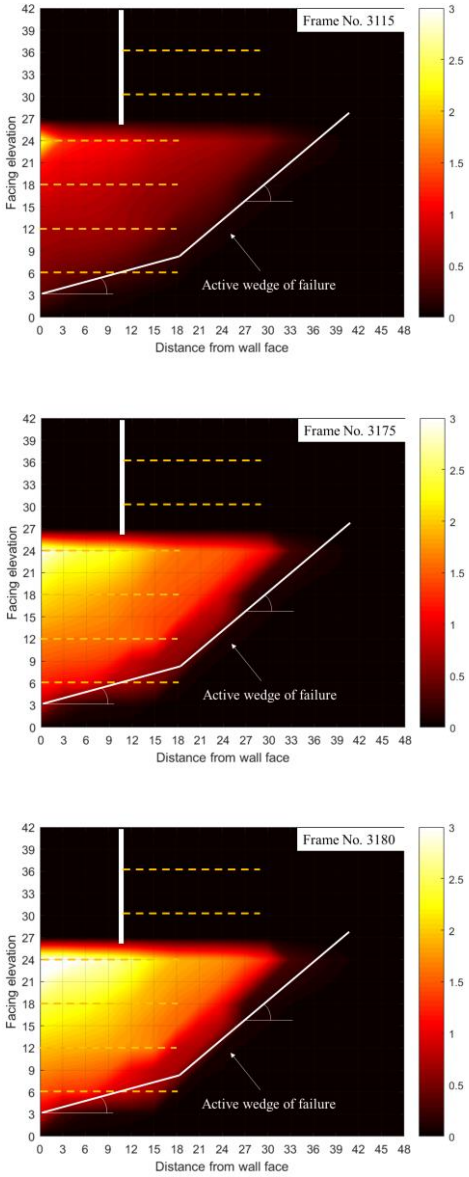

Figure 7 Sand horizontal displacement Test 102 during ground shaking

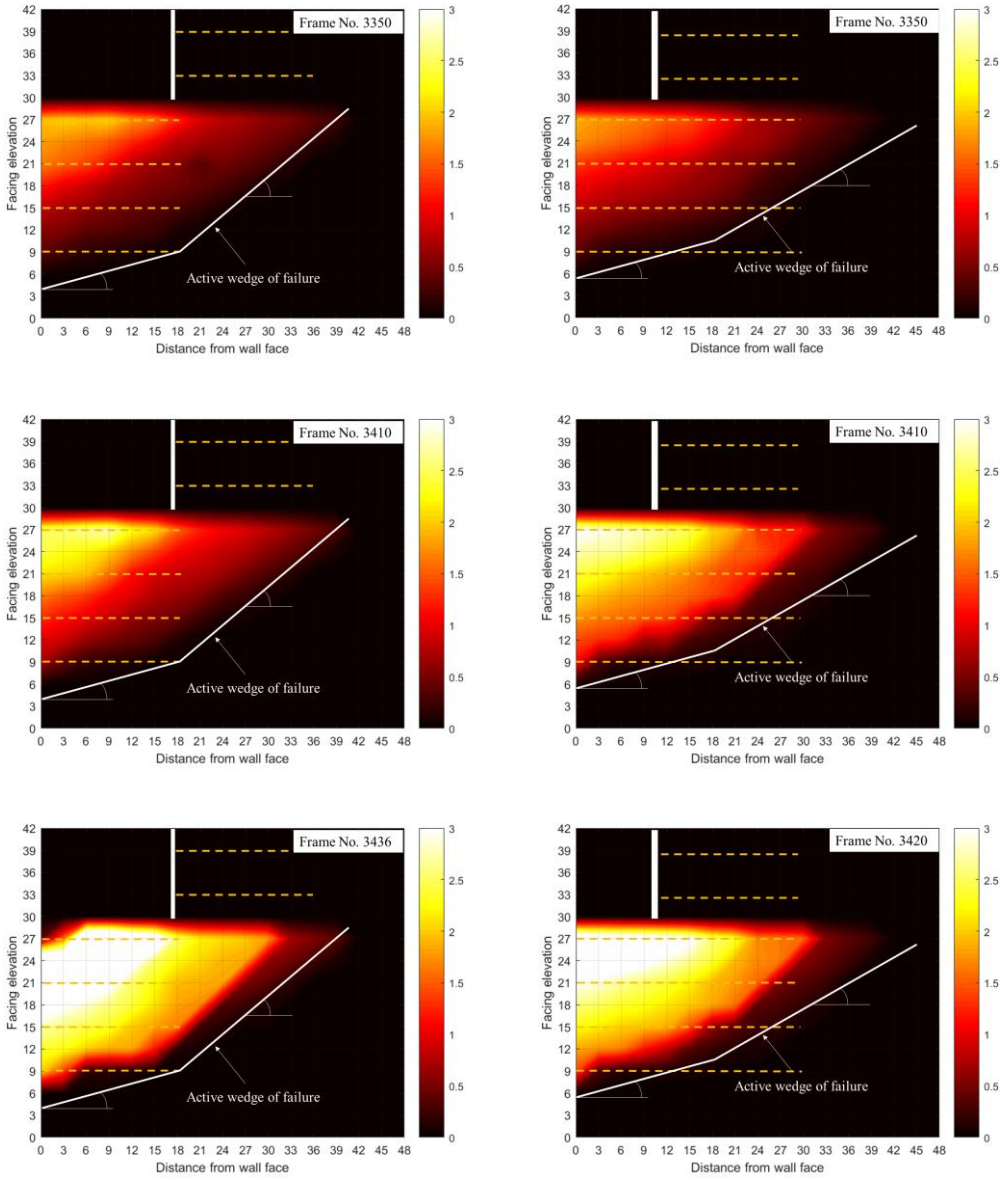

Figure 8 Horizontal sand displacements a) Test 103 and b) Test 104 during ground shaking

Figure 10 shows the comparison of the vertical displacement for test 103 and 104. The zone of compaction is different for each case. In test 103, the compaction zone length and depth were larger than test 104, which is attributed to the short reinforcement length of the lower tier. The compaction zone was also observed in front of the upper tier due to its sliding movement. In test 104, the compaction length and depth are reduced, and it

was not observed in front of the upper tier, which is attributed to longer reinforcement length since it is able to hold more mass together during seismic shaking preventing the additional sand deformations. Therefore, the two tiers interact through the surcharge from the upper tier acting on the lower tier and the deformation of the lower tier influencing the upper tier's behaviour. It can be concluded that the two tiers mutually affect each other and cause additional wall and soil deformation. Moreover, the offset displacement and reinforcement length of the lower tier greatly influence the sand movement in tiered walls.

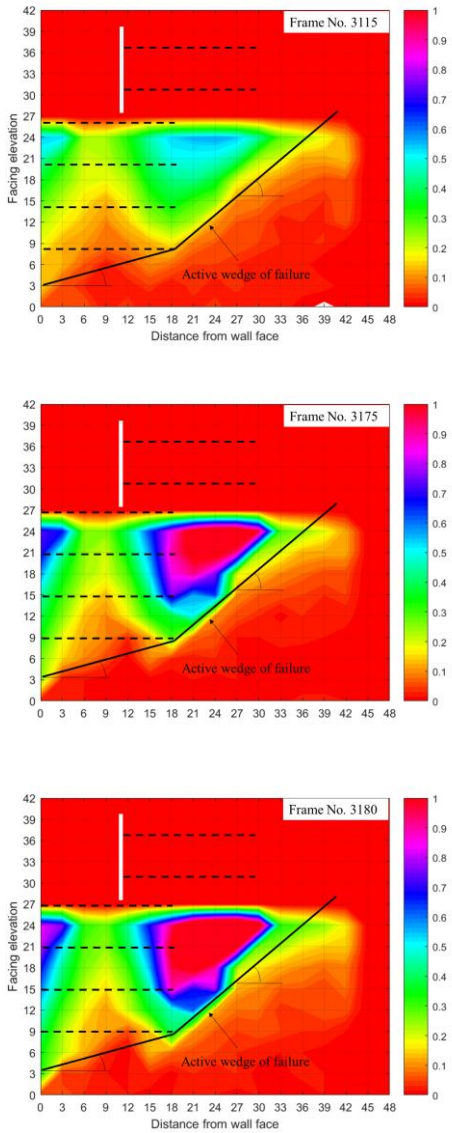

Figure 9(a) Sand vertical displacement Test 102 during ground shaking

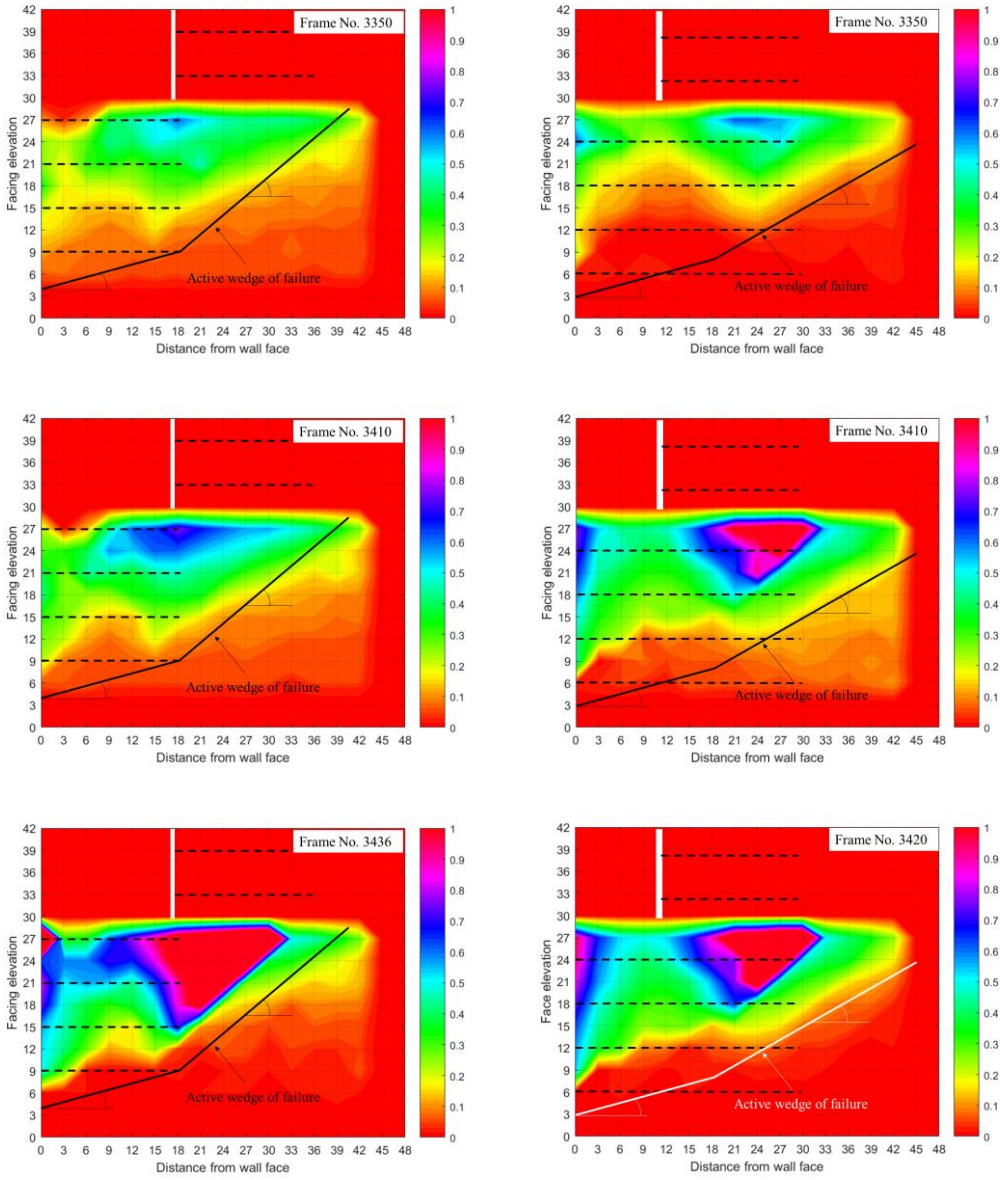

Figure 10(b) Vertical sand displacements a) Test 103 and b) Test 104 during ground shaking

Conclusion

This paper present results from a series of 1g shaking table model test on seismic deformation behaviour of two-tier reinforced soil wall. Influence of reinforcement length and offset distance was investigated. The following is the summary of the experimental observations:

- The facing lateral deformation of geosynthetics reinforced soil walls constructed in tiered arrangement was less than walls built in single tier or with very small offset distance; tiered walls were also able sustain greater ground motion amplitudes.
- Increasing the reinforcement length of the lower tier, reduced facing lateral deformation was observed in both tiers.
- The failure mechanism of all tested models consisted in a two-wedge geometry extending from the toe of the wall until the end of the bottom-most reinforcement layer and propagated toward the backfill surface. In all cases, no failure surface was observed in the reinforced zone of the upper tier.

References

Bathurst, R. J., & Hatami, K. (1998). Seismic Response Analysis of a Geosynthetic-Reinforced Soil Retaining Wall. Geosynthetics International, 5(1-2), 127-166.

Damians, I. P., Bathrust , R. J., Josa, A., & Lloret, A. (2015). Numerical Analysis of an Instrumented Steel-Reinforced Soil Wall. International Journal of Geomechanics, 15(1).

Guler, E., & Enunlu, A. K. (2009). Investigation of dynamic behavior of geosynthetic reinforced soil retaining structures under earthquake loads. Bulletin of Earthquake Engineering, 737-777.

Guler, E., & Selek, O. (2014). Reduced-Scale Shaking Table Tests on Geosynthetic-Reinforced Soil Walls with Modular Facing. Journal of Geotechnical and Geoenvironmental Engineering, 140(6).

Guler, E., Hamderi, M., & Demirkan, M. M. (2007). Numerical analysis of reinforced soil-retaining wall structures with cohesive and granular backfills. Geosynthetics International, 14(6), 330-345.

Hatami, K., & Bathrust , R. J. (2005). Development and verification of a numerical model for the analysis of geosynthetic-reinforced soil segmental walls under working stress conditions. Canadian Geotechnical Journal, 42(4), 1066-1085.

Hatami, K., & Bathrust , R. J. (2006). Numerical Model for Reinforced Soil Segmental Walls under Surcharge Loading. Journal of Geotechnical and Geoenvironmental Engineering, 132(6).

Huang, B., Bathrust , R. J., & Hatami, K. (2009). Numerical Study of Reinforced Soil Segmental Walls Using Three Different Constitutive Soil Models. Journal of Geotechnical and Geoenvironmental Engineering, 135(10).

Koseki, J., Munaf, Y., Sato, T., Tatsuoka, F., Tateyama, M., & Kojima, K. (1998). Shaking and Tilt Table Tests of Geosynthetic-Reinforced Soil and Conventional-Type Retaining Walls. Geosynthetics International, 73-96.

Krishna, A. M., & Latha, G. M. (2007). Seismic response of wrap-faced reinforced soil-retaining wall models using shaking table tests. Geosynthetics International, 14(6), 355-364.

Lee, K., Chang, N., & Ko, H. (2010). Numerical simulation of geosynthetic-reinforced soil walls under seismic shaking. Geotextiles and Geomembranes, 28(4), 317-334.

Ling, H. I., Mohri, Y., Leshchinsky, D., & Burke, C. (2005). Large-Scale Shaking Table Tests on Modular-Block Reinforced Soil Retaining Walls. Journal of Geotechnical and Geoenvironmental Engineering, 131(4).

Matsuo, O., Yokoyama, K., & Saito, Y. (1998). Shaking Table Tests and Analyses of Geosynthetic-Reinforced Soil Retaining Walls. Geosynthetics International, 5(1-2), 97-126.

Munoz, H., & Kiyota, T. (2020). Deformation and localisation behaviours of reinforced gravelly backfill using shaking table tests. Journal of Rock Mechanics and Geotechnical Engineering, 12(1), 102-111.

Panah, A. K., Yazdi, M., & Ghalandarzadeh, A. (2015). Shaking table tests on soil retaining walls reinforced by polymeric strips. Geotextiles and Geomembranes, 43(2), 148-161.

Sabermahani, M., Ghalandarzadeh, A., & Fakher, A. (2009). Experimental study on seismic deformation modes of reinforced-soil walls. Geotextiles and Geomembranes, 27(2), 121-136.

Watanabe, K., Munaf, Y., Koseki, J., Tateyama, M., & Kojima, K. (2003). Behaviour of several types of model retaining walls subjected to irregular excitation. Soils and Foundations, 43(5), 13-27.

Xiao, C., Han, J., & Zhang, Z. (2016). Experimental study on performance of geosynthetic-reinforced soil model walls on rigid foundations subjected to static footing loading. Geotextiles and Geomembranes.

Xu, P., Hatami, K., & Jiang, G. (2020). Shaking table study of the influence of facing on reinforced soil wall connection loads. Geosynthetics International, 27(4), 364-378.

Xu, P., Hatami, K., & Jiang, G. (2020). Study on seismic stability and performance of reinforced soil walls using shaking table tests. Geotextiles and Geomembranes, 48(1), 82-97.

Yazdandoust, M. (2017). Investigation on the seismic performance of steel-strip reinforced-soil retaining walls using shaking table test. Soil Dynamics and Earthquake Engineering, 97, 216-232.

Chapter 4: Capturing strain localization behind reinforced soil walls

Author 1

- *Albano Ajuda, PhD Candidate*
- *Department of Civil and Environmental Engineering, Saitama, Japan*

Author 2

- *Jiro Kuwano, Professor*
- *Department of Civil and Environmental Engineering, Saitama, Japan*

Abstract

This paper presents experimental results from shaking table test of four geogrid reinforced soil wall (GRSW) with an objective to investigate: (1) failure mechanism of GRSW, (2) soil-geogrid interaction during earthquakes and (3) the effect of multiple reinforcement stiffness along the wall height. Image analysis was employed to observe the progressive deformation, strain localization together with shear banding development along the soil-geogrid interface. It was found that the failure mechanism of the model walls strongly depends on the reinforcement stiffness arrangement. The deformation modes for wall with single reinforcement stiffness consisted mainly due to overturning with small base sliding, while walls constructed with multiple stiffness showed a zone of intense bulging deformation prior critical acceleration which implied high straining and a different progressive deformation. Moreover, it was observed that the shear band along the soil-geogrid in not stationary but rotates in an anticlockwise direction together with wall rotation and base shaking.

Introduction

Geosynthetics reinforced soil wall have been used in many civil engineering projects due to lower cost and significant performance under earthquakes as compared to traditional retaining wall systems as demonstrated by Tatsuoka et al. [1]. In addition, several post-earthquakes investigation on seismic response of reinforced soil walls from major earthquakes such as 1994 Northridge, Los Angeles earthquake Sandri [2], 1999 Ji-Ji, Taiwan earthquake Ling et al. [3], 2011 Tohuko, Japan Earthquake Kuwano et al. [4] demonstrated that reinforced soil walls structures are able to survive severe earthquake forces where traditional walls suffered severe damage or collapsed. For this reason, geosynthetics reinforced soil wall are one of the preferred structures around the world. Furthermore, the seismic behaviour of reinforced soil walls have been investigated by different methodologies such as shaking table, centrifuge and numerical. However, most the existed studies focus on the application of a single type of reinforcement type along the wall height. Bathurst & Hatami [5] investigated the seismic response of geosynthetics reinforced soil walls using numerical analysis in was concluded that the magnitude of permanent displacement diminished with increasing reinforcement stiffness and increasing reinforcement length. Matsuo et al. [6] showed that increasing the ratio of geogrid length to the wall height from 0.4 to 0.7 was the most effective method to reduce wall deformation, Roessig & Sitar [7] showed that stabilizing the slopes with stiffer reinforcements the magnitude of displacement induced by the earthquake is reduced. Sabermahani [8] demonstrate that the maximum horizontal wall deformation decreased as the stiffness of the reinforcement layers was increased and hence the stability of GRS model walls was improved under simulated earthquake loading. Furthermore, many studies have been carried out to investigate the failure mechanism of reinforced soil walls using a single reinforcement stiffness type

during seismic shaking through experimental studies such as Koseki et al. [9]; Watanabe et al. [10]; Yazdandoust [11] and Anastasopoulos et al. [12]. Recently, some attempts have been done in order to improve global stability as well to reduce the total construction cost of reinforced soil walls structures by combining different reinforcement materials or lengths along the reinforced soil wall height. Leschinsky [13] introduced the concept of hybrid geosynthetics reinforced retaining wall which consist in placing a shorter reinforcement layer in between longer reinforcement. It was observed that the inclusion of shorter reinforcement it is possible to reduce the connection force of primary reinforcement increase internal stability and reduce down drag effect. Jiang et al. [14] investigated the effect of secondary reinforcement on geosynthetics reinforced soil wall using numerical analysis. In their studies they focused in the effect of secondary reinforcement length, secondary reinforcement stiffness. It was found that the wall facing deflections decreased with an increase in the secondary reinforcement length and stiffness and also the incremental benefit of increasing the secondary reinforcement length and stiffness to reduce the maximum wall facing deflections becomes negligible when the secondary reinforcement length to wall height ratio (L/H) and stiffness is greater than a certain value and increase in secondary reinforcement stiffness can reduce the maximum tensile stress and connection stress in primary reinforcement. Lelli et al. [15] showed case studies of hybrid reinforced soil structure constructed in India, Albania and Turkey; these walls were constructed using geogrid as primary reinforcement and steel wires as secondary reinforcement. They reported that the choice was that these walls have more permeability and are cost effective as compared to conventional methods. Watanabe et al. [10] reported that placing longer reinforcement layer at higher elevations in the backfill can increase substantially the resistance against overturning. Kikumoto et al. [16] investigated the

influence of different reinforcement length arrangement along the wall height using model test and numerical analyses. Bearing capacity test were conducted on the backfill on the reinforced soil wall. They reported that the characteristics of bearing capacity and deformation behavior of the surrounding ground are totally different due the arrangement of the reinforcement. By placing longer reinforcement layers in the upper part of the wall and shorter in the lower part the initial stiffens sand bearing capacity was similar to walls with short uniform reinforcement length. On the opposite reinforcement arrangement, the deformation behavior was similar to wall with longer uniform reinforcement and the formation of the failure surface was interrupted by the reinforcement placed in the lower part. Hatami et al. [17] conducted a series numerical analysis using a computer program FLAC [18] on wrap-around walls. The walls were reinforced by different reinforcement stiffness along the wall height and subjected to a static loading. It was reported that deformation of walls constructed with multiple reinforcement stiffness in alternating manner was similar in magnitude and shape to walls constructed with a single reinforcement and by grouping the reinforcement with less stiffness either in the upper or lower large deformation occurred in regions with less stiff reinforcement. Miyata & Shinoda [19] reported case studies in Japan of reinforced soil walls constructed with different length as well multiple reinforcement types along the wall height. The wall was reported to suffer damage due to heavy rain. Moreover, it is well-know that soil-geosynthetics plays an important role in the deformation behaviour of reinforced soil walls and for this reason several laboratory test such as monotonic pullout and direct shear test have been conducted in order to characterize the soil-geosynthetics interface behaviour.

Recent attempts have been done using cyclic pullout test in order to observe the soil geosynthetics interaction under simulated earthquake loading. Furthermore, a few results have been showed by several researcher incorporating image-analysis For the author's best knowledge, no investigations have been conducted regarding hybrid wall or secondary reinforcement with respect to multiple reinforcement stiffness along the wall height subjected to earthquake loading. For this reason, in the present experimental program a series of four uni-axial shaking table model test were conducted on segmental reinforced soil walls using a uniform stiff reinforcement and multiple reinforcement stiffness along the wall height. The experimental program was divided in three series: (1) investigation on failure mechanism of walls constructed with a single reinforcement stiffness type was conducted in order to clarify their behaviour in terms of progressive failure, (2) shear banding development and strain localization along the soil geogrid interface and (3) effect of multiple reinforcement stiffness along the GRSW height, results from this experimental program were compared against each other. In the present experimental program geogrid segmental model walls were subjected to a seismic loading using a sinusoidal wave with a predominant frequency of 5 Hz until full collapse. To observe the facing displacement and failure mechanism image analysis was applied for physical model test.

Physical modelling

Shaking table

A computer controlled shaking table test was used to simulate seismic loading. The experimental program was conducted at Saitama University, Japan. The shaking table test was constructed on a plan dimension of 1300 mm (L) by 1000 mm (W) which is

seated on a pair of low friction bearing rails constrained to the horizontal direction equivalent to a single degree of freedom.

Model Container

The soil was poured in a rigid steel container built with the following dimension: 1300 mm (L), 300 mm (W) and 650 mm (W). One side of the soil container was constructed with a transparent Plexiglas in order visualize the wall and backfill deformation during model testing. To prevent scratches and to minimize side friction, a mylar sheet was placed over the one with square grid pattern. The rigid box was sufficiently rigid to keep plane strain conditions in the reduced-model. The far end boundary of the soil container was left rigid which may have some influence in the model dynamic response due to reflective waves and magnification as demonstrated previously Bathurst & Hatami [5], furthermore Lombardi et al. [20] found that the systems with absorbing boundaries showed a significant drop in transmissibility magnitudes particularly in the frequency range close to the fundamental frequencies of the soil deposits and their response demonstrated that the systems with foams were characterized by a considerably lower amount of energy which can be directly associated with minor generation and reflection of body waves from the artificial boundaries.

Laminar box is one the recommended solution for earthquake related studies, however, this solution is not adequate for irregular models as the wall will deform towards the backfill, which do not correspond to field behaviour, furthermore, it will be difficult to capture the deformation behaviour using CCD camera. However, this experimental program was designed to investigate solely the wall residual displacement and failure mechanism, therefore, it is expected that the reflective waves will not influence the parameters study in the present research program. For instance, Krishna & Latha [21]

showed that reflective waves do not have any influence in the displacement. Therefore, it is expected that wall residual displacement and shear strain which is calculated from displacement of the optical targets is not affected by the wave reflection.

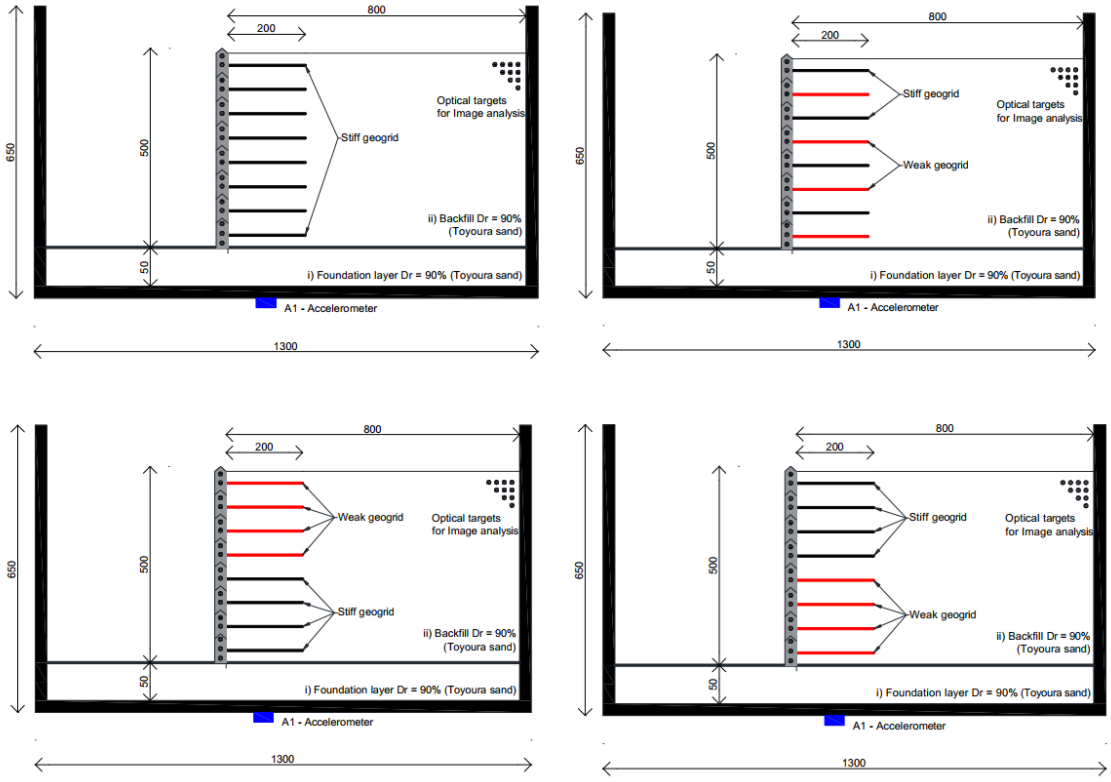

Figure 1 testes cases of reinforced soil

Segmental Wall Modelling

Pre-cast concrete facing panels are commonly used in Japan. Therefore, in the present research work the wall models were modeled as segmental walls with a total height of 500 mm, divided into a total of eight wall panels stacked on top of each other without additional connection so they can rotate against each other as shown in Figure 2. Each panel was built with the following dimension: 300 mm (W), 75 mm (H) and 30 mm thick as illustrated in Figure 2. The wall panels were built with a lightweight acrylic material, in both sides each wall panels Teflon sheets with the same height as the wall

panels was glued in the lateral sides of the wall panels to minimize friction between the rigid container as well to prevent any sand leakage during the model test. Similar wall height has been investigated by Watanabe et al. [10], Koseki, et al. [9] and Nakajima, et al. [22].

Foundation and Backfill material

Soil (Toyoura sand) was used to prepare the soil foundation. The sand layer was prepared by using a sand hopper and keeping a falling height of sand particles constant. The average relative density for both foundation and backfill was 90 % achieved using this method.

Reinforcement Modelling

In the present research program two types of biaxial geogrids with 200 mm long were used for the reinforcement layers as shown in Figure 2. The first reinforcement type is made of a stiff polypropylene (PP) geogrid and the second was made of a weak and flexible geogrid which is not commercially available for reinforced soil application was used only for experimental purposes in simulating the low reinforcement stiffness. Meantime, the thicknesses of the ribs of the weak geogrid was chosen to prevent breakage during the model testing. The geogrid reinforcement was clapped using bolts and nuts between two steel plates with same length as the wall panels. This type of connection was designed to prevent slippage of the geogrid during model testing. In order to characterize the basic behaviour of the geogrid reinforcement models, a series of pullout test were conducted. For this purpose, the geogrid was placed on a ground model consisting of dry Toyoura sand, air pluviation method was used to achieve the desired relative density of 90%. The ground model consists of 240 mm long, 300 mm

wide and 200 mm high; the geogrid was then was held by a steel clamp, wood plates with the same size as the steel clamps were used in the interior faces to reduce the friction effect. The clamp is connected to a jack through a load cell to measure the pullout force and the pullout displacement was measured using a displacement transducer (LVDT). The width and length of the geogrid were set to 30 cm by 30 cm. To simulate the stress state of the backfill layers in shaking table model tests, overburden pressures of the pullout tests were set equal to 5kPa, 10 kPa and 15 kPa using air pressure bag system. Pullout resistances are plotted against the pullout displacement for the case of stiff and weak stiffness geogrid as shown in Figure 3.

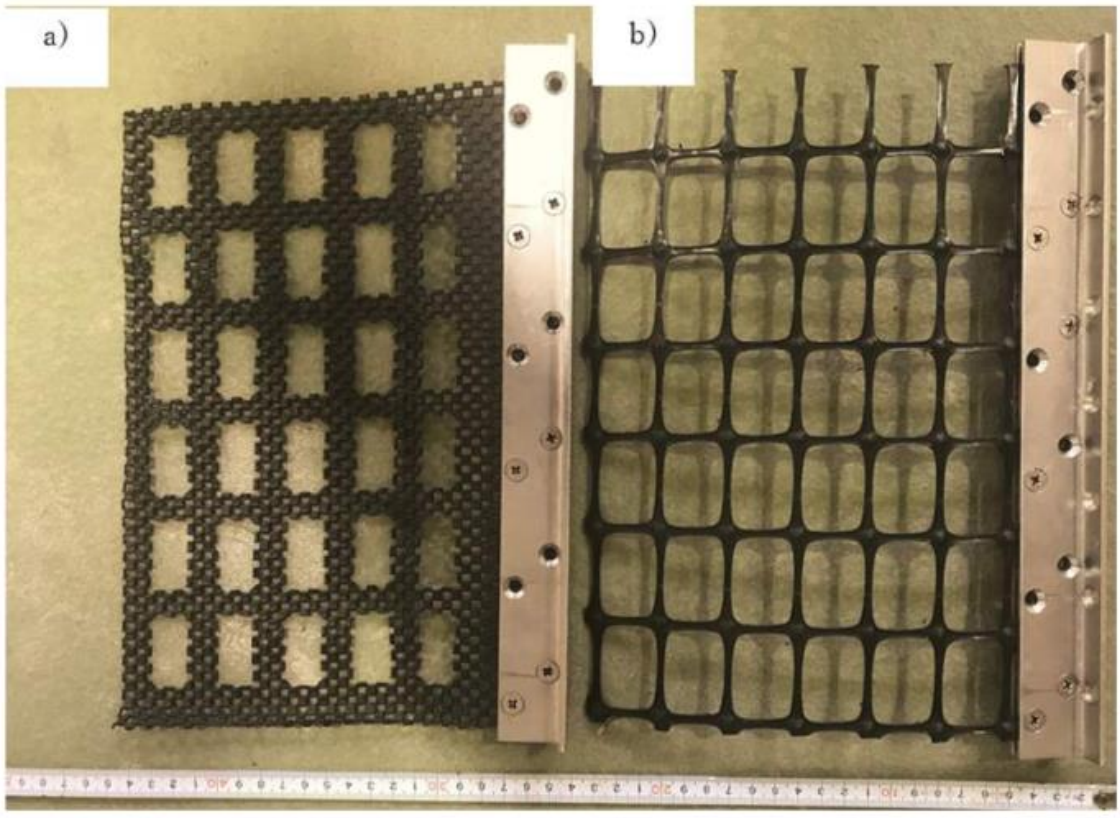

Figure 2 Reinforcment modelling a) Weak geogrid and b) Stiff geogrid

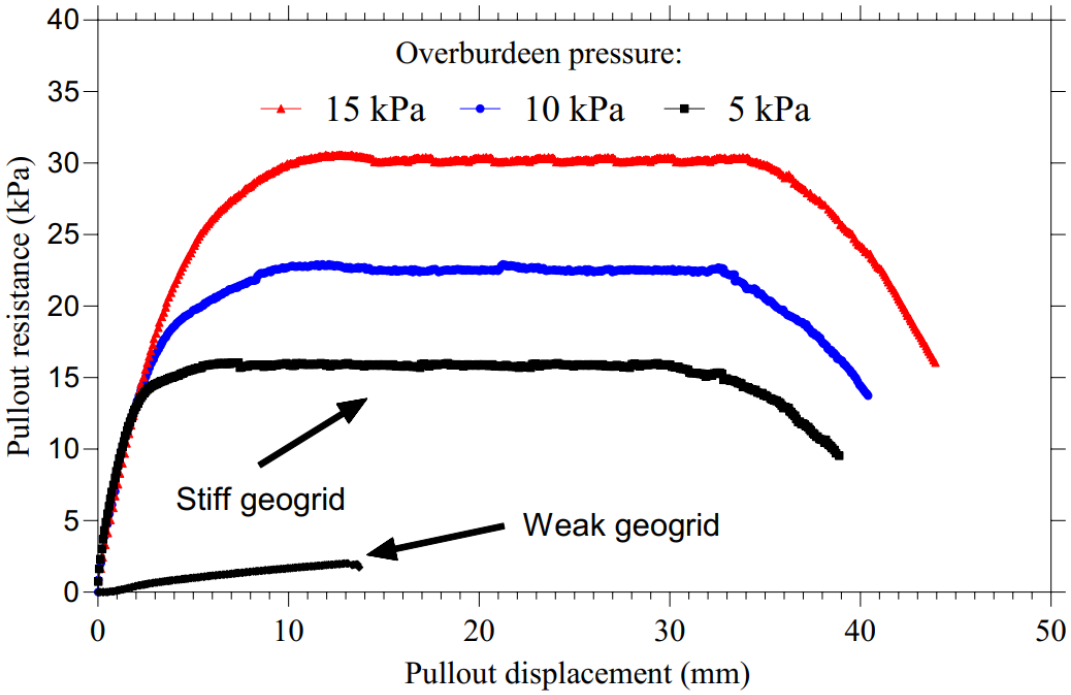

Figure 3 Pullout testing of the model geogrids

Testing Program and Model Instrumentation

A total of 4 geogrid reinforced soil walls were tested in this research in order to investigate the failure mechanism of geogrid reinforced soil walls, soil-geogrid interface during earthquakes and finally the effect of reinforcement stiffness arrangement along the wall height during seismic events. In order to obtain wall residual displacement at each shaking stage, two types of optical targets were used. The first optical targets were made of cartoon with a circular shape which was glued on one side of the wall segments. To investigate the soil displacement and strain a total of 240 optical targets was placed in the soil in contact with the plexiglass, due to the nature of the rubber it is expected that the friction between the optical target and the Plexiglas will not have any influence on the data obtained by this method, these targets were made of chloroprene rubber sponge and glued with an 8 mm long nail. One accelerometer is attached to the shaking table in all experiments to record the input ground motion.

Model preparation construction

The construction processes started from the bottom of the rigid container towards the top of the wall. First the soil foundation made of Toyoura sand was poured to the container with a thickness of 50 mm using air pluviation method to achieve a relative density of 90%. The second step consisted in placing the wall panels one by one on top of each other up to the final height of 500 mm, then the constructed wall was braced into the desired location. This bracing system also prevented lateral movement of the wall during backfilling. The third step consisted in placing the geogrid reinforcement layers and pouring the Toyoura sand using air pluviation method to achieve a relative density of 90% behind the wall in 30 mm layers, this thickness was chosen in order to place optical targets in the desired grid of 30 by 30 mm. The final step consisted in unbracing which started from the wall top towards the bottom as performed in the construction field. A light steel frame was attached to the shaking table together with the rigid container to accommodate the CCD camera in order to capture and record the wall displacement and the backfill deformation during model testing for further use in image processing.

Results and discussion

Seismic Facing Displacement

In regard to seismic facing displacements, Matsuo et al. [6] defined critical acceleration as which a sharp displacement occurs; El-Emam & Bathurst [25] as a sharp increase in the wall displacement-acceleration slope. Furthermore, the failure observed by Richardson et al. [26] was an outward wall rotation of 5.5% of its height; Huang & Wu [27] and Koseki, et al. [9] showed a displacement of 5% of the wall height. In the present experimental tests, the critical acceleration is observed when the wall top

displacement reached a value of 3% to the wall height as shown in Figure 10, at this moment clear failure surface or the active failure wedge was formed within the reinforced are and retained area. Similar observation has been reported by Ajuda et al. [28] and Izawa & Kuwano [29]. Figure 8 shows the displacement profiles with elevation for different types of geogrid stiffness arrangement along the wall height. It general, the wall displacements at each optical target increased with base acceleration. The deformation shape and amount of the tested models are clearly dependent on the stiffness arrangement along the wall height. For instance, in Test 3 the wall the displacement tends to be linear from the wall toe until reaching the region where the weak geogrid is placed, at this particular location the displacement profile changed and increased its magnitude toward the wall top leading to concave shape deformation of the wall panel. On the other hand, in Test 4 it can be seen an increase in sliding component, the displacement magnitude of the optical targets in the bottom half tends to increase with wall elevation up to mid-height where the reinforcement layer shifted to a stiff geogrid, at this elevation the displacement slightly tends to decrease due to the effect of the stiff geogrid. However, because the sliding component was larger, the stiff geogrid could not prevent such great top displacement and it just continued to slide horizontally leading to convex shape deformation. The deformation modes observed in grouped schemes walls is considered here as bulging deformation. Moreover, this bulging deformation shape tends to slightly reduce during critical acceleration and after this stage, the wall displacement profile become linear towards the catastrophic collapse. Sabermahani et al. [8] observed bulging deformation on walls constructed with the weakest type of reinforcements having extensive low stiffness where the wall facing showed a convex shape deformation. Also, Hatami et al. [17] observed bulging deformation on walls constructed with grouped reinforcement schemes walls subjected

to static loading using numerical analysis. Regarding the backfill settlements it is possible to observed from the CCD images the settlement behavior of each model. Wall constructed with single reinforcement stiffness clearly showed a relatively less backfill settlement and the angle of the drag down soil was shallower. On the other hand, walls construed with multiple reinforcement stiffness showed a large amount of settlement and the angle of the drag down soils is steeper, which induced large strain levels along the interface of reinforced and retained zone.

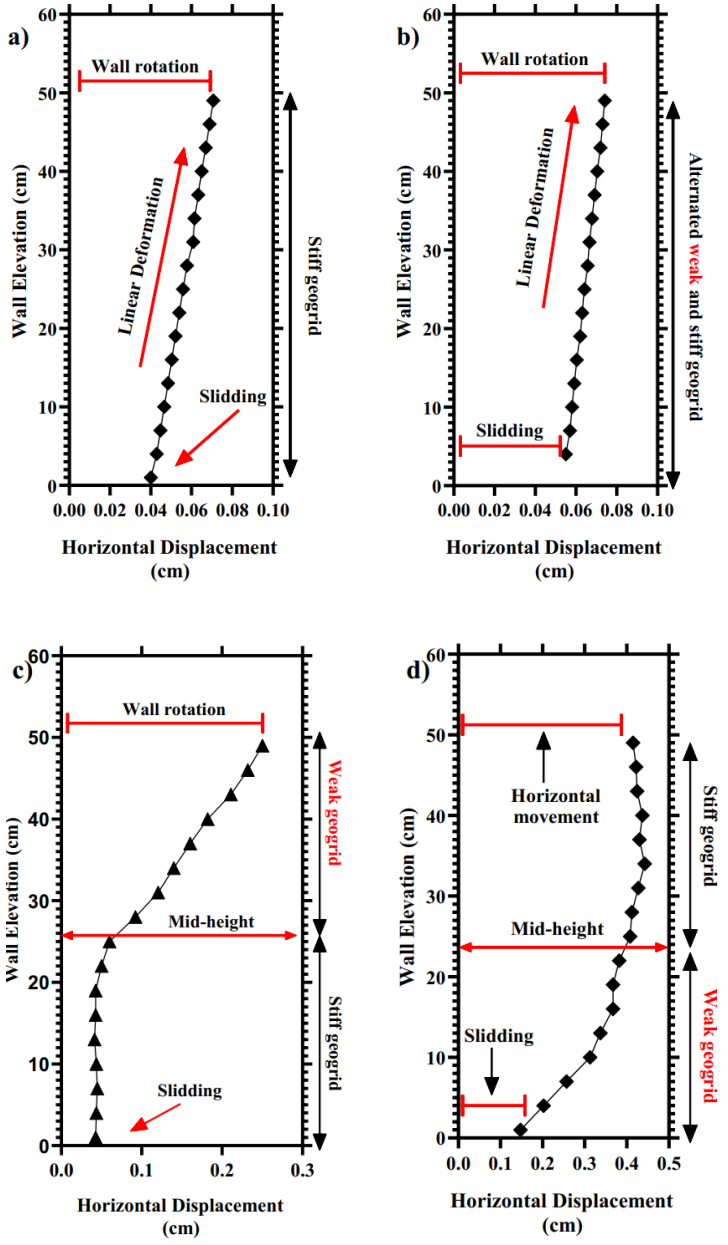

Figure 4 Facing lateral deformation a) test b) test c) test d) Test

Failure mechanism of geogrid reinforced soil walls

The direct recorded CCD images showing the progressive failure development of the models were a practical form to obtain the geometry of the failure surface and the failure mechanisms. An evaluation of the images retrieved during shaking table testing for wall constructed with a single and with multiple reinforcement stiffness is presented in Figure . It is obvious that irrespectively the reinforcement stiffness arrangement along the wall height, the model walls showed an identical failure pattern which extended from the wall toe at 16° from the horizontal towards the end of the first reinforcement layer and then progressed at 45° degrees upwards towards the backfill surface. Furthermore, we can observe that at the ground acceleration of 5 m/s2 the clear failure surface with a two wedge geometry already formed together with a large settlement of the backfill. Similar wedge geometry has been reported by Ajuda, et al. [28] and Izawa & Kuwano [29]. To further identify the failure pattern and the failure mechanism of the segmental geogrid reinforced soil wall a series of optical targets were placed in the backfill. Deformation of the soil together with the optical targets allowed to identify the failure pattern geometry as well the localized shear strains within the soil mass and along the soil-geogrid interface. Figure 11 shows the progressive deformation of Test 1 during base shaking of 4 m/s2 to 5 m/s2. The process of progressive failure in geogrid reinforced soil wall observed in the present experimental work can be explained in the following manner: (1) Before any shaking of the models, zero shear strain is obtained as the optical targets do not show any displacement corresponding to a static condition. (2) With the further application of base shaking, progressive strain localization started to be visible at the top backfill which progressed downwards in the last reinforcement layer in the interface between the reinforced and retained area with a very small amount of lateral wall deformation corresponding to a quasi-elastic response. (3) With further

application of base shaking inclined failure surface begin to appear in the top of the backfill toward the back of the wall while additional not well-defined shear bands propagated in the horizontal at a relatively low strain levels in the soil-geogrid interface and (4) with additional shaking cycles a second inclined failure surface become visible which propagated from the wall toe at 16° in the reinforced area intersecting the end of the first reinforcement layer and then intersecting the 45° inclined failure surface which allowed the creation of the active failure wedge where the soil inside this region slide horizontally and downwards to the back of the wall consequently large settlement of the ground surface occurred with additionally drag-down forces at the end of the reinforcement layers which extended up to the middle height of the wall. It was observed that after the active failure surface has been created and with continued application of base acceleration cycles, the wall continued to rotate to the outward direction and well-defined shear bands in the soil-geogrid interface propagated horizontally in large strain levels up to a half-length distance of the geogrid from the end tips of the geogrid layers towards the back of the wall. This behavior can be associated to the pullout failure mechanism similar to those observed in direct shear or pullout test. The active failure wedge was observed to be not an undamaged region, as can be observed through the movement of the optical targets as well from the non-uniform distribution of shear strain inside the active wedge and along the reinforcement layers, but a highly damaged region where multiple failure surfaces are possible to develop as also reported in Watanabe, et al. [10], Sabermahani, et al. [8] and Koseki, et al. [9]. Therefore, contradicting the current assumption in limit equilibrium that the active wedge translates as a rigid body. Furthermore, Tatsuoka et al. [30] pointed out that progressive failure is ignored in ordinary limit-equilibrium stability analysis which assumes that all shear band develops suddenly.

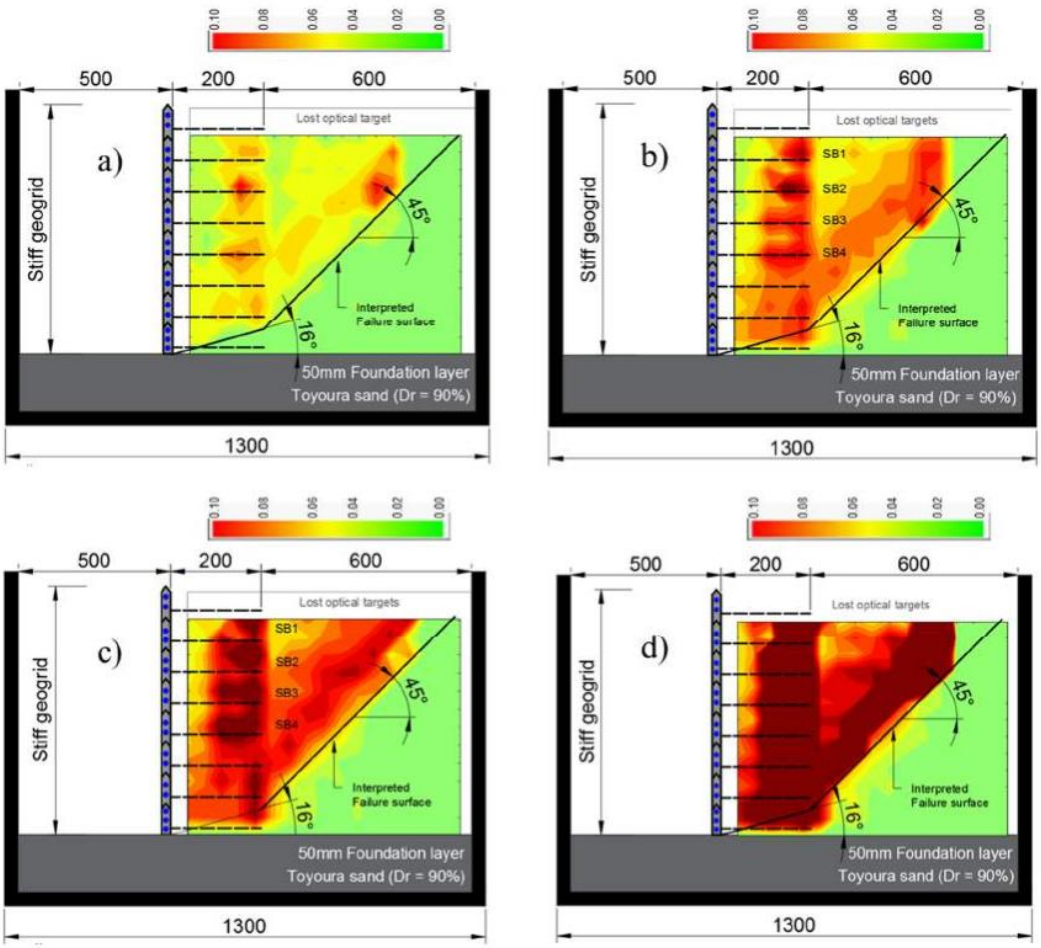

Figure 5 Failure mechansim of test 1 during ground shaking

Effect of multiple reinforcement stiffness on failure mechanism

The shear strain contour was obtained at the corresponding critical acceleration of 3% of the wall height as shown in Figure 6. It is possible to notice that the magnitude of maximum shear strain was dependent on the reinforcement stiffness arrangement during critical acceleration, the magnitude of maximum shear strain of Test 1 was much less as compared to the rest of the tested cases as it is more able of preventing the shear deformation owing to the stiff reinforcement layers, followed by Test 2. However, grouped reinforcement stiffness walls, Test 3 and Test 4 showed a large backfill

movement, consequently, an increased magnitude of shear strain along the failure surfaces which is attributed due to bulging deformation that is observed prior to the critical acceleration as shown in Figure 11. This behavior agrees with Leshchinsky [13] statement that bulging deformation of geosynthetics reinforced soil walls observed by AlHussaini & Perry [50] and Tatsuoka, et al. [30] implied large shear strains and a process of progressive failure. For Test 1, Test 2 and Test 3 the deformation of the active failure wedge was induced mainly by the large rotation of the wall top while in Test 3 and Test 4 the activation of the active failure surface is attributed to the sliding and bulging mechanism which was more predominant. However, the displacements were observed to be larger at the location where the weak geogrid is placed, in addition it was found that at the end of the shaking test, reinforcement stiffness arrangement is not very sensitive after passing the critical acceleration, at this stage all wall deformation became close to linear. Moreover, regarding the shear strain distribution in the backfill, it is evident that at the same base acceleration Test 1 and Test 2 did not show any strain level associated to the post-peak behavior while in Test 3 and Test 4 the shear bands already fully developed associated to strain softening leading to an early catastrophic collapse. This is because the geogrid used in this experiment is extremely weak that it allows significant strain levels to be develop very quickly, therefore, allowing a reduction in the shearing resistance with continuous progress of plastic strains until exceeding the previous strain levels required to activate the soil residual strength as compared to the stiffer geogrid reinforcement. The post-failure performance of Test 1 and Test 2 may be attributed to the large movements that the stiff geogrid is able to withstand after achieving its ultimate tensile strength. However, this behavior is different than that of the GRSW constructed with a combination with a weaker geogrid in grouped arrangement, namely Test 3 and Test 4 which shows a rapid drop in tensile

strength after it was reached their peak tensile strength leading to an early failure, Ajuda et al. [28] demonstrated that by increasing the reinforcement stiffness, the failure surface start to appear at late shaking steps and tilting angles. Therefore, under seismic loading the post-failure behavior of the models until the catastrophic collapse of GRSW not only depends on the post-peak behavior of the backfill soil, the geogrid reinforcements, but also on the reinforcement stiffness arrangement. Despite multiple reinforcement stiffness along the GRS wall, the failure surfaces angles observed in the present models during the shaking table test remained the same at the failure stages. For instance, Izawa & Kuwano [51] investigated the behavior of geogrid reinforced soil walls subjected to pseudo-static loading using a centrifuge tilting table test together with a two-wedge analysis. It was reported that failure surfaces have different geometries under different geogrid tensile strength. Therefore, the failure surface behaviour observed in the present study suggest that despite multiple reinforcement stiffness along the reinforced soil wall system the failure surface angle will be governed by its reinforcement length and the highest reinforcement stiffness.

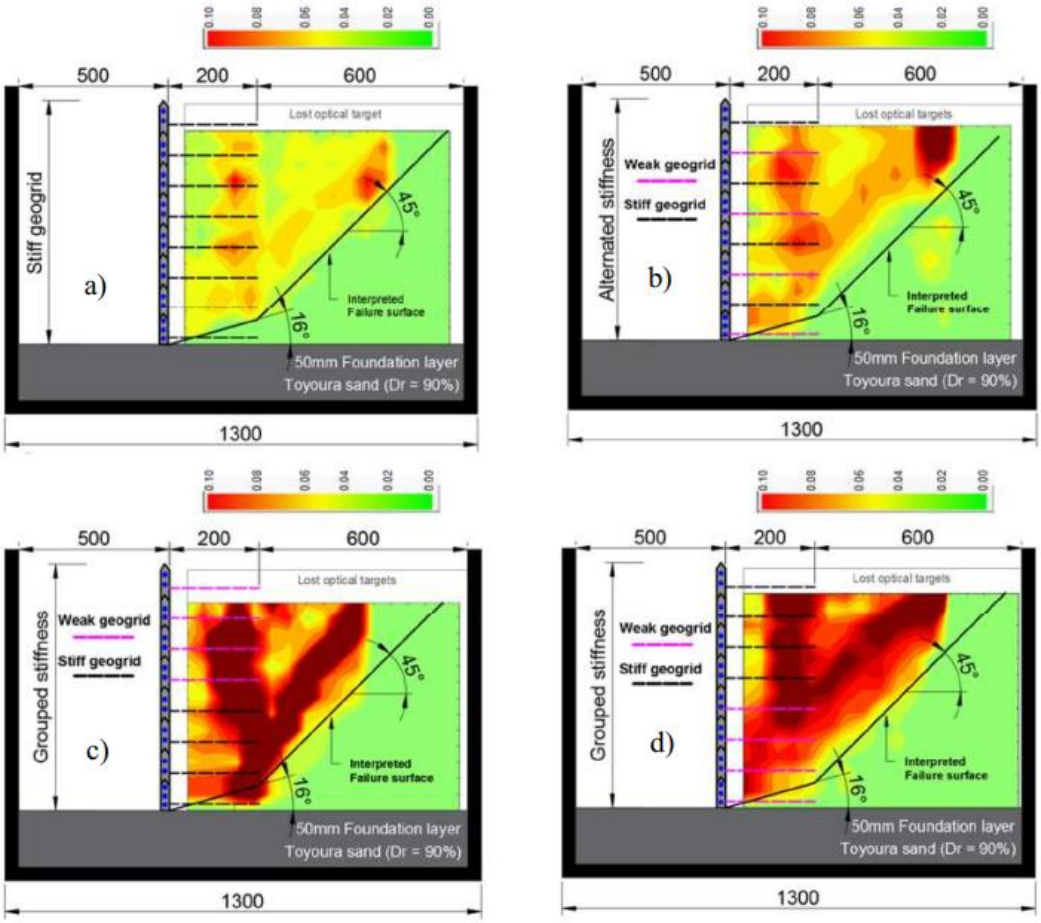

Figure 6 Failure process of tested models

Conclusion

A total of four model scale segmental geogrid reinforced soil wall were study regarding (1) the failure mechanism of GRSW and the effect of multiple reinforcement stiffness along the wall height. For this purpose. The following is the summary of the test results observed in the experiments:

- Wall displacement increased with base acceleration and the critical acceleration was observed at 3% of the wall height at this point clear failure surfaces were observed within the reinforced and retained zone corresponding to the development of the active failure wedge;

- The shape and amount of deformation of wall with alternating was similar to wall with stiff geogrid reinforcement only; However, grouped reinforcement schemes showed an increase in displacement in particular in the region where the weak reinforcement was placed which implied high strain levels and a different progressive deformation of the backfill soil as compared to wall constructed with stiff geogrid only;

- Shaking table test results indicate that the initiation of soil softening, and the failure of the wall occurred earlier in wall constructed with weak geogrid reinforcement in grouped arrangement;

- It was found that the shear band along the soil-geogrid interface become fully developed after the active failure wedge has been developed on the reinforced soil wall;

- It was found that the post-failure behavior of the models until final structure collapse not only depends on the post-peak behavior of the backfill soil, geogrid reinforcements, but also in the geogrid reinforcement stiffness arrangement along the wall height, in particular for walls constructed with a combination with stiff and weak geogrid in grouped schemes;

- Despite different reinforcement stiffness arrangement along the wall height, failure surface angles remained almost the same for all models which might

suggest that stability of this walls will be governed by the reinforcement length and the highest reinforcement stiffness;

References

[1] F. Tatsuoka, J. Koseki, M. Tateyama and K. Horii, Performance of Soil Retaining Walls during the Great Hanshin-Awaji Earthquake, Bulletin of ERS, no. 28, pp.43-57, 1995.

[2] D. Sandri, A performance summary of reinforced soil structures in the greater Los Angeles area after the Northridge earthquake, Geotextiles and Geomembranes, vol. 15, no. 4-6, pp. 235-253, 1997. https://doi.org/10.1016/S0266-1144(97)10006-1

[3] H. I. Ling, D. Leshchinsky and N. N. Chou, Post-earthquake investigation on several geosynthetic-reinforced soil retaining walls and slopes during the Ji-Ji earthquake of Taiwan, Soil Dynamics and Earthquake Engineering , vol. 21, no. 4, pp. 297-313, 2001. https://doi.org/10.1016/S0267-7261(01)00011-2

[4] J. Kuwano, Y. Miyata and J. Koseki, Performance of reinforced soil walls during the 2011," Geosynthetics International, vol. 21, no. 3, pp. 179-196, 2014. https://doi.org/10.1680/gein.14.00008

[5] R. J. Bathrust and K. Hatami, Seismic response analysis of a geosynthetic reinforced soil, Geosynthetics International , vol. 5, no. 1-2, pp. 127-166, 1998. https://doi.org/10.1680/gein.5.0117

[6] O. Matsuo, T. Tsutsumi, K. Yokoyama and Y. Saito, "Shaking Table Tests And Analyses of Geosynthetic-Reinforced Soil Retaining Walls," Geosynthetics International, vol. 5, no. 1-2, pp. 97-126, 1998. https://doi.org/10.1680/gein.5.0116

[7] L. N. Roessig and N. Sitar, "Centrifuge Model Studies of the Seismic Response of Reinforced Soil Slopes," Journal of Geotechnical and Geoenviromental Engineering, pp. 388-400, 2006. https://doi.org/10.1061/(ASCE)1090-0241(2006)132:3(388)

[8] M. Sabermahani, A. Ghalandarzadeh and A. Fakher, Experimental study on seismic deformation modes of reinforced-soil walls, Geotextiles and Geomembranes, vol.27, no. 2, pp. 121-136, 2009. https://doi.org/10.1016/j.geotexmem.2008.09.009

[9] J. Koseki, Y. Munaf, M. Tateyama, M. Kojima and T. Sato, Shaking and Tilt Table Test of Geosynthtic-Reinforced Soil and Conventional-Type Retaining Walls, vol.5, no. 1-2, pp. 73-96, 1998. https://doi.org/10.1680/gein.5.0115

[10] K. Watanabe, Y. Munaf, J. Koseki, M. Tateyama and K. Kojima, "Behaviors of several types of model retaining walls subjected to irregular excitation," Soils abd Foundations, vol. 43, no. 5, pp. 13-27, 2003. https://doi.org/10.3208/sandf.43.5_13

[11] M. Yazdandoust, "Assessment of Horizontal Seismic Coefficient for Three Different Types of Reinforced Soil Structure Using Physical and Analytical Modeling," International Journal of Geomechanincs , vol. 19, no. 7, 2019. https://doi.org/10.1061/(ASCE)GM.1943-5622.0001344

[12] I. Anastasopoulos, T. Georgarakos, V. Georgiannou, V. Drosos and R. Kourkoulis, "Seismic performance of bar-mat reinforced-soil retaining wall: Shaking table Test using versus numerical analysis with modified kinematic hardening constitutive model," Soil Dynamics and Earthquake Engineering , vol. 30, no. 10, pp. 1089-1105, 2010. https://doi.org/10.1016/j.soildyn.2010.04.020

[13] D. Leshchinsky, Design Dilema: Use peak or residual strengh of soil, Geotextiles and Geomembranes, pp. 111-125, 2001. https://doi.org/10.1016/S0266-1144(00)00007-8

[14] Y. Jiang, J. Han and R. L. Parsons, Numerical evaluation of secondary reinforcement effect on geosynthetic-reinforced retaining walls, Geotextiles and geomembranes , 2019. https://doi.org/10.1016/j.geotexmem.2019.103508

[15] M. Lelli, R. Laneri and P. Rimoldi, Innovative reinforced soil structures for high walls and slopes Innovative reinforced soil structures for high walls and slopes, 2015. https://doi.org/10.1016/j.proeng.2015.11.099

[16] M. Kikumoto, T. Nakai, S. M. Hossain, K. Ishii, A. Watanabe and F. Zhang, Mechanical Behaviour of Geosynthetic-reinforced Soil Retaining Wall, Geoshanghai International Conference, 2010. https://doi.org/10.1061/41108(381)41

[17] K. Hatami, R. J. Bathrust and P. Di Pietro, "Static Response of Reinforced Soil Retaining Walls with Nonuniform Reinforcement," The International Journal of Geomechanics, vol. 1, no. 4, pp. 477-506, 2001.

DOI: 10.1080/15323640108500164

[18] G. C. Itasca, "FLAC - Fast Lagrangian Analysis of Continua, v 4.00,," Minneapolis, MN, USA, 2001.

[19] Y. Miyata and M. Shinoda, A Case Study of Damages of Geogrid Reinforced Soil Walls Triggered By Rainfall, 6th Asian Regional Conference on Geosynthetics, New Dehli, India, 2016.

[20] D. Lombardi, S. Bhattacharya, F. Scarpa and M. Bianchi, "Dynamic response of a geotechnical rigid model container with absorbing boundaries," Soil Dynamics and Earthquake Engineering, vol. 69, pp. 46-56, 2015.

[21] A. M. Krishna and M. G. Latha, "Container boundary effects in shaking table tests on reinforced soil wall models," International Journal of Physical Modelling in Geotechnics, vol. 9, no. 4, pp. 01-14, 2009. https://doi.org/10.1680/ijpmg.2009.090401

[22] S. Nakajima, J. Koseki, K. Watanabe and M. Tateyama, Simplified procedure to evaluate earthquake-induced residual displacement of geosynthetic reinforced soil retaining wall," Soils and Foundation, vol. 50, no. 5, pp. 659-677, 2010. https://doi.org/10.3208/sandf.50.659

[23] M. M. El-Emam and R. J. Bathrust, Experimental Design, instrumentation and Interpretation of Reinforced Soil Wall Response Using a Shaking Table Test," International Journal of Physical Modelling in Geotechnics , vol. 4, no. 4, pp. 13-

32, 2004. https://doi.org/10.1680/ijpmg.2004.040402

[24] S. Lai, Similitude for shaking table tests on soil-structure-fluid model in 1g gravitational field," Soils and Foundations, vol. 29, no. 1, pp. 105-118, 1989. https://doi.org/10.3208/sandf1972.29.105

[25] M. M. El-Emam and R. J. Bathurst, Influence of reinforcement parameters on the seismic response of reduced-scale reinforced soil retaining walls, Geotextiles and Geomembranes, pp. 33-49, 2007. https://doi.org/10.1016/j.geotexmem.2006.09.001

[26] G. N. Richardson, K. L. Lee, A. C. Fong and D. L. Feger, Seismic Testing of Reinforced Earth Walls, Journal of the Geotechnical Engineering Division, vol. 103, no. 1, pp. 1-17, 1977.

[27] C. -C. Huang and H. -J. Wu, Seismic displacement analysis of a reinforced soil model wall considering progressive development of reinforcement force, Geosynthetics International, vol. 16, no. 3, pp. 1751-7613, 2009. https://doi.org/10.1680/gein.2009.16.3.222

[28] A. A. Ajuda, J. Kuwano, S. Takamine and K. Yasukawa, Shaking table test on seismic performance of geogrid reinforced soil wall, 7th International Conference on Earthquake Geotechnical Engineering, Rome, Italy, 2019.

[29] J. Izawa and J. Kuwano, Evaluation of extent of damage to geogrid reinforced soil walls subjected to earthquakes, Soils and Foundations, vol. 51, no. 5, pp. 945-958,

2011. https://doi.org/10.3208/sandf.51.945

[30] F. Tatsuoka, M. Tateyama and O. Murata, Earth retaining wall with a short geotextile and a rigid facing, Rio de Janeiro, Brazil, Balkema, Rottedam, 1988.

[31] M. Alfaro, N. Miura and D. Bergado, Soil-Geogrid Reinforcement Interaction by Pullout and Direct Shear Tests, Geotechnical Testing Journal, vol. 18, no. 2, pp. 157-167, 1995. https://doi.org/10.1520/GTJ10319J

[32] D. Cazzuffi, L. Picarelli, A. Ricciuti and P. Rimoldi, Laboratory Investigations on the Shear Strength of Geogrid Reinforced Soils, pp. 119-137, 1993. https://doi.org/10.1520/STP24317S24

[33] F. B. Ferreira, C. S. Vieira and M. L. Lopes, Direct shear behaviour of residual soil–geosynthetic interfaces – influence of soil moisture content, soil density and geosynthetic type," Geosynthetics International, vol. 22, no. 3, pp. 257-272, 2015. https://doi.org/10.1680/gein.15.00011

[34] M. J. Lopes and M. L. Lopes, Soil-Geosynthetic Interaction - Influence of Soil Particle Size and Geosynthetic Structure," Geosynthetics International, vol. 6, no. 4, pp. 261-282, 1999. https://doi.org/10.1680/gein.6.0153

[35] C.-N. Liu, J. G. Zornberg, T.-C. Chen, Y.-H. Ho and B.-H. Lin, Behavior of Geogrid-Sand Interface in Direct Shear Mode," Journal of Geotechnical and Geoenvironmental Engineering , vol. 135, no. 12, pp. 1863-1871, 2009. https://doi.org/10.1061/(ASCE)GT.1943-5606.0000150

[36] M. R. Abdi and H. Mirzaeifar, Experimental and PIV evaluation of grain size and distribution on soil-geogrid interaction in pullout test, Soils and Foundations, vol. 57, no. 6, pp. 1045-1058, 2017. https://doi.org/10.1016/j.sandf.2017.08.030

[37] R. Bathrust and F. Ezzein, Geogrid and Soil Displacement Observations During Pullout Using a Transparent Granular Soil," Geotechnical Testing Journal, vol. 38, no. 5, pp. 673-685, 2015. https://doi.org/10.1520/GTJ20140145

[38] N. H. Giang, J. Kuwano, J. Izawa and S. Tachibana, Influence of unloading–reloading processes on the pullout resistance of geogrid, Geosynthetics International, vol. 17, no. 4, pp. 242-249, 2010. https://doi.org/10.1680/gein.2010.17.4.242

[39] A. M. Morsy, J. G. Zornberg, J. Han and D. Leshchinsky, A new generation of soil-geosynthetcis interaction experimentation," Geotextiles and Geomembranes , 2019. https://doi.org/10.1016/j.geotexmem.2019.04.001

[40] X. Peng and J. G. Zornberg, Evaluation of soil-geogrid interaction using transparent soil with laser illumination," Geosynthetics International, vol. 26, no. 2, pp. 1-47, 2019. https://doi.org/10.1680/jgein.19.00004

[41] K. Hatami and R. J. Bathrust, Parametric analysis of reinforced soil walls with different backfill material properties," Las Vegas, Nevada, USA, 2005.

[42] M. Yazdandoust, Assessment of Horizontal Seismic Coefficient for Three Different Types of Reinforced Soil Structure Using Physical and Analytical Modelling," International Journal of Geomechanics, 2019.

[43] E. M. Palmeira, Soil-Geosynthetic Interaction: Modelling and Analysis, Geotextile and Geomembranes, Vol, 27, no. 5, pp. 368-390 https://doi.org/10.1016/j.geotexmem.2009.03.003

[44] L. Zhang and C. Thornton, A numerical examination of the direct shear test,25 Geotechnique, vol. 57, no. 4, pp. 343-354, 2007. https://doi.org/10.1680/geot.2007.57.4.343

[45] W. Po-Kai, K. Matsushima, F. Tatsuoka and T. Uchimura , Shear Zone Formation in Reinforced Soil Subjected to Direct Shear, in 第 37 回地盤工学研究発表会, 2002.

[46] D. Lesniewska, M. Niedostatkiewicz and J. Tejchman, Experimental Study on Shear Localisation in Granular Materials Within Combined Strain and Stress Field, An International Journal for Experimental Mechanics , vol. 48, no. 5, 2012. https://doi.org/10.1111/j.1475-1305.2012.00838.x

[47] B. Soltanbeigi, A. Altunbas and O. Cinicioglu, Influence of dilatancy on shear band characteristics of granular backfills," European Journal of Environmental and Civil Engineering, 2019. https://doi.org/10.1080/19648189.2019.1572542

[48] P. Vangla and G. M. Latha, Influence of Particle Size on the Friction and Interfacial Shear Strength of Sands of Similar Morphology," International Journal of Geosynthetics and Ground Engineering, 2015. https://doi.org/10.1007/s40891-014-0008-9

[49] E. M. Palmeira and G. W. Milligan, Scale effects in direct shear test on sands, Proceedings of the XII International Conference on Soil Mechanics and Foundation Engineering Rio de Janeiro, Brazil, 1989.

[50] M. Al-Hussaini and E. B. Perry, Analysis of rubber membrane-strip reinforced earth wall, Soil Reinforcing and Stablizing Techniques in Engineering Practice, Proceedings of a Symposium Jointly Organized by New South Wales Institute of Technology and the University of New South Wales, Sydney, Australia, 1978.

[51] J. Izawa and J. Kuwano, Centrifuge modelling of geogrid reinforced soil walls subjected to pseudo-static loading," International Journal of Physical Modelling in Geotechnics, vol. 10, no. 1, pp. 1-18, 2010. https://doi.org/10.1680/ijpmg.2010.10.1.1

Appendix 1

Sand total deformations on hybrid reinforced retaining walls

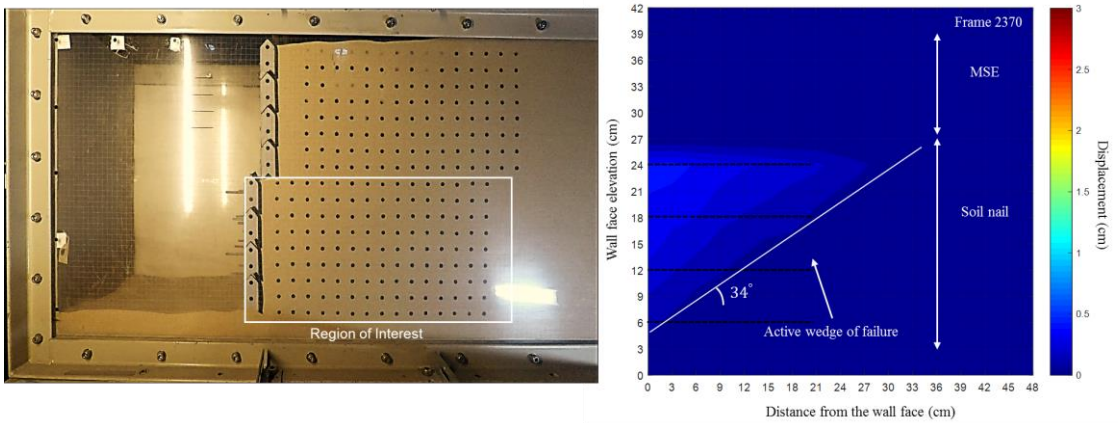

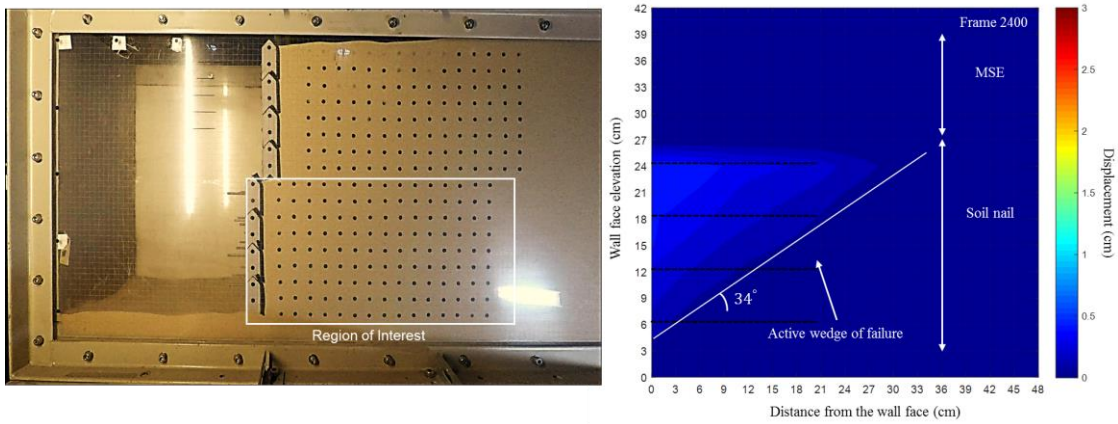

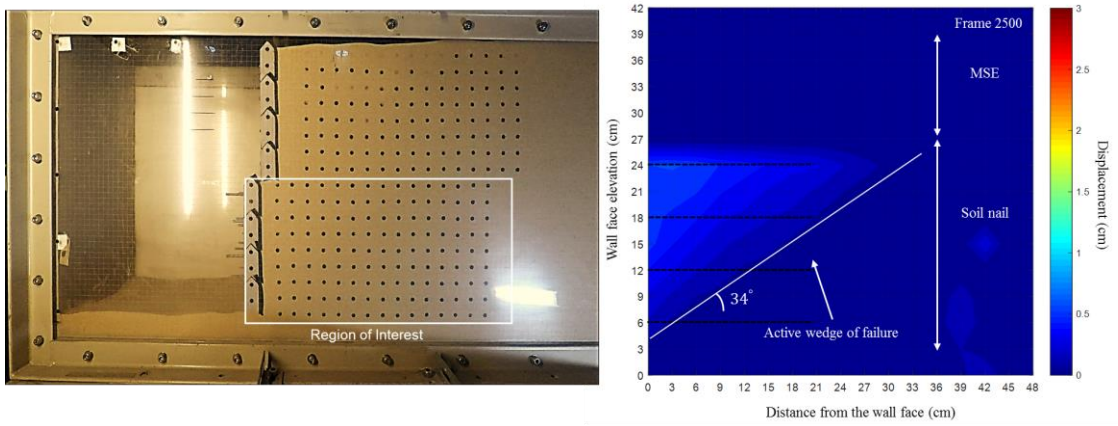

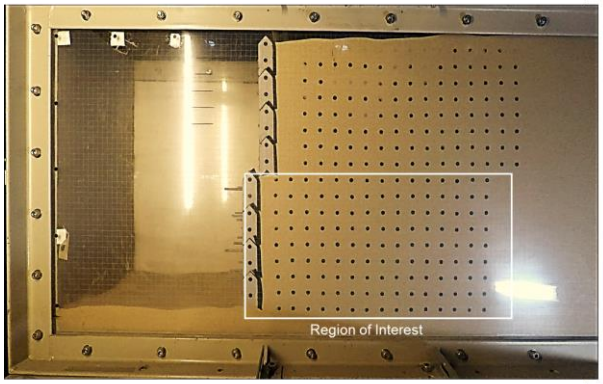
Region of Interest

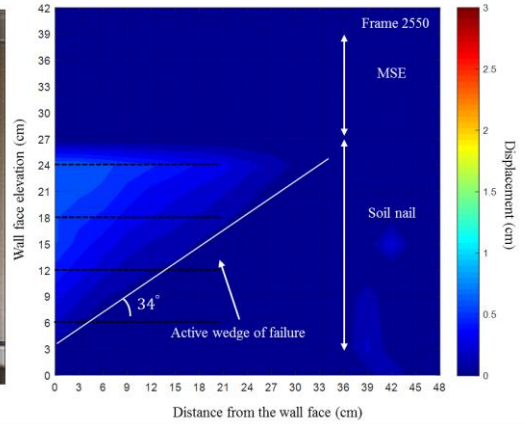
Frame 2550
MSE
Soil nail
34°
Active wedge of failure
Wall face elevation (cm)
Distance from the wall face (cm)
Displacement (cm)

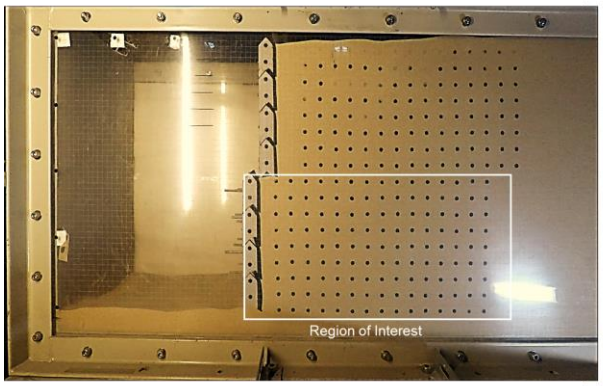
Region of Interest

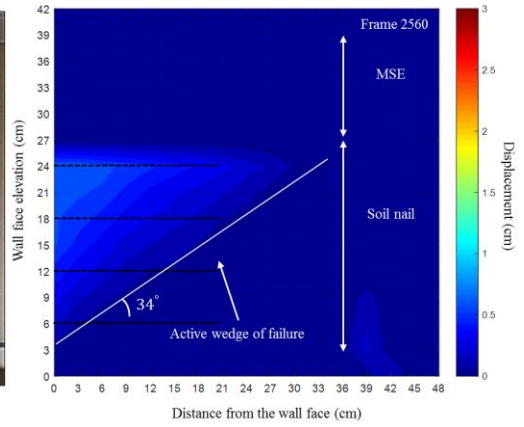
Frame 2560
MSE
Soil nail
34°
Active wedge of failure
Wall face elevation (cm)
Distance from the wall face (cm)
Displacement (cm)

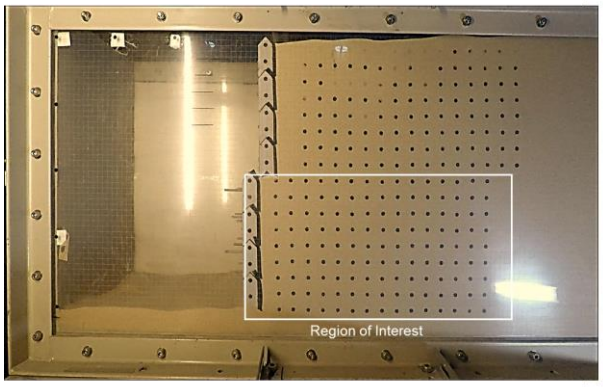
Region of Interest

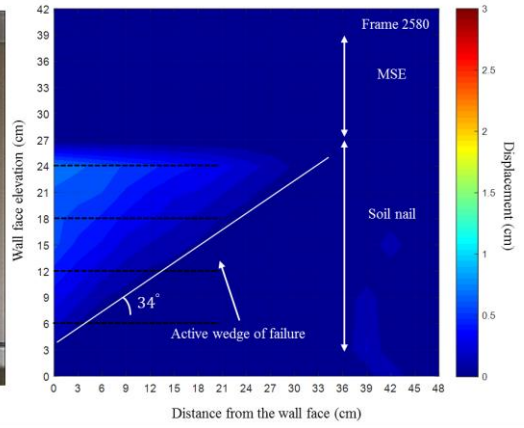
Frame 2580
MSE
Soil nail
34°
Active wedge of failure
Wall face elevation (cm)
Distance from the wall face (cm)
Displacement (cm)

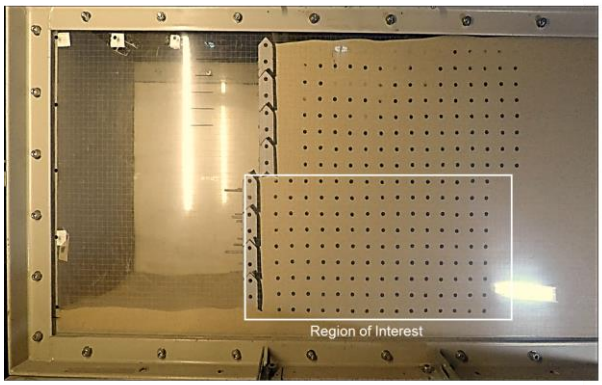
Region of Interest

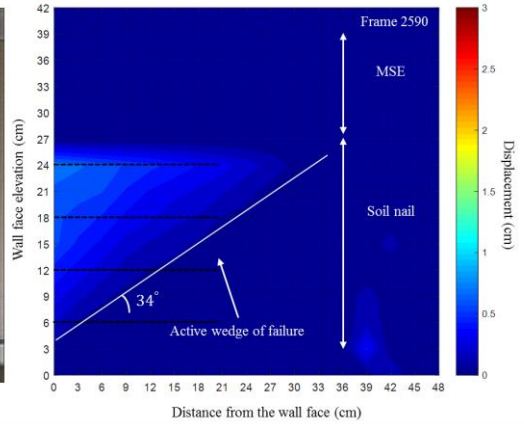
Frame 2590
MSE
Soil nail
34°
Active wedge of failure
Wall face elevation (cm)
Distance from the wall face (cm)
Displacement (cm)

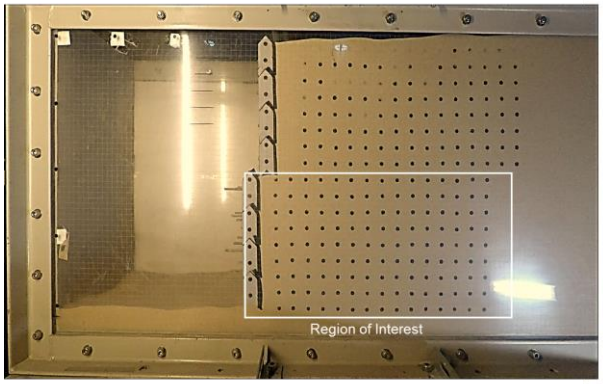
Region of Interest

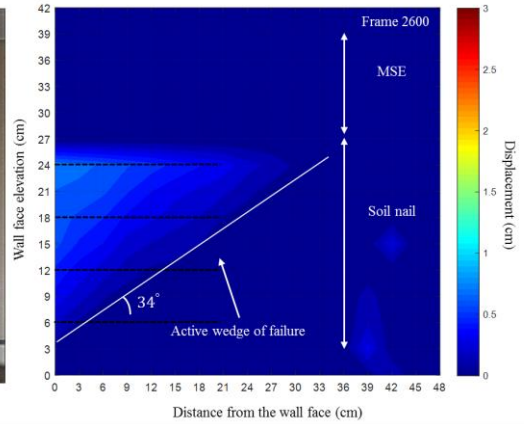
Frame 2600
MSE
Soil nail
34°
Active wedge of failure
Wall face elevation (cm)
Distance from the wall face (cm)
Displacement (cm)

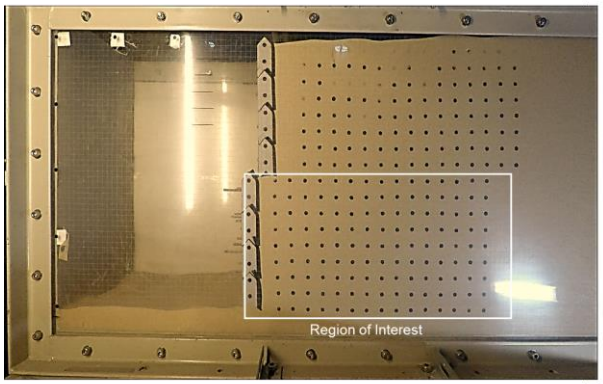
Region of Interest

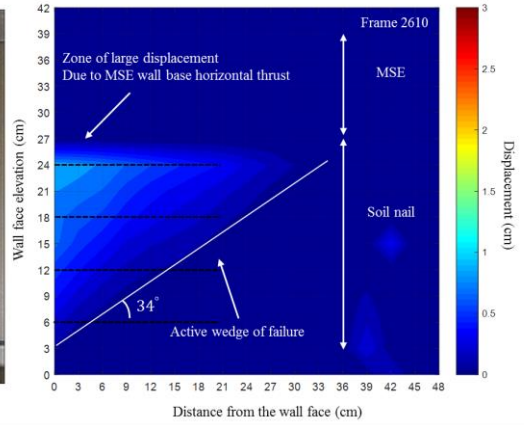
Frame 2610
Zone of large displacement
Due to MSE wall base horizontal thrust
MSE
Soil nail
34°
Active wedge of failure
Wall face elevation (cm)
Distance from the wall face (cm)
Displacement (cm)

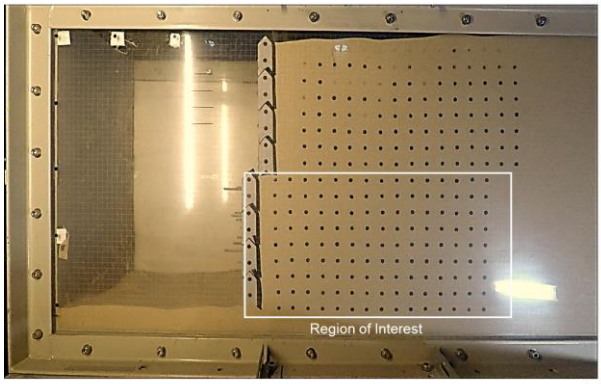
Region of Interest

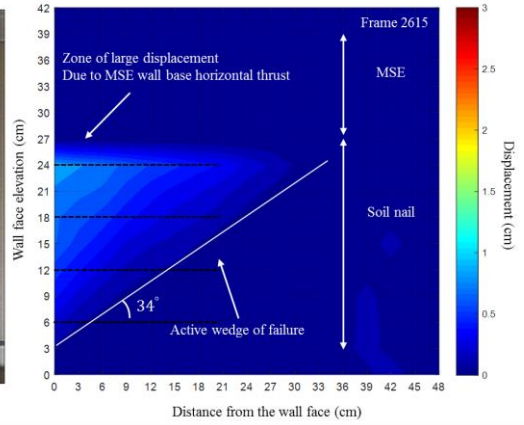
Frame 2615
Zone of large displacement
Due to MSE wall base horizontal thrust
MSE
Soil nail
34°
Active wedge of failure
Wall face elevation (cm)
Distance from the wall face (cm)
Displacement (cm)

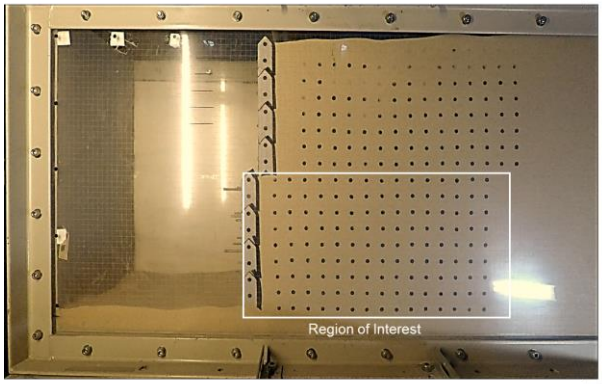
Region of Interest

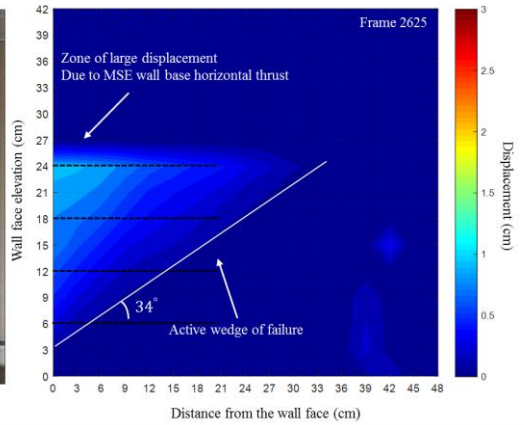
Frame 2625
Zone of large displacement
Due to MSE wall base horizontal thrust
34°
Active wedge of failure
Wall face elevation (cm)
Distance from the wall face (cm)
Displacement (cm)

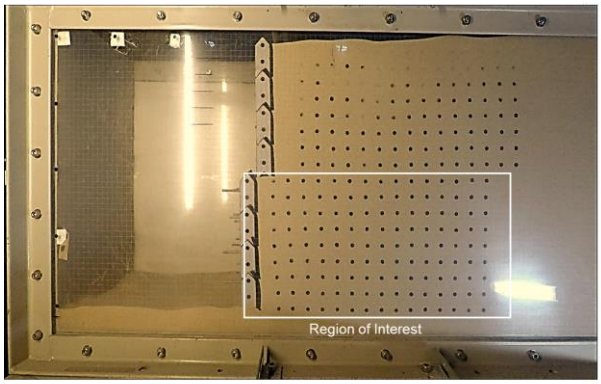
Region of Interest

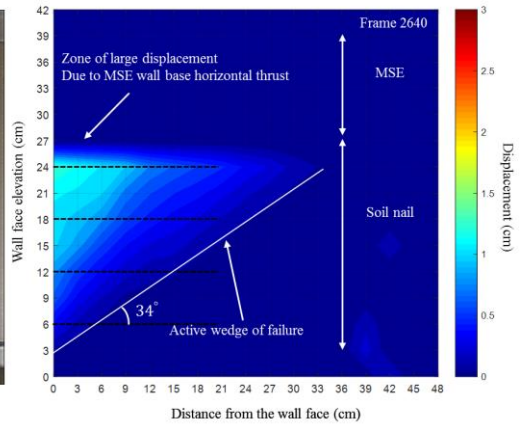
Frame 2640
Zone of large displacement
Due to MSE wall base horizontal thrust
MSE
Soil nail
34°
Active wedge of failure
Wall face elevation (cm)
Distance from the wall face (cm)
Displacement (cm)

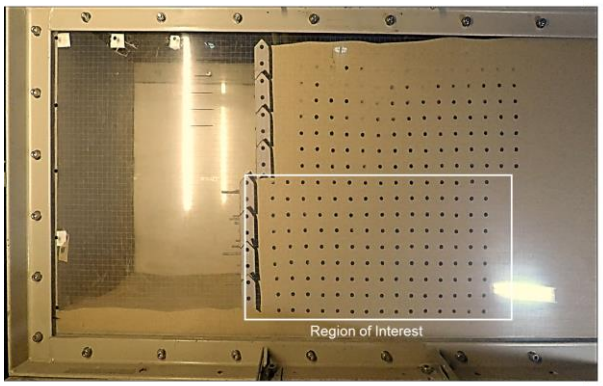
Region of Interest

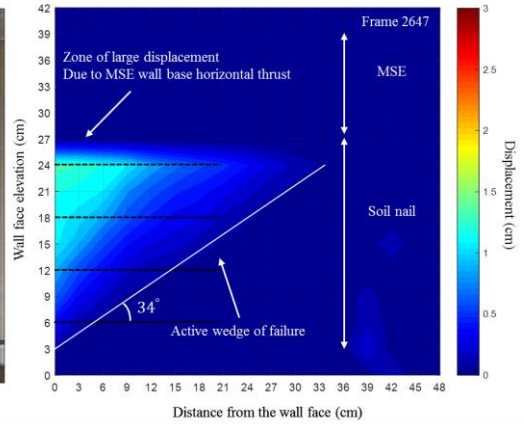
Frame 2647
Zone of large displacement
Due to MSE wall base horizontal thrust
MSE
Soil nail
34°
Active wedge of failure
Wall face elevation (cm)
Distance from the wall face (cm)
Displacement (cm)

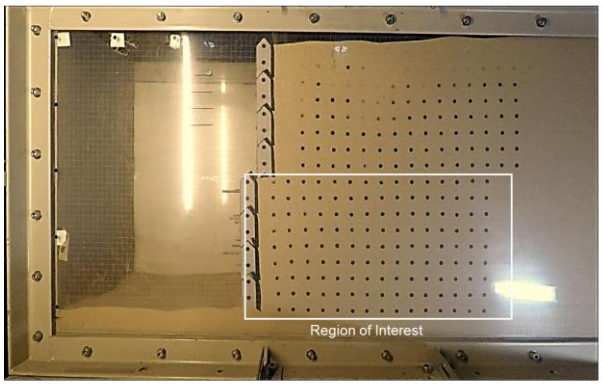
Region of Interest

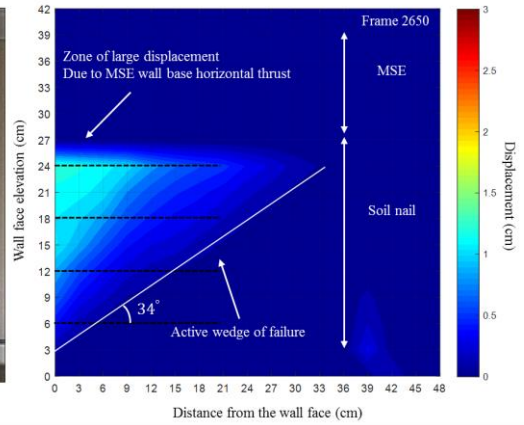
Frame 2650
Zone of large displacement
Due to MSE wall base horizontal thrust
MSE
Soil nail
34°
Active wedge of failure
Wall face elevation (cm)
Distance from the wall face (cm)
Displacement (cm)

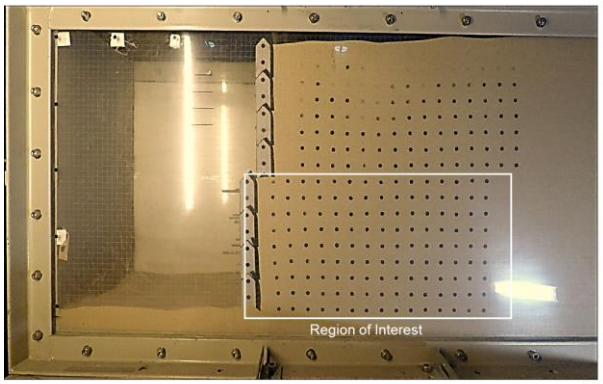
Region of Interest

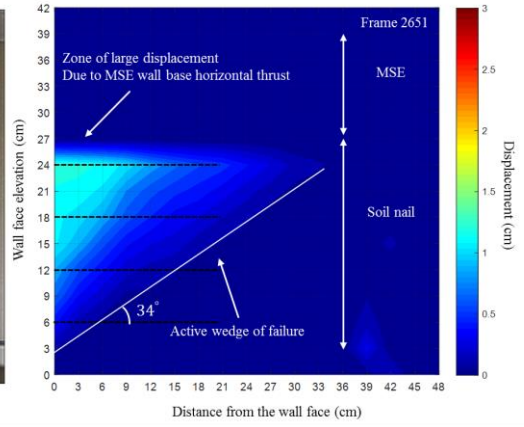
Frame 2651
Zone of large displacement
Due to MSE wall base horizontal thrust
MSE
Soil nail
34°
Active wedge of failure
Wall face elevation (cm)
Distance from the wall face (cm)
Displacement (cm)

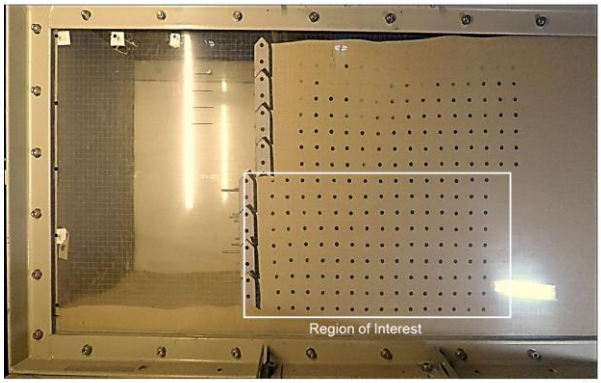
Region of Interest

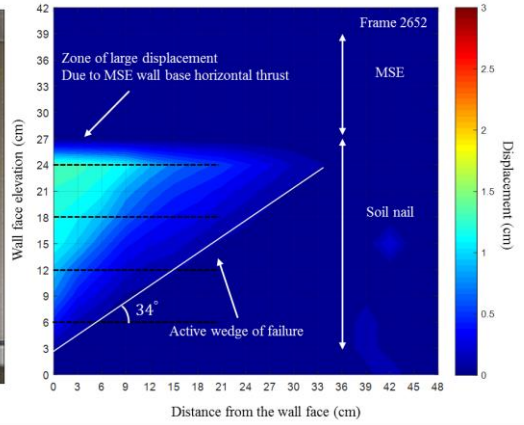
Frame 2652
Zone of large displacement
Due to MSE wall base horizontal thrust
MSE
Soil nail
34°
Active wedge of failure
Wall face elevation (cm)
Distance from the wall face (cm)
Displacement (cm)

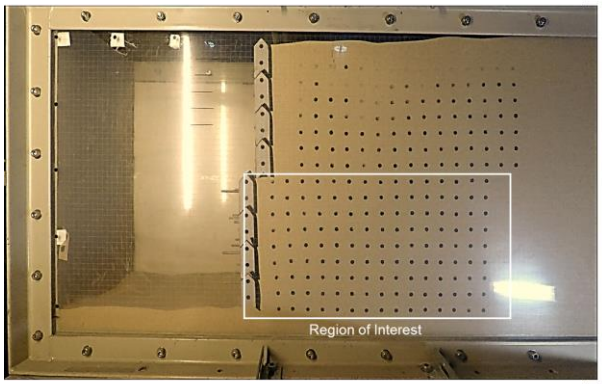
Region of Interest

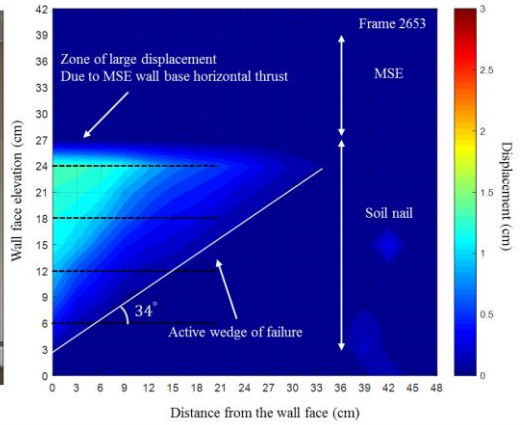
Frame 2653
Zone of large displacement
Due to MSE wall base horizontal thrust
MSE
Soil nail
34°
Active wedge of failure
Wall face elevation (cm)
Distance from the wall face (cm)
Displacement (cm)

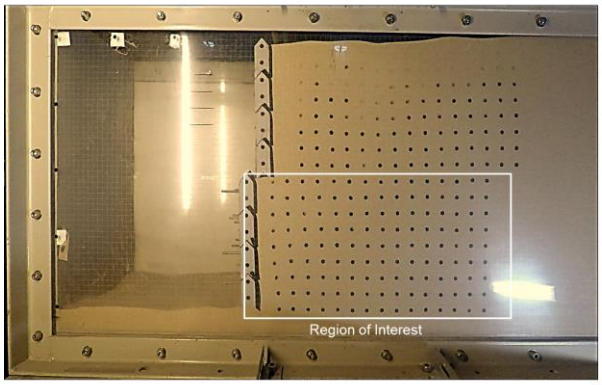
Region of Interest

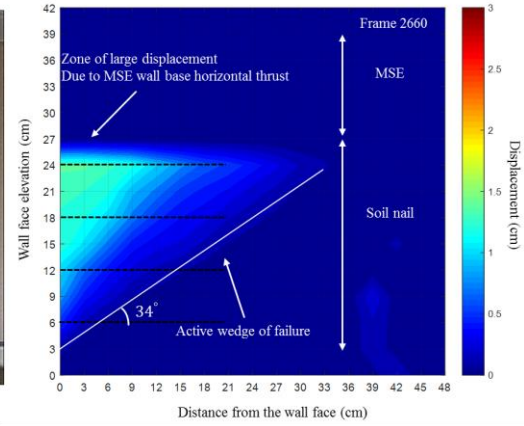
Frame 2660
Zone of large displacement
Due to MSE wall base horizontal thrust
MSE
Soil nail
34°
Active wedge of failure
Wall face elevation (cm)
Distance from the wall face (cm)
Displacement (cm)

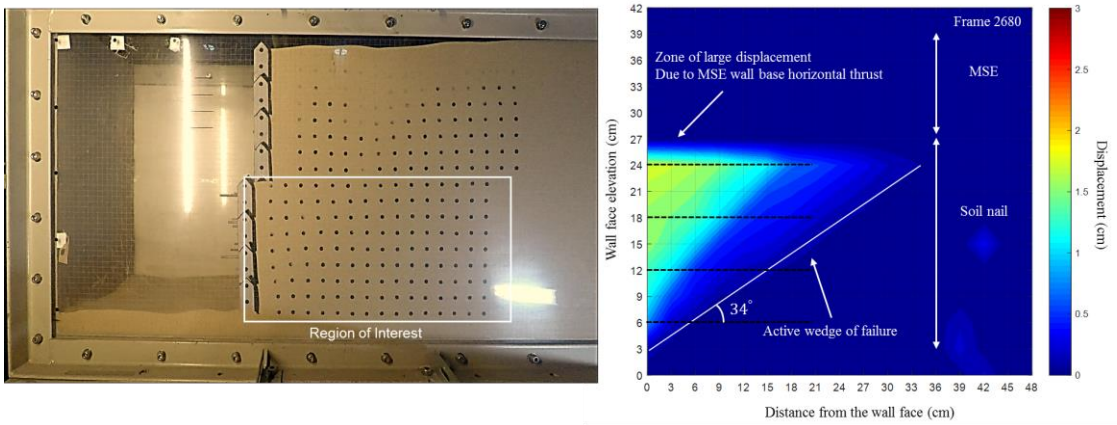
Region of Interest
Frame 2680
Zone of large displacement
Due to MSE wall base horizontal thrust
MSE
Soil nail
34°
Active wedge of failure
Wall face elevation (cm)
Distance from the wall face (cm)
Displacement (cm)

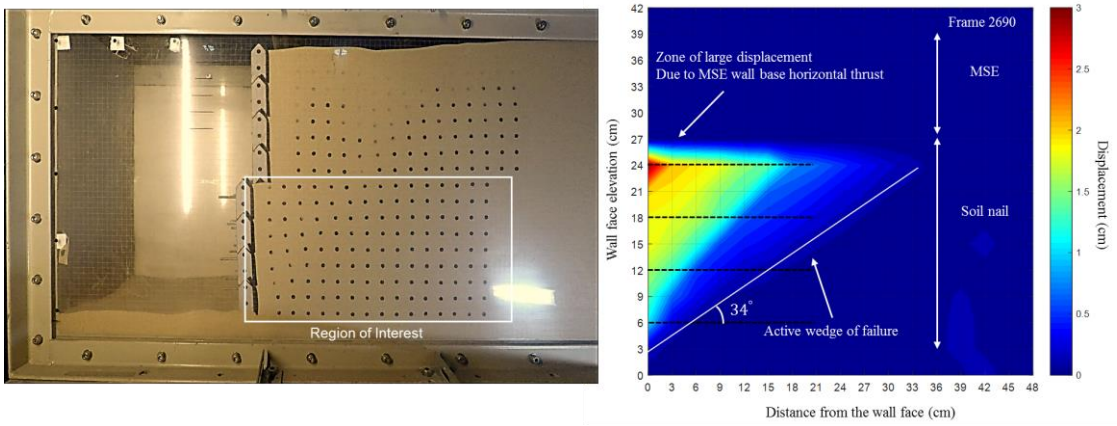
Region of Interest
Frame 2690
Zone of large displacement
Due to MSE wall base horizontal thrust
MSE
Soil nail
34°
Active wedge of failure
Wall face elevation (cm)
Distance from the wall face (cm)
Displacement (cm)

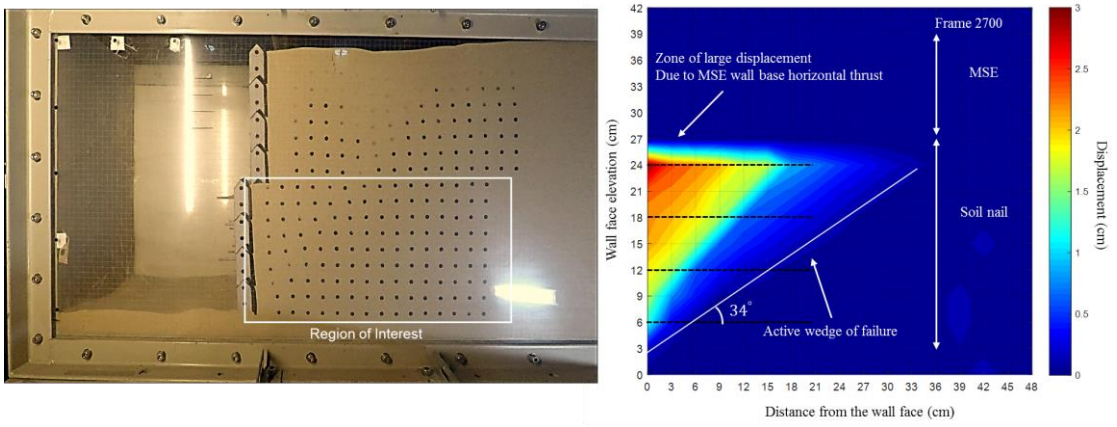
Region of Interest
Frame 2700
Zone of large displacement
Due to MSE wall base horizontal thrust
MSE
Soil nail
34°
Active wedge of failure
Wall face elevation (cm)
Distance from the wall face (cm)
Displacement (cm)

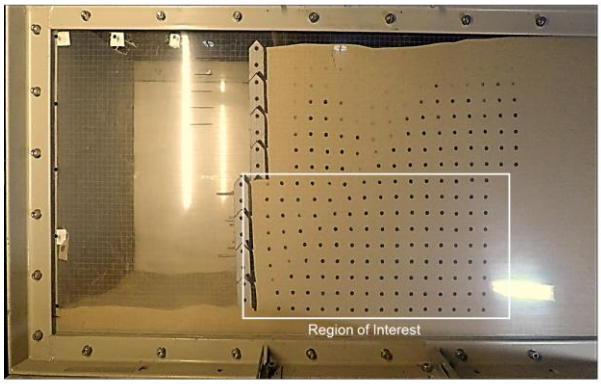
Region of Interest

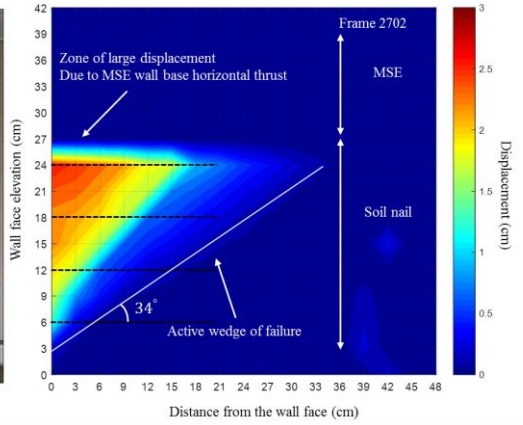
Frame 2702
Zone of large displacement
Due to MSE wall base horizontal thrust
MSE
Soil nail
34°
Active wedge of failure
Wall face elevation (cm)
Distance from the wall face (cm)
Displacement (cm)

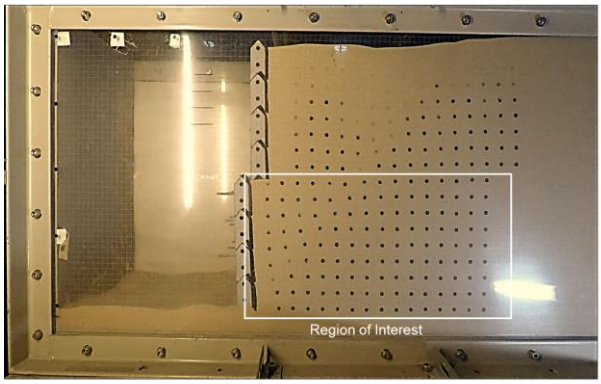
Region of Interest

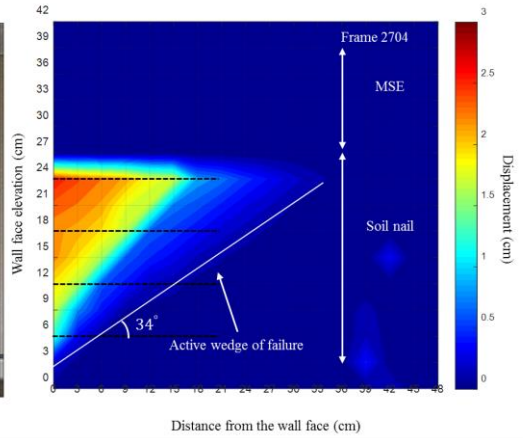
Frame 2704
MSE
Soil nail
34°
Active wedge of failure
Wall face elevation (cm)
Distance from the wall face (cm)
Displacement (cm)

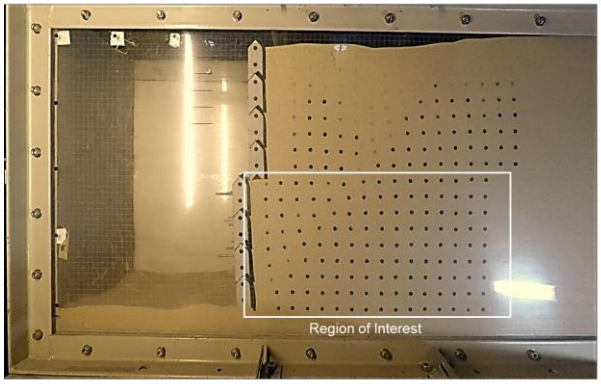
Region of Interest

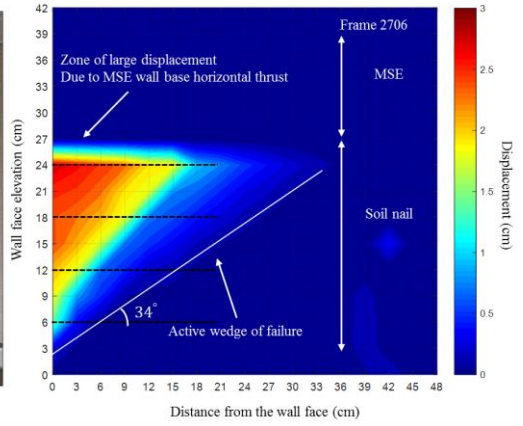
Frame 2706
Zone of large displacement
Due to MSE wall base horizontal thrust
MSE
Soil nail
34°
Active wedge of failure
Wall face elevation (cm)
Distance from the wall face (cm)
Displacement (cm)

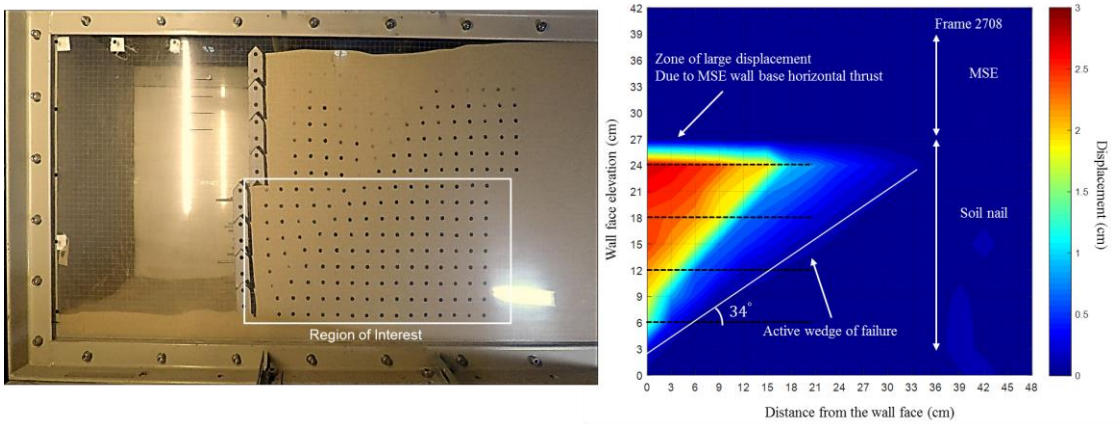
Region of Interest
Frame 2708
Zone of large displacement
Due to MSE wall base horizontal thrust
MSE
Soil nail
34°
Active wedge of failure
Wall face elevation (cm)
Distance from the wall face (cm)
Displacement (cm)

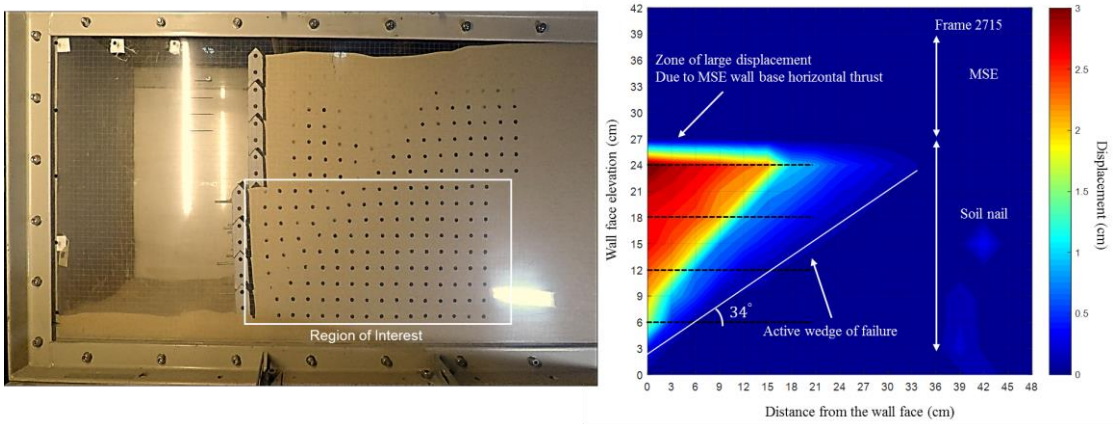
Region of Interest
Frame 2715
Zone of large displacement
Due to MSE wall base horizontal thrust
MSE
Soil nail
34°
Active wedge of failure
Wall face elevation (cm)
Distance from the wall face (cm)
Displacement (cm)

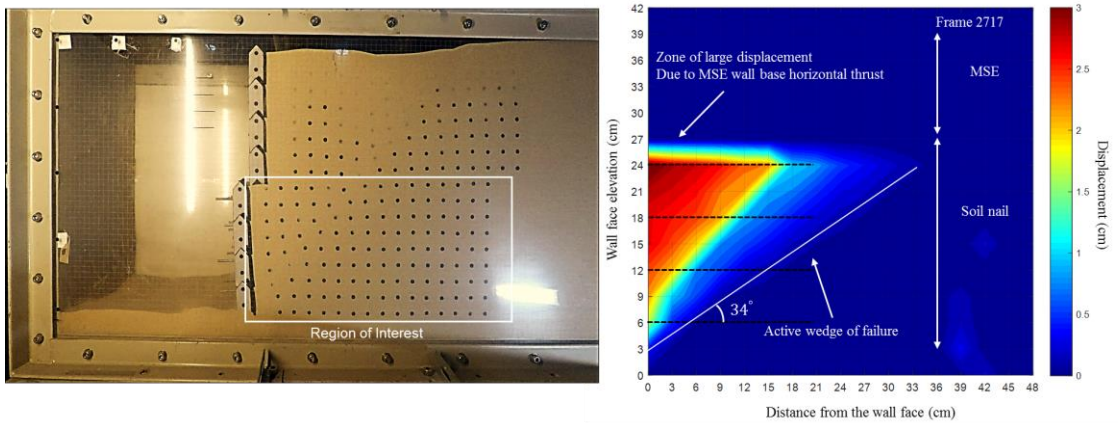
Region of Interest
Frame 2717
Zone of large displacement
Due to MSE wall base horizontal thrust
MSE
Soil nail
34°
Active wedge of failure
Wall face elevation (cm)
Distance from the wall face (cm)
Displacement (cm)

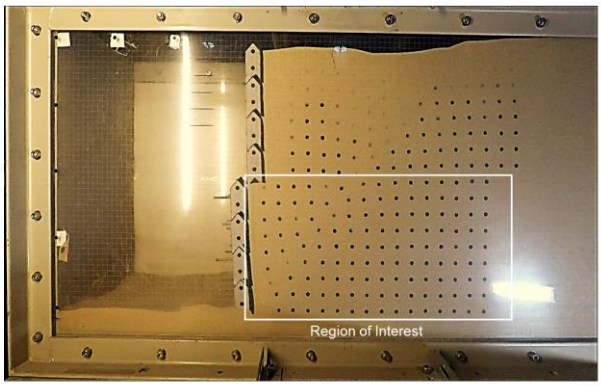
Region of Interest

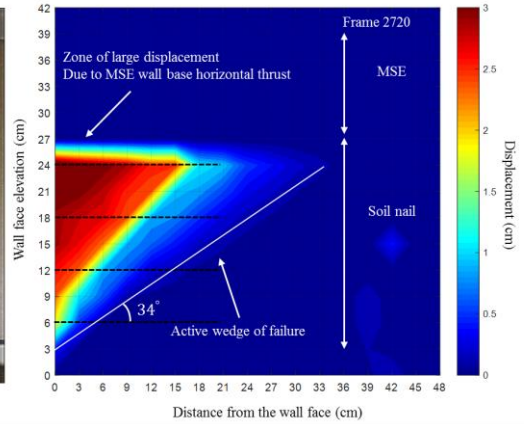
Frame 2720
Zone of large displacement
Due to MSE wall base horizontal thrust
MSE
Soil nail
34°
Active wedge of failure
Wall face elevation (cm)
Distance from the wall face (cm)
Displacement (cm)

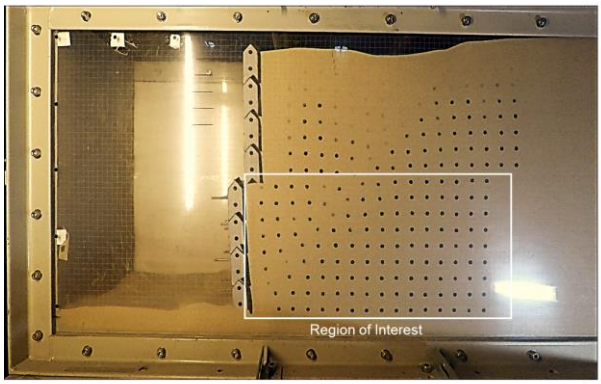
Region of Interest

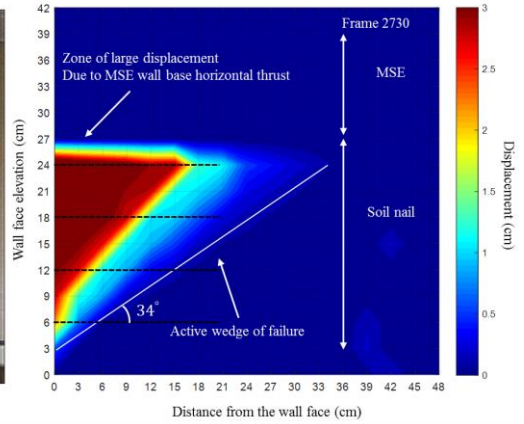
Frame 2730
Zone of large displacement
Due to MSE wall base horizontal thrust
MSE
Soil nail
34°
Active wedge of failure
Wall face elevation (cm)
Distance from the wall face (cm)
Displacement (cm)